Evolving and adaptive strategies for consensus and synchronization of multi-agent systems

Ph.D Thesis

Francesco Scafuti

Tutor

Ch.mo prof. Mario di Bernardo

University of Naples Federico II
Department of Electric Engineering and Information Technology
Naples, Italy
2016

Abstract

We investigate evolving and adaptive strategies, in network of dynamical agents, for solving general types of consensus and synchronization.

First, we analyse the problem of max/min consensus in directed networks of integrators. Extending edge snapping method with a three-well potential, we are able to show the effectiveness of our strategy to achieve general types of consensus, different from the average. Theoretical results are validated via a number of numerical examples.

Then we move to synchronization of coupled non identical oscillators. We design an evolutionary strategy for network synchronization. Our results suggest that heterogeneity is the driving force determining the evolution of state-dependent functional networks. Minimal emergent networks show enhanced synchronization properties and high levels of degree-frequency assortativity. We analyse networks of $N = 100$ and $N = 1000$ Kuramoto oscillators showing that hubs in the network tend to emerge as nodes' heterogeneity is increased.

Finally, we study synchronization of multi-agent systems from a contraction theory viewpoint. Contraction theory is a useful tool to study convergence of dynamical systems and networks, recently proposed in the literature. In detail, we recall three strategies: virtual systems method, convergence to a flow-invariant subspace and hierarchical approach. While the former is simple to apply, the latter is suited for larger networks.

Contents

1 Introduction **1**

1.1 Outline of the thesis 3

2 Complex Evolving Networks of dynamical agents: an overview **5**

2.1 Networks: Dynamics and structure 6

2.1.1 Dynamics and Coupling 6

2.1.2 Network structure 7

2.1.2.1 Network Models 9

2.2 Synchronization 11

2.2.1 Master Stability Function 12

2.3 Consensus 14

2.4 The third ingredient: Evolution 16

2.4.1 Edge Snapping 19

2.4.2 NetEvo 21

2.5 Summary 22

3 The Kuramoto model **23**

3.1 The origins 23

3.2 The model 24

3.3 Developments 26

3.3.1 Critical coupling for the onset of synchronization 26

3.3.2 Explosive synchronization 28

3.4 Summary 29

4 Modified edge-snapping techniques **30**
4.1 General consensus and three-well potential 30
4.2 Hybrid Edge Snapping 32
4.3 Directed edge snapping 35
4.4 Summary 37

5 An evolutionary strategy for network synchronization **39**
5.1 Problem statement 40
5.2 Methodology 41
5.3 Analysis of emergent network structures 43
5.4 Larger networks 47
5.5 Robustness properties varying the parameters 50
5.6 Applications to networks of oscillators 51
5.7 Summary 53

6 Dynamics, stability and robustness of evolving strategies **54**
6.1 Dynamics of adaptively coupled Kuramoto oscillators: a brief overview . . . 54
6.2 Dynamics of two oscillators coupled via Edge Snapping 56
6.3 Two oscillators model 60
6.4 Summary 66

7 Synchronization via contraction theory **67**
7.1 Mathematical Preliminaries 68
7.2 Contraction Theory and Incremental Stability 69
7.2.1 Example 70
7.2.2 Properties of contracting systems 71
7.3 Synchronization and Contraction Theory 73
7.4 Virtual system method 74
7.4.1 Synchronization of networks with an all-to-all topology 74
7.4.2 Example 75
7.4.3 Synchronization of networks with a generic topology 78
7.5 Convergence to a flow-invariant linear subspace 78
7.5.1 Example 83
7.6 Hierarchical approach 85
7.6.1 Example 87

7.7 Summary 89

8 Conclusions **90**

Bibliography **92**

List of Figures

2-1 Different MSF shapes 13
2-2 MSF for a Scale-free network of N=200 Lorenz systems. 14
2-3 Undirected edge snapping. Bistable potential (2-14) driving the evolution of each k_{ij}. 20
2-4 Network of $N = 50$ integrators: (a) Evolution of the agent dynamics under the undirected edge-snapping strategy; (b) Evolution of the coupling gains. . 21
2-5 Schematic illustration of how NetEvo works. 22

4-1 Three-well potential (4-7) driving the evolution of each σ_{ij}. 33
4-2 Network of $N = 50$ integrators: (a) Evolution of the agent states towards max-consensus; (b) evolution of the coupling gains. 35
4-3 Network of $N = 50$ integrators: (a) Evolution of the agent states towards min-consensus; (b) evolution of the coupling gains. 36
4-4 Network of $N = 50$ integrators: (a) Max-consensus is achieved through directed edge snapping; (b) all the coupling gains converge to the equilibrium values. 37
4-5 Network of $N = 50$ integrators with $x_1(0) = -300$: (a) χ-consensus is achieved through directed edge snapping, with $\chi < \chi_{\max}$; (b) all the coupling gains converge to the equilibrium values. 38
4-6 Network of $N = 50$ integrators: (a) Min-consensus is achieved through directed edge snapping; (b) all the coupling gains converge to the equilibrium values. 38

5-1 Schematic description of the evolutionary edge-snapping strategy. Step 1 (variation): computation of link activation probabilities by running the edge-snapping strategy from many different random initial conditions. Step 2 (selection): selection of those links whose activation probability is above some threshold value p^*. 41

5-2 (a) Standard deviation of the link activation probability p_{ij} as a function of the number of trials n_S. (b) Order parameter and relative number of links of the minimal ES structure as a function of the number of trials n_S. 42

5-3 (a) Link activation probabilities p_{ij} in the case of $N = 6$ generated by the variation stage of the evolutionary ES strategy; (b) Selection of the threshold probability value p: order parameter R, relative number of links $\bar{M}$. The arrow on the x-axis indicates the critical threshold p^* which gives the minimal ES network; (c) Minimal Edge-Snapping Network; (d) Optimal network maximizing R obtained by Exhaustive search and a Monte Carlo based method. 44

5-4 Heterogeneity induces functional structural properties of the network. P matrix as a function of the heterogeneity parameter σ when $N = 20$. 44

5-5 Structural properties of the emergent minimal ES network with $N = 100$ and $\sigma = 0.2$. (a) Standard deviation of the link activation probabilities p_{ij} as a function of σ. (b) Maximum (red dashed line) and minimum (black solid line) value of Node Degree k_i as a function of σ. (c) Activation probability of each link against the value of the difference between the natural frequencies of the oscillators at the endpoints. (d) Node degree k_i vs. ω_i. (e) Order parameter R (red solid line) and relative number of links $\bar{M}$ (blue solid line) of the ES network as a function of the threshold probability value p. For comparison, the value R is depicted for an all-to-all network (purple dashed line) and for randomly generated networks (blue dot-dashed line) with the same number of links. The arrow on x-axis represents the threshold p^* to give the minimal ES network. (f) Order parameter R of the phase oscillators interconnected by the minimal ES network when the overall coupling strength K is increased (red solid) and decreased (blue dashed). We set $N = 300$ and $\sigma = 0.2$. . . . 45

5-6 Frequency-degree plots for different values of network heterogeneity σ. We set $N = 1000$. 48

5-7 Robustness analysis of the emergent minimal ES network. (a) Variations of the control input gain α (b) Variations of the damping factor d (c) Variations of the height of the barrier b 50

5-8 Emergent minimal ES network with $N = 10$ and $\sigma = 1$. (a) Link activation probabilities p_{ij} generated by the variation stage of the evolutionary ES strategy; (b) Minimal ES network obtained selecting $p^* = 0.91$. (c) Order parameter of the minimal ES network as a function of the threshold probability value p^* (blue solid line). For comparison, the value is depicted of the order parameter for randomly generated networks (red solid line) with the same number of links. The vertical (purple dotted line) represents the threshold we choose at the selection stage to find the minimal ES network. As can be seen, the order parameter of the minimal ES network rapidly decrease in the proximity of the threshold we choose. Indeed the network does not guarantee any phase locked solution above that threshold. (d) Relative number of links $\bar{M}$ of the minimal ES structure (when compared to the number of links of the all-to-all structure). 52

6-1 (a) Nullclines and equilibria of system (6-6). Blue dots are stable and red dots are unstable equilibria. (b) Some trajectories of system (6-6) rooted in several initial conditions, with $k = 0$ and ψ varying from 0 to 2π. 58

6-2 Parameters variation (equilibrium A). Red(black) line are associated to stable(unstable) solutions. Green dots are related to the amplitude of stable limit cycles. 59

6-3 Behaviour of equilibrium A varying $\Delta\omega$. Red(black) line are associated to stable(unstable) solutions. Green dots are related to the amplitude of stable limit cycles. 60

6-4 Parameters variation (equilibrium B). Red (black) lines are associated to stable (unstable) solutions. 61

6-5 Behaviour of equilibrium B varying $\Delta\omega$. Red (black) lines are associated to stable(unstable) solutions. 62

6-6 Schematic illustration of condition (6-12). Red dotted line divides the plane in two regions $\rho^+ > \Delta\omega/2$ and $\rho^+ < \Delta\omega/2$. Function g^R is obtained for $\Delta\omega = 1$. 63

6-7 Schematic illustration of functions g^R and g_L. Red dotted line divides the plane in two regions $\rho^+ > \Delta\omega/2$ and $\rho^+ < \Delta\omega/2$. Functions g^R and g^L are obtained for $\Delta\omega = 1$. 65

7-1 Norm of the error (blue solid line) between two trajectories $x(t)$ and $z(t)$ rooted in different initial conditions $x_0 = [0.4 \;\; 0.2]^T$, $z_0 = [0.3 \;\; 0.1]^T$. For the sake of comparison, the behaviour of $|x_0 - z_0|e^{-ct}$ is depicted (dashed black line). (Reproduced from [22]). 71

7-2 A schematic representation of the three-genes Repressilator circuit (a). Simulation results (b). (Reproduced from [22]) 76

7-3 The network structure of the example 7.5.1 (left panel). Simulation of the network (7-15) with parameters $a = 0$, $b = 2$, $c = 6$, coupling gains $\sigma_1 = 7$, $\sigma_2 = 10$, $k_1 = 1$, $k_2 = 10$, and $u(t) = 3\sin(t)$. The initial conditions are uniformly distributed in the interval $[-4,\ 4]$ (right panel). (Reproduced from [22]) 85

7-4 The network used for the simulation of FN neurons. (Reproduced from [22]) 87

7-5 Simulation of (7-21) with $\gamma_1 = 0.05$ and $\gamma_2 = 7$ (left panel). The behaviour of $u(t)$ is shown ($0 \geq t \geq 10$) in the right panel. (Reproduced from [22].) . . 89

List of Tables

5-1 Comparison results ($N = 1000$). Minimal network is obtained for $\sigma = 0.14$. The optimal structure is computed as in [80]. NetworkCM was obtained with the Configuration Model algorithm [50], given the degree distribution of minimal network. All quantities referring to NetworkCM are averaged over 10 realizations. 49

7-1 Vector Norms, Induced Matrix Norms and Matrix Measure 68

CHAPTER 1

Introduction

Networked systems are ubiquitous nowadays: gene regulatory networks, smart grids, the Internet, World Wide Web, sensor networks, neural networks are all examples of ensembles of connected agents that interact with each other to achieve some common objective [11, 84]. Network science has been quickly developed in the last few years, as an efficient tool to study such systems. In this area, a network is a set of dynamical agents linked to each other through a web of interconnections [8, 88, 51]. The most interesting and facing feature of networked systems is their ability to show emergent behavior that cannot be explained in terms of the individual dynamics of each single agent in the network. Synchronization and coordination are probably the simplest of these kind of phenomena [63, 18, 53]. Examples also come from nature, where flocks of birds spontaneously emerge, or the fascinating synchronous flashing of fireflies in Amazonia, suddenly takes place.

Networks paradigm has been used in a wide class of systems ranging from engineering, to biology and sociology. In all of those cases a fundamental is how to control the whole system, represented by an artificial neural network or a grid of power generators and consumers, so as to achieve a desired behavior [45, 60]. Basically, network control strategies can be formulated in terms of rules acting on: (i) the set of links; (ii) the set of nodes or (iii) the evolution of the network structure. Link based network control is represented by a rule, often called the protocol, that each agent has to apply to treat information coming from neighbors, i.e. nodes that share a link. Examples range from diffusive linear protocol [88] to distributed PID control [10]. The idea behind controlling nodes' dynamics, instead, is typically called pinning control [13] and relies on adding a virtual leader node, the pinner, unidirectionally linked to a small fraction of the entire nodes set. Pinner node produces the control action that is

propagated to the rest of the nodes through their interconnections. One of the key assumptions of the control strategies presented so far, is the time-invariant nature of links weights and the interconnection structure. In particular, it is assumed that the strength associated to the interaction between nodes does not change over time. Also, the structure defining the web of interconnections among nodes is supposed to be constant. Anyway, examples in nature show that in flocks of birds, swarm or flashing of fireflies, individuals are able to form or suppress connections between themselves and adapt the strength of the interactions [35]. As a result, interconnections are continuously rearranged, allowing network structure to evolve. Moreover, there are often situations in which the nature of interconnections is intrinsically time-varying. This is the case, for example, of autonomous vehicles equipped with limited sensing area devices for the communication and interconnection [91]. Also, even if network structure can be assumed fixed, links failures could occur, determining a variation of interconnections that one has to cope with. Thus, controlling agents behavior via the evolution of the network structure and/or adaptation of coupling strength is a useful and viable method recently established in Network Science [18, 7]. Another fundamental is how to evolve network structure so as to promote synchronization. Indeed, a pressing open problem in Network Science is to link structural properties of networks to their functionalities, in terms of, for example, synchronization performances or group coordination capabilities (see [85] and reference therein).

Recent advances in this direction can be found in literature [23]. Although these results are useful to better understand what are the features promoting desired network functionalities, they often rely on centralized strategies. In other words, they require global information on the entire network. However, in the control of networked systems (see for example [62] and reference therein) decentralization is a key feature. Indeed in many real-world applications, each node only knows its state and those of its neighbours. Thus, it is of utmost importance to design decentralized strategies for network control and synchronization.

The aim of this thesis is to study decentralized evolving strategies for consensus and synchronization. The work builds on extensions to edge snapping method, independently developed in [20]. Edge snapping is a general way to evolve an undirected network of identical nonlinear oscillators. It was proposed in the nonlinear control literature and used in a number of applications [19]. Here, we tailor this method so as to guarantee consensus in directed networks. Moreover, based on edge snapping, we develop an evolutionary strategy for synchronization in networks of heterogeneous agents.

Related independent work on the evolution of network structure for synchronization can be found in the literature. For instance in [33] a framework is proposed to enhance synchronization, based on network evolution. Moreover, in [80] the problem of finding correlations between network structure and synchronization performances is formulated as that of optimizing some synchronization measure. In both cases, even though authors derive nice conclusions on the network properties of synchrony optimized structures, the approach taken is heavily centralized. Thus, the work presented in this thesis nicely complement these strategies, relying on simple and decentralized evolving rules.
Further work involved in this thesis deals with the study of synchronization from a contraction theory perspective. Contraction theory is a promising approach to study convergence of dynamical systems and networks [1], since it provides global results based on a constructive method. Indeed, most of the methods to analyse the synchronized state are local (e.g. they are obtained from a linearised version of the model) or rely on finding Lyapunov functions.

1.1 Outline of the thesis

In Chapter 2 we give an overview on networks of dynamical agents, from structure and dynamics to the evolving paradigm. Also synchronization and consensus are presented, showing how it is possible to study their stability. Then we recall two strategies for network evolution, namely Edge snapping and NetEvo.

In Chapter 3 we recall the Kuramoto model. First we present preliminary studies about mutually coupled oscillators that led to the work of Kuramoto. Then we show developments of Kuramoto model, relying on finding critical coupling for the onset of synchronization. Also we present explosive synchronization recently proposed in the literature of Kuramoto model.

In Chapter 4 we present two evolving strategies for consensus. Specifically we extend edge snapping to directed networks, through directed edge snapping and hybrid edge snapping. Numerical examples are also given to support theoretical finding.

In Chapter 5 an evolutionary method for synchronization in a network of oscillators is introduced. An analysis of emergent networks of $N = 100$ oscillators is given together with a discussion in the case of larger networks. The method is then validate on a network of

chaotic oscillators. Finally we give an application of the proposed strategy in the case of oscillator array models for associative memory functions.

In Chapter 6 we present the Two oscillators model for the analysis of robustness of Edge Snapping in the case of heterogeneous Kuramoto oscillators, used in Chapter 5.

In Chapter 7 Contraction theory is presented as a viable tool to study the convergence properties of networks of dynamical agents and then in Chapter 8 conclusions are drawn.

The results in Chapter 4 are obtained in collaboration with Dr. Pietro De Lellis (Department of Electrical Engineering and Information Technology, University of Naples Federico II, Italy) and were presented in [21]. The results in Chapters 5 and 6 have been developed together with Prof. Takaaki Aoki (Faculty of Education, University of Kagawa, Japan) and can be found, in part, in [76, 75]. The results in Chapter 7 have been obtained in collaboration with Dr. Giovanni Russo and Davide Fiore and can be found in [22].

CHAPTER 2

Complex Evolving Networks of dynamical agents: an overview

Recently, there has been a tremendous interest in the study of complex networks, see [84, 8, 88]. Such networked systems are composed by a set of agents (the nodes), that are linked with each other through a web of interconnections (the edges). Studying complexity of the emerging collective behaviours is a fascinating but difficult task to perform. Indeed, the whole system can show new emergent behaviours that none of the individual agents is able to present. In this scenario, we can expect that even if the dynamics of each node is simple to study, the behaviour of the network cannot be easily predicted and unexpected motions or coordinated evolution could emerge. Synchronization and consensus are typical coordination problems widely studied in literature, see for example [18, 53, 64, 63]. Another fundamental is controllability of complex networks, see [45, 60] and reference therein.

There are many other aspects characterizing complex networks, from the entangled interconnection structure to node diversity and evolution of network structure. With this in mind, we can summarize the three fundamental aspects of a complex network in terms of: *dynamics, structure of interconnections, evolution process.*

In this chapter we will review the key fundamental concepts in the theory of complex networks. Specifically, after recalling the main features of networks in terms of structure and dynamics, we will focus on networks whose interconnection structure is time-varying, i.e. evolving complex networks.

2.1 Networks: Dynamics and structure

2.1.1 Dynamics and Coupling

We start by considering a general network, in which every node is connected to some neighbors (see Section 2.1.2). Furthermore we take into account the most general case, by placing at each node a different dynamical system with its own vector field. As we will see in Chapter 5, heterogeneity of nodes' dynamics can be fundamental in determining network functionalities.
The dynamics of each node can be written as

$$\dot{\mathbf{x}}_i = \mathbf{f}_i(\mathbf{x}_i) + c \sum_{j \in \mathcal{N}_i} \mathbf{g}_i(\mathbf{x}_i, \mathbf{x}_j) \qquad i = 1, \ldots, N \tag{2-1}$$

where

- $N \in \mathbb{R}$ is the number of nodes
- $\mathbf{x}_i \in \mathbb{R}^n$ is the n-dimensional state vector of i-th agent.
- $\mathbf{f}_i \in \mathbb{R}^n$ represents the dynamics of node i.
- $\mathcal{N}_i$ is the set of neighbors of node i, e.g. nodes j that are connected to node i (see Section 2.1.2 for more details).
- $\mathbf{g}_i(\mathbf{x}_i, \mathbf{x}_j) \in \mathbb{R}^n$ is called the coupling function. It describes how node i treats information coming from node j. Namely, dynamics of node i is affected by all of states $\mathbf{x}_j : \ j \in \mathcal{N}_i$, according to $\mathbf{g}_i$.
- $c \in \mathbb{R}$ is the coupling strength since it provides a measure of the coupling force between two or more nodes. It can vary in time and it can be different for each pair of connected nodes, that is $c = c_{ij}(t)$.

If we suppose that each node is an oscillator (i.e. the system has a stable limit cycle [81]) or a chaotic oscillator (i.e. the system shows a non-periodic behaviour coming from motion over a strange attractor [82]), an interesting phenomenon could emerge. It has been shown (see [84] and references therein) that in this case the network can synchronize, that is all the oscillators settle over the same spatio-temporal orbit. We will discuss in depth about synchronization, in Section 2.2.

Another possible type of collective behaviour is called *swarming*. The main examples come from nature, like migration of birds in some direction (specifically named *flocking*), or swarm behaviour in fish (also known as *schooling*). It is easy to imagine the usefulness of understanding the emergence of this behaviours if one has to carry out the control of a collection of mobile robots, or in the control of unmanned air vehicles, or the handling of a distributed sensors network.
As we have seen above, another crucial ingredient in the model of complex networked systems is the law through which agents can communicate with each other. If we consider diffusive coupling [88], (2-1) becomes

$$\dot{\mathbf{x}}_i = \mathbf{f}_i(\mathbf{x}_i) + c \sum_{j \in \mathcal{N}_i} (\mathbf{x}_j - \mathbf{x}_i) \qquad i = 1, \ldots, N \tag{2-2}$$

Linear diffusive coupling is only one of the many possible communication protocols. It is surely suitable to all those cases where the interaction is a smooth process, like in the case of laser arrays where coupling could be performed through the overlapping of each laser electric field [84].

2.1.2 Network structure

The structure of a network is usually modelled by means of graphs. Generally speaking, a graph is a set of elements (nodes or vertex), connected to each other by edges. More precisely, an undirected graph $\mathcal{G}$ is defined by the couple $(\mathcal{V}, \mathcal{E})$, where $\mathcal{V} = 1, \ldots, N$ is the set of nodes and $\mathcal{E} \subset \mathcal{V} \times \mathcal{V}$ is the set of edges. Clearly if nodes i and j are connected to each other, then $(i, j) \in \mathcal{E}$; further, they are called *neighbors* and this relation is expressed by $i \sim j$. The set of all neighbors of the node i is $\mathcal{N}_i = \{j \in \mathcal{V} : j \sim i\}$; the *degree* of a node is the number of its neighbors. In a *direct graph*, instead, the edges are oriented from a starting vertex (*head*) to an ending one (*tail*), so the neighborhood relationship is not symmetric and we can define an *in-degree* (number of edges for which the actual node is the tail) and an *out-degree* for each node (number of edges for which the actual node is the head). A *path* $i_0, i_1, \ldots, i_L$ is a finite sequence of nodes such that $i_{k-1} \sim i_k, k = 1, \ldots, L$; an undirected graph is said to be *connected* if there exists a path between any pair of distinct nodes.
The *adjacency matrix* $\mathbf{A} \in \mathbb{R}^{N \times N}$ of the graph $\mathcal{G}$ is defined as

$$A_{ij} = \begin{cases} 1 & \text{if } (i, j) \in \mathcal{E}, \\ 0 & \text{otherwise.} \end{cases}$$

Furthermore, if $\mathcal{G}$ has M edges, we can define the node-edge *incidence matrix* $\mathbf{B} \in \mathbb{R}^{N\times M}$ as

$$B_{ij}\begin{cases}1 & \text{if node } i \text{ is the head of the edge } j,\\ -1 & \text{if node } i \text{ is the tail of the edge } j,\\ 0 & \text{otherwise.}\end{cases}$$

Finally, a matrix that play a central role in complex network modelling and analysis is the *Laplacian matrix* defined by

$$\mathbf{L} := \mathbf{B}\mathbf{B}^T$$

For an undirected graph the *Laplacian* is a symmetric matrix with zero row sum; it is also positive semidefinite and its spectrum can be ordered as follows

$$0 = \lambda_1(\mathbf{L}) \leq \lambda_2(\mathbf{L}) \leq \cdots \leq \lambda_N(\mathbf{L})$$

The multiplicity of the zero eigenvalue is equal to the number of the connected components of the graph. It is useful observing, that denoting by $\mathbf{D} \in \mathbb{R}^{N\times N}$ the matrix $\mathbf{D} = \text{diag}(d_i)$, $i = 1, \ldots, N$ where d_i is the degree of node i, we have

$$\mathbf{L} = \mathbf{D} - \mathbf{A}$$

The relationship above, allows us to rewrite Equation (2-2) as follows

$$\dot{\mathbf{x}}_i = \mathbf{f}_i(\mathbf{x}_i) - c\sum_{j=1}^{N} L_{ij}\mathbf{x}_j \qquad i = 1, 2, \ldots, N \tag{2-3}$$

Now, with the aim of finding some characteristics that could allow to analyze a real networks, it is useful to briefly review some crucial observables of complex networks:

Average path length It is simply the distance L (in terms of number of edges along the path) between any two nodes, averaged over all pair of distinct nodes;

Diameter It represents the maximum distance between any pair of nodes;

Clustering coefficient It reflects a property of the network also known as transitivity and relies on the fact that, if node i and node j are both neighbors of a node k, there might be an higher or lower probability that there is an edge also between i and j. Rigorously, the *clustering coefficient* is the average fraction of neighbors of a node, that are also neighbors of each other. Then, indicating with k_i the degree of node i, we can immediately recover the clustering coefficient of the actual node, as: $C_i = \frac{2E_i}{k_i k_i - 1}$ where E_i is the effective number of neighbors that are neighbors among themselves. The clustering coefficient C is defined as the average of C_i over all nodes;

Degree distribution This quantity is encoded by the function $P(k)$ that provides the probability that a randomly chosen node of the network, has a degree equal to k. It is worth recalling at this stage, the notion of average degree, that is simply the average of the nodes degree k_i over all i and is denoted as $\langle k \rangle$. This parameter helps us, among others, to highlight the homogeneous degree of the network. If $P(k)$ is a Gaussian bell shaped function, for example, then we can expect that nodes will have comparable degree values;

Assortative mixing A network is said to show assortative mixing if the nodes in the network that have many connections tend to be connected to other nodes with many connections. Moreover connections in many technological and biological networks attach vertices of very different degree with stronger likelihood. This case is referred to as disassortative mixing. A measure of assortativity is usually given by the Pearson correlation coefficient of the degrees at either ends of an edge and lies in the range $[-1, 1]$.

2.1.2.1 Network Models

The main interesting aspect of the network structure, is that of finding how to place edges and nodes so that the whole network has specific proprieties, in terms, for example of the previous measures. The output of this task is the generation of *network models*.
The simplest models are the so-called *regular coupled networks* [88, 51]. To this category, belong *all-to-all networks*, in which any node is connected to all the other $N-1$; it is simple to see that it has $L = C = 1$. Another regular network is the *K-nearest-neighbor lattice*, where each node is connected to his K-nearest neighbors ($K/2$ to each side, with $K > 1$ even). For this network we have $C \sim \frac{3(K-2)}{4(K-1)} \sim \frac{3}{4}$ and $L \sim \frac{N}{2K}$; note that $L \to \infty$ as N grows, that is $N \to \infty$. Like the all-to-all configuration, this network is perfectly homogeneous, with all nodes sharing the same degree ($N-1$ for the all-to-all, K for the K-nearest neighbors). Finally, there is the *star coupled network* in which a main node is connected to all other $N-1$ nodes, just like the center of a star. This kind of network encodes *two characteristics of many real-networks, like small avarage path length ($L \to 2$ as $N \to \infty$) and high clustering ($C \to 1$ as $N \to \infty$).*
A very different type of networks from regular networks are *Random Networks*, studies of which are dated about *'60s* when *Erdös* and *Renyi* formalized this concept. The idea is very simple: start with N isolated nodes and then choosing at random two of them (distinct),

connect those vertex with probability p. The interesting result is that, in this way, we obtain $L \sim \frac{ln(N)}{ln(<k>)}$, where $< k >$ is the average degree; so L increases "slowly" when N grows ($\lim_{N\to\infty} \frac{ln(N)}{N} = 0$). This is a property of many real networks, although the clustering coefficient of a random network is typically too small ($C = p = \frac{<k>}{N} \ll 1$) compared to that of real networks.

To overcome the limitations of random graphs we have just mentioned, Watts and Strogatz engineered a better model that they named *Small World Network* [89]. Starting from a regular K-nearest neighbors lattice, they introduced randomness with the task of rewiring with a specified probability p, each edge of the initial network, connecting one end of the edge, to another one chosen at random. This process introduces $pNK/2$ long range connections, that allow (with increasing p) to obtain: *(i)* Small average path length; *(ii)* High clustering. That is, starting from a regular network ($p = 0$), before obtaining completely random network ($p = 1$), there is a threshold ($p = \bar{p} \in]0, 1[$) above which the network can embed the advatages of regular and random networks. The name *small-world* is a consequence of the long-range connection effect: indeed in this way it is possible to have edges between two nodes that are at the opposite side of the network (like in a friendship network where a person A would likely know other people that are not confined to those who live "near" A).

Although small-world networks incorporate two main aspects of large-scale real networks, they have still an unrealistic *Degree distribution*. In fact Watts and Strogatz model is characterized by a $P(k)$ very similar to a normal distribution, that roughly means all nodes have a degree around a mean value. In real networks this almost never happens. What we expect, indeed, is the presence of "few" nodes (currently named *hubs*) with huge degree and the rest of vertices with a "small" degree. This leads to a degree distribution $P(k) \sim k^{-\gamma}$, that is a *power-law degree distribution*.

Albert and *Barabási* proposed in [6] a model named *Scale-free network* to obtain this degree distribution.

1. Start with $m_0 < N$ nodes connected to each other as you want;
2. Add a new node to the network and connect it to $m \leq m_0$ existing nodes i, with a probability:
$$\Pi_i = \frac{k_i}{\sum_j k_j}$$
3. Repeat 2 till $N - m_0$ nodes have been added.

The resulting network will have N nodes and $m(N-m_0)+l_0$ edges (with l_0 being the initial number of edges),but most of all it will be characterized by a power law degree distribution:

$$P(k) \sim 2m^{\frac{1}{\beta}}k^{-\gamma}, \qquad \text{with} \quad \gamma = \frac{1}{\beta} + 1 = 3$$

It has also been seen [88] that scale free networks have a smaller average path length and higher clustering coefficient, compared with random graphs of the same size and average degree.

2.2 Synchronization

Let us consider a network of coupled identical oscillators modelled by

$$\dot{\mathbf{x}}_i = \mathbf{f}(\mathbf{x}_i) - c\sum_{j=1}^{N} L_{ij}\mathbf{h}(\mathbf{x}_j) \qquad i = 1, 2, \ldots, N \tag{2-4}$$

where $\mathbf{h}$ is a generic output function. One of the most interesting and well studied form of collective behavior is synchronization. Indeed in a network such as that in Equation (2-4), it can happen that each subsystem behaves in the same fashion, that is all nodes follow the same spatiotemporal evolution. This phenomenon is common in science and a milestone in this issue was the work of the Dutch scientist Christiaan Huygens [8]. For his experiments, he built a system of two pendulum clocks hooked on a wood support. The ends of the holder, were backed on two chairs. The more remarkable thing he saw, was the synchronization of the clocks. The synchrony motion was recovered also after an external perturbation. He sensed that this behaviour was due to the horizontal and imperceptible oscillations of the beam, that was the *coupling mean* between the two pendulum clocks. This phenomenon is the same that one can observe in cardiac pacemakers (where heart beats are paced by a sequence of pulses from electronic generator) or the circadian rhythms of an organism. Also, in neuroscience, it is sometimes desirable that a web of interconnected neurons, settles on a stable synchronized state.
Formally, we can define synchronization as follows

Definition 2.2.1 (Synchronization)**.** *Network (2-4) is said to achieve asymptotic syncronization if and only if:*

$$\mathbf{x}_1(t) = \mathbf{x}_2(t) = \cdots = \mathbf{x}_N(t), \qquad as \quad t \to \infty$$

That is all network trajectories converge towards the synchronization manifold

$$\mathcal{S} := \left\{ [\mathbf{x}_1^T, \ldots, \mathbf{x}_N^T] \in \mathbb{R}^{nN} \ : \ \mathbf{x}_1 = \cdots = \mathbf{x}_N \right\} \tag{2-5}$$

2.2.1 Master Stability Function

In this Section, the problem of studying the stability of a synchronous state is examined. There are approaches based on *Lyapunov theory* or others that relies on *Contraction Theory* (see Chapter 7 and references therein). The result we want to illustrate here, is that proposed by *Pecora* and *Carroll* in [56], better known as the *Master Stability Function* method. Since we want to study behaviour of (2-4) near a syncronized state, say $\mathbf{x}_s(t)$, we can linearize the system about $\mathbf{x}_s(t)$. This leads to:

$$\dot{\xi}_i = \mathbf{J_f}(\mathbf{x}_s)\xi_i + c\sum_{j=1}^{N} L_{ij}\mathbf{J_h}(\mathbf{x}_s)\xi_j \qquad i = 1, \ldots, N \tag{2-6}$$

where

- $\mathbf{J_f}(\mathbf{x}_s) \in \mathbb{R}^{n\times n}$ and $\mathbf{J_h}(\mathbf{x}_s) \in \mathbb{R}^{n\times n}$ are respectively the *Jacobian Matrices* of $\mathbf{f}(\mathbf{x}_i)$ and $\mathbf{h}(\mathbf{x}_i)$ with respect to $\mathbf{x}$ and evaluated at $\mathbf{x}_i = \mathbf{x}_s$;
- $\xi_i = [\mathbf{x}_i(t) - \mathbf{x}_s(t)]^T$ is the vector of the variations about $\mathbf{x}_s(t)$ of each state vector $\mathbf{x}_i(t)$.

Now, supposing $\mathbf{L}$ to be diagonalizable, we can also block diagonalize (2-6), obtaining the following relationship:

$$\dot{\zeta}_k = [\mathbf{J_f}(\mathbf{x}_s) + c\lambda_k\mathbf{J_h}(\mathbf{x}_s)]\zeta_k \qquad k = 1, \ldots, N \tag{2-7}$$

We have obtained a decoupled system that locally describes the behaviour of (2-6) over N transverse directions. In [56] authors refer to the dynamics along each of the N-1 the directions (excluding the one corrresponding to the trivial eigenvalue) as *transverse modes*, and they observe that $\lambda_0 = 0$ is associated to the synchronization manifold $\mathbf{x_1} = \mathbf{x_2} = \cdots = \mathbf{x_N}$. So it is clear that the synchronization state $\mathbf{x_s}(t)$ will be stable if all other transverse modes are stable. A possible criterion to prove that, is by imposing a negative Maximum Lyapunov Exponent for all modes. This yelds the definition of the *Master Stability Function Equation* as:

$$\dot{\zeta}_k = [\mathbf{J_f}(\mathbf{x}) + (\alpha + j\beta)\mathbf{J_h}(\mathbf{x})]\zeta_k \qquad k = 1, \ldots, N \tag{2-8}$$

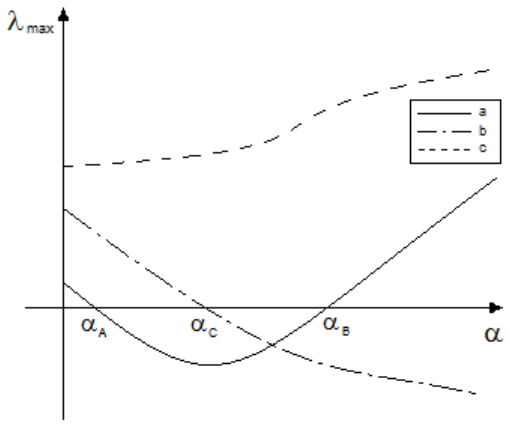

Figure **2-1**: Different MSF shapes

To evaluate the *Master Stability Function*, is then necessary to calculate the Maximum Lyapunov exponent for the generic equation (2-8), obtaining a $\lambda_{max}(\alpha + j\beta)$. Finally if we want to stabilize a synchronous state, we have simply to chose some c in (2-6) for which $\lambda_{max}(c\lambda_k) < 0 \quad \forall\, 2 \leq k \leq N$.

At this stage we can provide a measure of *Synchronizability* in terms of the values of c for which we can stabilize all transverse modes (we group this values in the set $\mathcal{C}$). So it is clearly that the larger is $\mathcal{C}$, the greater is network synchronizability.

If we consider the case of real eigenvalues for the Laplacian matrix $\mathbf{L}$(i.e. the Laplacian Matrix is symmetric and thus the underlying network is bidirectional), we can expect that the MSF could assume three different shapes depending on f and h functions as shown in Figure **2-1**. Type (c) simply represent a case in which the synchronization state can never be stabilized, no matter the value of the coupling strength c; the (b) type, indeed, is characterized by a certain threshold, α_C in the picture, after which λ_{max} becomes negative, that implies a stable behaviour of the synchronized state. In this case we have simply to choose c, such that $\lambda_2(\mathbf{L})c > \alpha_C$. Finally case (a) requires conditions on both smallest and largest eigenvalues of $\mathbf{L}$. In fact, we have two thresholds, say α_A and α_B, that identify an interval where negative values of MSF are obtained. To garantee synchronization, is then necessary to choose c in such a way that $\lambda_2(\mathbf{L})c > \alpha_A$ and $\lambda_N(\mathbf{L})c < \alpha_B$. These conditions suggest that, in general, to enlarge the set $\mathcal{C}$ above, one has to maximize: the eigenratio $1/R = \frac{\lambda_N(\mathbf{L})}{\lambda_2(\mathbf{L})}$ in case c, and the smallest eigenvalue $\lambda_2(\mathbf{L})$ if $\mathbf{f}$ and $\mathbf{h}$ yield an MSF of type (b).

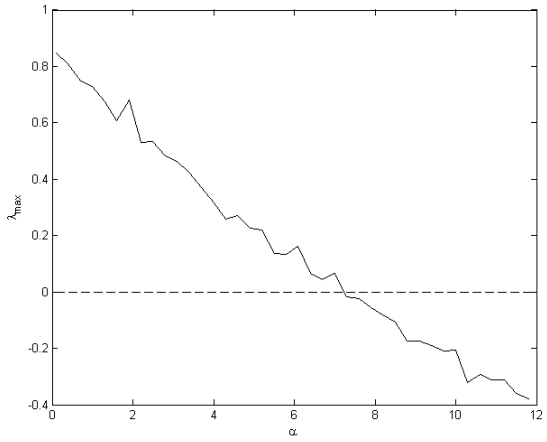

Figure **2-2**: MSF for a Scale-free network of N=200 Lorenz systems.

To provide a concrete example of MSF, we have considered a Scale-free network of $N = 200$ *Lorenz* systems coupled through the first state variable:

$$\begin{aligned} \dot{x}_i^{(1)} &= 10(x_i{}^{(2)} - x_i{}^{(1)} - c\sum_{j=1}^{N} L_{ij} x_j{}^{(1)} \\ \dot{x}_i^{(2)} &= 28x_i{}^{(1)} - x_i{}^{(1)} x_i{}^{(3)} - x_i{}^{(2)} \qquad\qquad i = 1, \ldots, N \\ \dot{x}_i^{(3)} &= x_i{}^{(1)} x_i{}^{(2)} - 8/3 x_i{}^{(3)} \end{aligned} \tag{2-9}$$

where the superscripts indicate the component of the state vector. As we can see in Figure **2-2**, for the networked system (2-9) we obtain a MSF that looks like b-type in Figure **2-1**. In this case the set of coupling gains for which the syncronization state is stable, is $\mathcal{C} = [c_0, \infty)$, with c_0 such that $\lambda_{max}(c_0\lambda_2(\mathbf{L})) < 0$. Thus it is clear that, with this kind of MSF, only λ_2 plays a role in determining the stability of the synchronization manifold.

2.3 Consensus

In the framework of multi-agent systems a relevant issue is the so-called *Consensus Problem*. Indeed, when a set of units need to cooperate, it is meaningful that they are able to agree upon some shared variable, also when all-to-all communications are not allowed. Let us associate, without loss of generality, a scalar variable x_i to the agent i, and suppose that they are able to exchange their state variable to each neighbour in a network of N nodes, encoded by the *undirected graph* $\mathcal{G} = (\mathcal{V}, \mathcal{E})$. We say that node i and j *agree*, if $x_i = x_j$, while they

are said to disagree if $x_i \neq x_j$. Furthermore we have to distinguish between unconstrained and constrained consensus problems. An **unconstrained consensus problem** is simply the alignment or agreement problem in which it suffices that the state of all agents asymptotically be the same. In the **constrained problem**, instead, agents have to carry out the distributed computation of a particular function $\chi(\mathbf{x}) : \mathbb{R}^N \to \mathbb{R}$, where $\mathbf{x} \in \mathbb{R}^N$ is the vector collecting all the agents' states. Solving the constrained consensus problem is a cooperative task and requires participation of all the agents. Indeed, simply suppose a single agent decides not to cooperate with the rest of the agents and keep its state unchanged [52]. Then, the overall task cannot be performed despite the fact that the rest of the agents reach an agreement. For instance, the most considered constrained consensus problem is the so-called *average-consensus*, that is $\chi(\mathbf{x}) = Ave(\mathbf{x}) = \frac{1}{N}\sum_{i=1}^{N} x_i$.
Now let the agents' dynamics be given by the following differential equations:

$$\begin{aligned} &\dot{x}_i = u_i \\ &u_i = \sum_{j \in \mathcal{J}_i} (x_j - x_i) \quad x_i(0) = z_0 \qquad i = 1, \ldots, N \end{aligned} \tag{2-10}$$

The above dynamics reveals that each agent is a simple integrator and updates its variable because of the mismatch between its state and those of its neighbours. The system in (2-10) can be rewritten in a compact form, as:

$$\dot{\mathbf{x}} = -\mathbf{L}\mathbf{x} \tag{2-11}$$

where $\mathbf{L}$ is the Laplacian matrix of the graph $\mathcal{G}$. The linear protocol (2-10), under the assumption that the graph $\mathcal{G}$ is connected, ensures that agents reach globally asymptotically an average-consensus as shown in [52].
Moreover in the case of a directed graph $\mathcal{G}$, it is possible to show that protocol (2-10) ensures, if the digraph contains at least a spanning tree [1], that consensus is achieved. In particular one has $x_i(t) \to \sum_{i=1}^{N} \nu_i x_i(0)$ as $t \to \infty$, where $\nu_i \geq 0$ and $\mathbf{1}_N{}^T \nu = 1, \mathbf{L}^T \nu = 0$. Moreover, in [52] is pointed out that if the digraph $\mathcal{G}$ is strongly connected and balanced, then protocol in Equation (2-10) allows to reach an *average-consensus*.
In the field of multi-vehicles, and more generally, roving systems sometimes it is possible to model the kinematic equation of each planar agent, as a double integrator. This is the

[1] A digraph contains a spanning tree if there is a node (root), s.t. there exist directed paths starting from the root and reaching each node in the digraph. Moreover, it is balanced if for each node the in-degree is equal to the out-degree and finally it is said to be is strongly connected if there exists a directed path between every pair of nodes in the same graph

case of holonomic vehicles, for which all motion directions are unconstrained and from each point the agent is capable to move to all possible directions. Since this is true, the motion equation can be also decoupled along each axis of the motion (for example x and y in the plane). We argue here that also if agents are non-holonomic, and then their kinematic equations are non-linear, through a feedback linearization procedure one can obtain a double integrator dynamics. So it is useful to analyze the following linear consensus protocol for double integrators dynamics:

$$\begin{aligned} \dot{\mathbf{p}}_i &= \mathbf{v}_i \\ \dot{\mathbf{v}}_i &= \mathbf{u}_i \qquad i = 1, \ldots, N \\ \mathbf{u}_i &= -\sum_{j=1}^{N} a_{ij}[(p_j - p_i) + \gamma(v_i - v_j)] \end{aligned} \tag{2-12}$$

where a_{ij} are the elements of the Adjacency Matrix. In [63] it is demonstrated that if the graph $\mathcal{G}$ is undirected and connected, then system (2-12) reaches asymptotically a consensus, for any $\gamma > 0$. In the case of directed graphs, instead, having a spanning tree only a necessary condition is needed to achieve consensus, i.e. if system (2-12) reaches consensus, then the underlying digraph $\mathcal{G}$ has a spanning tree. A necessary and sufficient condition, indeed, is given in term of the spectral properties of the following matrix

$$\Theta = \begin{bmatrix} 0_{N\times N} & I_N \\ -\mathbf{L} & -\gamma\mathbf{L} \end{bmatrix}$$

In particular, (2-12) achieves consensus asymptotically if and only if Θ has exactly two zero eigenvalues and all other eigenvalues have negative real parts. Specifically $p_i \to \sum_{i=1}^{N} g_i p_i(0) + t\sum_{i=1}^{N} g_i v_i(0)$ and $v_i \to \sum_{i=1}^{N} g_i v_i(0)$ as $t \to \infty$, where $g_i \geq 0, \mathbf{1}_N{}^T\mathbf{g} = 1$ and $\mathbf{Lg} = \mathbf{0}$.
In the literature many other protocols for reaching consensus are provided, also in the case of additive noise or disturbances on the dynamics, delays and non-ideal links. Finally some efforts are made also to cover the case in which the dynamics of each agent is not a simple or double integrator, but a generic nonlinear function [68], [95].

2.4 The third ingredient: Evolution

So far, we analysed two of three main features of networks, e.g. dynamics and structure. In this Section we will discuss what happens if we allow the network structure to evolve. Indeed, in many applications the network topology evolves according to the agents' dynamics

[49, 12, 29, 96]. For example, in networks of mobile robots [96] each node is equipped with wireless communication devices and can sense only the nodes in its proximity. Clearly, the communication topology changes with the nodes' dynamics, and controlling its evolution can be crucial to control the motion of the mobile agents. For example, in [91], a control algorithm is presented that allows a network of mobile agents to achieve a desired goal in the presence of structural constraints via the controlled activation/deletion of some of its edges. Other examples include road networks, power grids, neural or genetic networks (see [34] and references therein).

Thus, static network models lack these fundamental characteristics that are displayed by many complex systems. The recent efforts are among the few to consider time-dependent couplings. Nonetheless, the central feature of evolving networks is, basically, a feedback action between nodes' state and network structure. Indeed, while links evolution affects nodes' dynamics, the state of each agent is responsible for updating network structure. To formally describe this feature, *adaptive networks* and *evolving dynamical networks* have been proposed as more realistic models of complex systems [34, 32]. There are several formalisms introduced to describe the co-evolution of network structure and dynamics. One of the first attempts is represented by *Dynamic Graphs* introduced in [78]. The idea is to define dynamical equations to describe how the weight of each edge in the network changes over time. As these weights vary the network structure also varies with the most extreme cases being the addition of an edge as a very weak weight becomes strengthened, and the loss of an edge as a weight tends toward zero. Although dynamic graphs provide access to many existing theoretical results, one major limitation remains. Dynamics are defined over a fixed size network, prohibiting the description of evolutionary processes that involve growth. To this aim, in [32] a definition of Evolving Dynamical Network (EDN) is provided. The definition is given in two steps. First the notion of a dynamic graph is generalized, creating a structure to describe both network topology and dynamics. This structure is then used to define an EDN, allowing for changes to the underlying topology and dynamics to take place. Authors in [32] consider a directed graph $\mathcal{G} = (\mathcal{V}, \mathcal{E})$ where $\mathcal{V} = \{v_1, v_2, \ldots, v_n\}$ is the set of nodes and $\mathcal{E} = \{e_1, e_2, \ldots, e_n\}$ with $e_i \in \mathcal{V} \times \mathcal{V}$ is a set of directed edges. Now, a state is associated to each node and edge so as to enable dynamics to take place on the fixed graph $\mathcal{G}$. The current state of node $v_i \in \mathcal{V}$ and edge $e_i \in \mathcal{E}$ will be given by $\mathbf{v}_i \in \mathbf{V}_i$ and $\mathbf{e}_i \in \mathbf{E}_i$, respectively, with $\mathbf{V}_i$ and $\mathbf{E}_i$ being the sets of admissible state values. Thus a Generalized Dynamic Graph (GDG) can be defined as

Definition 2.4.1 (Generalized Dynamic Graph [32]). *A generalized dynamic graph for a fixed network structure $\mathcal{G} = (\mathcal{V}, \mathcal{E})$ is a collection $(\mathcal{V}, \mathcal{E}, \mathbf{V}, \mathbf{E}, \mathbf{U}, \mathbf{T}, \Phi)$ where*

- $\mathcal{V} = \{v_1, v_2, \ldots, v_n\}$ *is the set of nodes.*
- $\mathcal{E} = \{e_1, e_2, \ldots, e_n\}$ *with $e_i \in \mathcal{V} \times \mathcal{V}$ is a set of directed admissible edges.*
- $\mathbf{V} = \mathbf{V}_1 \times \mathbf{V}_2 \times \cdots \times \mathbf{V}_n$ *represents node state space, with $\mathbf{V}_i$ being the sets of admissible state values for node v_i.*
- $\mathbf{E} = \mathbf{E}_1 \times \mathbf{E}_2 \times \cdots \times \mathbf{E}_n$ *represents node state space, with $\mathbf{E}_i$ being the sets of admissible state values for edge e_i.*
- $\mathbf{U} = \mathbf{U}_1 \times \mathbf{U}_2 \times \cdots \times \mathbf{U}_p$ *is a set of control inputs.*
- $\mathbf{T}$ *is the set of times.*
- $\Phi : \mathbf{V} \times \mathbf{E} \times \mathbf{U} \times \mathbf{T} \to \mathbf{V} \times \mathbf{E}$ *represents some dynamics mapping for the states.*

Mapping Φ in Definition 2.4.1 is very general, including deterministic and probabilistic operators. For instance, it could be given by a difference equations as

$$\mathbf{v}_i(t+1) = f_i[\mathbf{v}_i(t), \{\mathbf{v}_j(t) : v_j \in \mathcal{N}_i\}, \{\mathbf{e}_j(t) : e_j = (v_k, v_i)\}, \mathbf{u}(t)] \quad \forall j, k$$
$$\mathbf{e}_i(t+1) = g_i[\mathbf{e}_i(t), \{\mathbf{v}_j(t) : (v_j, v_k) = e_i \vee (v_k, v_j) = e_i\}, \mathbf{u}(t)] \quad \forall j, k$$

where f_i is a function of the current node, the state of any incoming edge and the state of any adjacent node, while g_i is a function of current edge and the state of any connected node. Moreover, $\mathcal{N}_i$ is the set of neighbors of node i and $\mathbf{u}(t)$ is a control input.
An important feature of GDG is that the mapping Φ can drive states $\mathbf{v}_i$ and $\mathbf{e}_i$ toward zero, thus removing them from the network structure. Although GDG allows to capture many features of evolving networks, they still consider a fixed underlying structure $\mathcal{G} = (\mathcal{V}, \mathcal{E})$ and given mapping Φ. To allow for the exploration of alternatives, authors in [32] consider the set of all possible GDGs, $\mathcal{D}$, and define

Definition 2.4.2 (Evolving Dynamical Network [32]). *An Evolving Dynamical Network (EDN) is a collection $(\mathcal{D}, \Omega, I, \tau)$ where*

- $\mathcal{D}$ *is the set of GDGs.*

- $\Omega = \{\omega_1, \omega_2, \dots\}$ *is a set of structural operators such that* $\omega_i \in \Omega$ *is a mapping* $\omega : \mathcal{D} \to \mathcal{P}$ *where* $\mathcal{P}$ *is a probability distribution over the set* $\mathcal{D}$.
- I *is a set of inputs from the environment or to be used for control purposes.*
- $\tau : I \times \mathcal{D} \to \Omega$ *is the evolutionary plan determining the operator* $\omega_i \in \Omega$ *to be applied when transitioning from one structure to the next.*

In other words, set $\mathcal{D}$ represents all possible GDGs. Of those reached by the evolutionary process, say $\mathcal{D}_1, \mathcal{D}_2, \mathcal{D}_3, \dots \in \mathcal{D}$, each consists of a state space over which network dynamics can take place in accordance with the associated dynamical mappings, that is Φ. Evolution of the network structure, state space, and dynamics mapping occurs through the evolutionary mapping τ, that enables the network to grow.
In what follows, we recall a fundamental strategy for the evolution of complex networks, namely *edge snapping* and a useful software framework to simulate evolving networks called *NetEvo* . Indeed, the first part of the thesis deals with extensions to edge snapping mechanism so as to achieve general types of consensus. It will be also used in an evolutionary manner, as illustrated in Chapter 5.

2.4.1 Edge Snapping

Edge Snapping [20] is an adaptive strategy that induces an unweighted self-emerging network structure, by adapting the coupling gains. Specifically, the gains dynamics are given by

$$\ddot{k}_{ij} + d\dot{k}_{ij} + \frac{\partial}{\partial k_{ij}} V(k_{ij}) = g(e_{ij}) \tag{2-13}$$

where $k_{ij} \in \mathbb{R}$ is the coupling gain associated to edge (i, j) and d is the damping. Moreover, with reference to Equation (2-13), a bistable polynomial potential was selected

$$V(s_{ij}) = bk_{ij}^2(k_{ij} - 1)^2. \tag{2-14}$$

This smooth bistable potential has two local minima corresponding to the desired equilibria of the system: $k_{ij} = 0$ (non-active edge) and $k_{ij} = 1$ (active edge), while the parameter b represents the height of the barrier between the two equilibria. With this choice of V, system (2-13) can be viewed as a Duffing-Holmes oscillator, firstly introduced in [37] to model a buckled beam undergoing forced lateral vibrations. When considering edge snapping, the forcing is not periodic as in [37], but it is bounded. The driving function was selected as

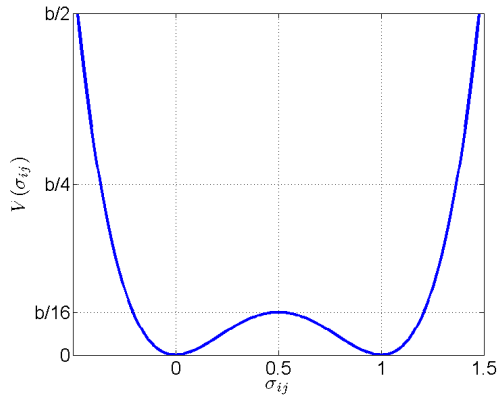

Figure **2-3**: Undirected edge snapping. Bistable potential (2-14) driving the evolution of each k_{ij}.

$g(e_i - e_j) = \mathcal{G}(|e_i - e_j|)$, with $\mathcal{G}$ chosen from the set of strictly increasing functions of *class* k_∞ [2].

Now, consider a network of integrators

$$\dot{x}_i = \sum_{\substack{j=1 \\ j \neq i}}^{N} k_{ij}^2 (x_j - x_i) \tag{2-15}$$

where the k_{ij}^2 is considered so that the coupling gains are positive for all $t \geq 0$. In this way, none of the possible emerging topologies is unstable, as shown in [58]. Also, the network of integrators asymptotically reaches average consensus, that is,

$$\lim_{t \to \infty} (\chi_{\text{ave}}(x(0)) - x_i(t)) = 0,$$

for all $i = 1, \ldots, N$ [20]. Moreover, almost all solutions of (2-13) converge towards $\sigma_{ij} = 0/1$. Specifically, if we exclude the trivial case in which $s_{ij}(0) = \frac{1}{2}, \forall (i,j)$ and $e(0) = 0$, the network evolves to a final topology, whose structure depends on the initial conditions, the damping d, and the parameter b.

To illustrate the effectiveness of the approach, we report the results of a numerical simulation. Namely, we consider a network of $N = 50$ integrators, and we select the damping d equal to 5. The nodes' initial conditions are selected from a normal distribution with zero mean and standard deviation equal to 15, while all the $k_{ij}(0)$ are set to 0, so that at the onset of the

[2] A function $F : I \to \mathbb{R}$ is positive definite if $F(x) > 0, \forall x \in I, x \neq 0$ and $F(0) = 0$. A function $f : \mathbb{R}_{\geq 0} \to \mathbb{R}_{\geq 0}$ is of *class* k if it is continuous, positive definite and strictly increasing. A unbounded function of *class* k belongs to *class* k_∞.

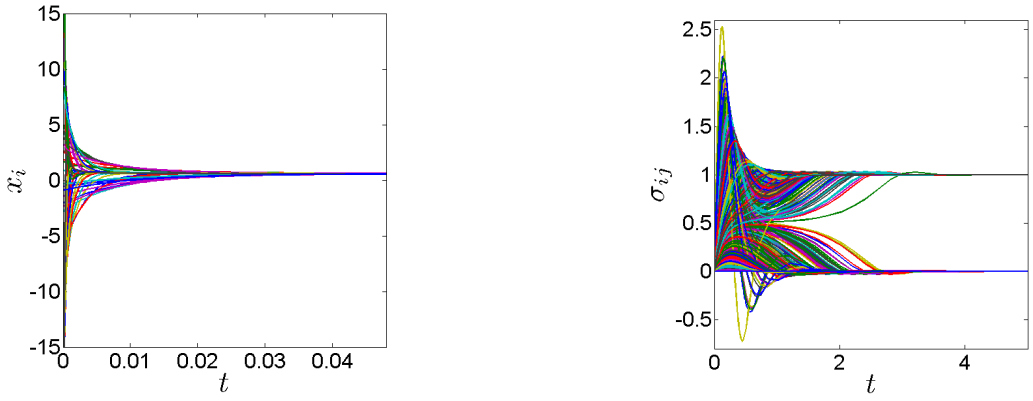

(a) (b)

Figure **2-4**: Network of $N = 50$ integrators: (a) Evolution of the agent dynamics under the undirected edge-snapping strategy; (b) Evolution of the coupling gains.

evolution the network is completely disconnected. The height of the barrier b is chosen equal to 15. As shown in Figure **2-4**a, the average consensus problem is asymptotically solved by the classical edge snapping mechanism, and all nodes converge to $\chi_{\text{ave}} = 0.59$. In addition, all coupling gains asymptotically converge to 0 or 1, see Figure **2-4**b.

2.4.2 NetEvo

NetEvo is a computational framework designed to help understand the evolution of dynamical complex networks [33]. It provides flexible tools for the simulation of dynamical processes on networks and methods for the evolution of underlying topological structures. To bring together simulation and evolution in a coherent way, the framework uses the idea of a supervisor, illustrated in Figure **2-5**. Evolution of the system is performed by the supervisor which can be viewed as a form of optimiser. This takes as input an initial topology, simulated output from the system and user defined constraints, and aims to return an optimal or enhanced topology. Changes to the system are assessed by using a certain performance measure Q, with smaller values representing an improved performance. By default, NetEvo provides a supervisor that uses a Simulated Annealing meta-heuristic to search for near optimal configurations. This method has been shown to perform well for a wide range of problems with an unknown prior structure.

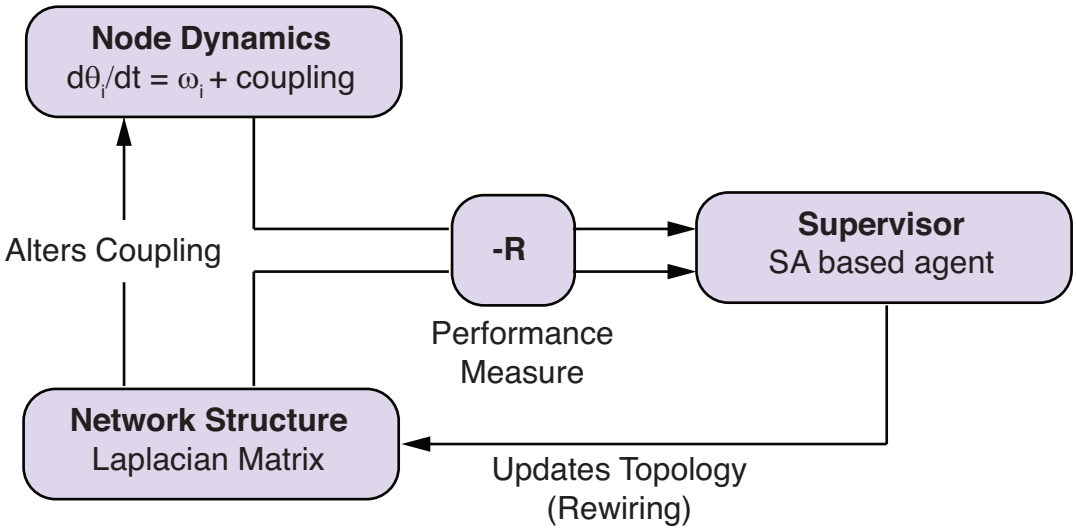

Figure **2-5**: Schematic illustration of how NetEvo works.

2.5 Summary

In this Chapter we reviewed the basic concepts of complex networks of dynamical agents. Starting from the dynamics of nodes and the structure of interconnections, we provided an overview on evolving networks that represent the main subject of this thesis, as we will see in Chapter 4 and Chapter 5. Next Chapter, instead, introduces the reader to networks of Kuramoto oscillators, namely coupled phase oscillator models. We anticipate that our work builds on edge snapping method. We will extend it to directed networks and general types of consensus. Moreover, we will develop a method in networks of heterogeneous Kuramoto oscillators that will allows us to find a link between the structure of the emerging networks and their functionalities, in terms, for instance, of network synchronization.

CHAPTER 3

The Kuramoto model

In Chapter 5 we will present a method, based on edge snapping, that will help us to link structure of emergent networks to their functionalities, i.e. their synchronization properties. We will focus on networks of phase oscillators and, specifically, we will use coupled Kuramoto oscillators. Thus, this Chapter deals with one of the most important paradigms for synchronization phenomena. Indeed, the Kuramoto model, yet very simple, is able to capture the main features of the onset of synchronization. This provides the easiest way to study large ensemble of oscillators interacting with each other. Preliminary studies date back to 75's, when Kuramoto began working on collective synchronization. His work rigorously formalizes Winfree's intuition to formulate the problem as the interaction of a huge population of limit-cycle oscillators.

3.1 The origins

The first attempts to analyse collective synchronization are due to Wiener [90], who firstly proposed a mathematical framework to study the onset of synchronization. His guess was that collective coordination mechanisms were involved in the generation of alpha rhythms in the brain, and those mechanisms are quite general and ubiquitous. They can be found also in other biological systems such as pacemaker cells in the heart or metabolic synchrony in yeast cell suspension. However, his formalism based on Fourier integrals, has turned out to be too much complicated, resulting in a dead point. A more fruitful approach was proposed by Winfree [92], later in 1967. In his seminal paper, Winfree proposed a formulation based on the interaction of a huge population of limit-cycle oscillators. As stated, the problem would

be intractable, but he argued simplification would arise if the coupling strength among oscillators is weak and the oscillators nearly identical. Under such assumptions, the whole dynamics can be separated into two timescales: a fast timescale in which oscillators run at their natural frequency and can be characterized solely by their phase, and a slow dynamics where agents interact with each other through the weak coupling and frequency differences. Thus, the model proposed by Winfree is

$$\dot{\theta}_i = \omega_i + \left(\sum_{j=1}^{N} X(\theta_j) \right) Z(\theta_i), \qquad i = 1, \ldots, N$$

where θ_i is the phase of oscillator i and ω_i its natural frequency. The evolution of oscillator i is affected by the phase of each other oscillator j, through $X(\theta_j)$. Moreover, the sensitivity function $Z(\theta_i)$, measures the response of node i to the influence of all other oscillators.
Based on numerical evidence, Winfree found spontaneous synchronization emerges as a threshold process, akin to a phase transition. Indeed, as the coupling among oscillators is increased, a transition is observed from an incoherent state, with all oscillators running at different frequencies, to a synchronized state. Despite the importance of his finding and the intuition about modelling the entire dynamics as a coupled phase oscillators system, the work of Winfree lacked a theoretical framework supporting the numerical evidence. Later, Kuramoto [41], starting from Winfree's results, proposed his model able to capture the onset of synchronization in a population of coupled phase oscillators.

3.2 The model

Kuramoto started his studies from the model

$$\theta_i = \omega_i + \frac{K}{N} \sum_{j=1}^{N} \Gamma_{ij}(\theta_j - \theta_i), \quad i = 1, \ldots, N \tag{3-1}$$

that describes the long term evolution of weakly coupled, nearly identical limit-cycle oscillators [42]. In Equation (3-1), θ is the phase of each oscillator and ω_i its natural frequency. Even tough Equation (3-1) represents a reduction of a more complex system, it is still difficult to analyse. Kuramoto recognised that simplifications would occur in the case of equally weighted, all-to-all, sinusoidal coupling of the form

$$\Gamma_{ij}(\theta_j - \theta_i) = \frac{K}{N} \sin(\theta_j - \theta_i) \tag{3-2}$$

The frequencies ω_i are distributed according to a probability density $g(\omega)$. For simplicity, in his model Kuramoto considered only unimodal and symmetric functions $g(\omega)$, about the mean value Ω. In particular, $g(\Omega + \omega) = g(\Omega - \omega)$ for all ω formalizes symmetry about the mean value. Another interesting property of the Kuramoto model is its rotational symmetry. Indeed, we can set the mean frequency $\Omega = 0$, by redefining $\theta_i \to \theta_i + \Omega t$ for all i, that corresponds to going into a rotating frame at frequency Ω. Thus the governing equations remains

$$\theta_i = \omega_i + \frac{K}{N} \sum_{j=1}^{N} \sin(\theta_j - \theta_i), \quad i = 1, \ldots, N \tag{3-3}$$

where ω_i are now the deviations from the mean Ω, obtained by subtracting Ω from the equation of each oscillator. Thus, thanks to the rotational symmetry in the model, the unimodal hypothesis translates in the fact that $g(\omega)$ is nowhere increasing in the interval $[0, +\infty)$, having set the mean value Ω to zero.
A network of Kuramoto oscillators can be seen as a swarm of points moving on a unitary circle in the complex plane. Moreover, the order parameter defined as

$$R(t)e^{i\phi(t)} = \frac{1}{N} \sum_{j=1}^{N} e^{i\theta_j(t)} \tag{3-4}$$

is a macroscopic quantity that can be interpreted as the collective rhythm produced by the whole population. It takes value in the interval $[0, 1]$, with $r \approx 1$ when the population acts as a giant oscillators and $r \approx 0$ if oscillators are scattered around the circle. Note that $r = 1$ if and only if all the oscillators share the same instantaneous phase $\theta_1(t) = \theta_2(t) = \ldots \theta_N(t)$. The quantity ϕ, instead, can be seen as the average phase. An interesting feature of the Kuramoto model is that Equation (3-3) can be rewritten in terms of the order parameter. Indeed, multiplying both sides of Equation (3-4) by $e^{-i\theta_i}$ yields

$$R(t)e^{i(\phi(t)-\theta_i(t))} = \frac{1}{N} \sum_{j=1}^{N} e^{i(\theta_j(t)-\theta_i(t))} \tag{3-5}$$

that corresponds to two equations, one for the real part and the other for the imaginary one. Equating the imaginary parts one obtains

$$R(t) \sin(\phi(t) - \theta(t) = \frac{1}{N} \sum_{j=1}^{N} \sin(\theta_j(t) - \theta_i(t)) \tag{3-6}$$

Substituting in Equation (3-3) yields

$$\dot{\theta}_i = \omega_i - \frac{KR(t)}{N} \sin(\phi - \theta_i), \quad i = 1, \ldots, N \tag{3-7}$$

Equation (3-7) clearly shows that each oscillator is interacting with each other via the macroscopic quantities R and ϕ. In particular the phase of i-th oscillators is pulled towards the average phase ϕ. Moreover, there is a positive feedback loop between coupling K and coherence R. Indeed, as the population becomes more coherent, R grows and so the effective coupling KR increases, which tends to recruit even more oscillators into the synchronized cluster. If the coherence is further increased by the new recruits, the process will continue; otherwise, it becomes self-limiting.

One of the characterization of the Kuramoto model is the curve $R - K$, that describes how the order parameter changes as the coupling strength is varied. Numerical simulations show that the order parameter remains close to zero until a certain threshold, say K_c, is crossed. Then for $K > K_c$ the order parameter grows exponentially, reflecting the formation of small clusters that merge, as K is increased, in a giant cluster, yielding $r \approx 1$.

Kuramoto analysis, assuming $N \to \infty$, predicts the behaviour presented so far. Kuramoto's exact formula for the critical coupling at the onset of collective synchronization is given by

$$K_c = \frac{2}{\pi g(0)}$$

3.3 Developments

Starting from the pioneering work by Kuramoto, and due to the increasing interest in Complex Networks, extensions to the Kuramoto model have been proposed in the literature, from those considering general type of interconnection to those where the coupling is time-varying. In this section we will highlight some of those developments that will be relevant for the rest of the thesis.

3.3.1 Critical coupling for the onset of synchronization

A first research direction on the Kuramoto model is concerned with finding necessary and/or sufficient conditions ensuring synchronization. These results come mainly from the Control Theory community and assume there is a finite number of oscillators. Before showing the

main results in that direction, it is worth defining some concepts about synchronization in a network of phase oscillators.
We start by recalling a weaker form of synchronization

Definition 3.3.1 (Frequency synchronization)**.** *The oscillators are said to achieve frequency synchronization if*

$$\lim_{t\to\infty} \left|\dot{\theta}_j(t) - \dot{\theta}_i(t)\right| = 0 \qquad \forall i, j = 1, \ldots, N$$

Then, we define phase synchronization as

Definition 3.3.2 (Phase synchronization)**.** *The oscillators are said to achieve phase synchronization if*

$$\lim_{t\to\infty} |\theta_j(t) - \theta_i(t)| = 0 \qquad \forall i, j = 1, \ldots, N$$

Note that phase synchronization is not attainable when oscillators have heterogeneous natural frequencies [24].
Let us assume that natural frequencies are supported on a compact interval $\omega_i \in [\omega_{min}, \omega_{max}]$. Then, a necessary condition for the existence of synchronized solutions, is given in [14, 39] as

$$K > \frac{N(\omega_{max} - \omega_{min})}{2(N-1)} \tag{3-8}$$

A looser but still insightful necessary condition is $K > 2\sigma$ [36] where σ is the variance of the natural frequencies. Moreover, in [14], sufficient conditions for exponential synchronization of the oscillator frequencies to the mean natural frequency of the group were also developed. An interesting case is investigated in [39] where authors considered a general type of interconnection among the oscillators. The Kuramoto model for a generic unweighted network structure can be written, using tools from graph theory (see Chapter 2), as

$$\dot{\theta} = \omega - \frac{K}{N}\mathbf{B}\sin(\mathbf{B}^T\theta) \tag{3-9}$$

where $\theta = [\theta_1, \ldots, \theta_N]^T$ collects the phases of the oscillators and $\omega = [\omega_1, \ldots, \omega_N]^T$ the natural frequencies. Moreover, $\mathbf{B}$ is the incidence matrix of the unweighted network structure. Synchronization is best defined in a grounded system, where the phase are defined with respect to a reference variable. This can be achieved by any projection $V_{N\times N-1}$ with

$$\mathbf{V}^T\mathbf{V} = \mathbf{I}, \quad \mathbf{V}\mathbf{V}^T = \mathbf{I} - \frac{\mathbf{1}_N\mathbf{1}_N^T}{N}, \quad \mathbf{V^T 1_N} = \mathbf{0}$$

Thus, $\mathbf{V}$ is a matrix collecting the $N-1$ vectors orthogonal to $\mathbf{1}_N$, which generates the grounded coordinates $\bar{\theta} = \mathbf{V}^T\theta$ and $\bar{\omega} = \mathbf{V}^T\omega$. The grounded Kuramoto model is

$$\dot{\bar{\theta}} = \bar{\omega} - \frac{K}{N}\mathbf{V}^T\mathbf{B}\sin\left(\mathbf{B}^T\mathbf{V}\theta\right) \tag{3-10}$$

As the coupling K is decreased, there is a critical value K_L below which no fixed point exists, resulting in a running solution for the grounded system (3-10). This means that the system cannot be fully synchronized for $K < K_L$. In [39], a sufficient condition for frequency synchronization is given as

$$K \geq 2\frac{\sqrt{N}\|\omega\|_2}{\lambda_2(\mathbf{L})} \tag{3-11}$$

3.3.2 Explosive synchronization

Several works have verified the occurrence of discontinuous synchronization transitions in the tradition Kuramoto model since 90's [65]. However in 2011, Gómez-Gardenez et.al. [30] showed the occurrence of a discontinuous transition, or explosive synchronization as called by them. Authors pointed out that the correlation between network structure and frequency allocation is the mechanism behind such transition. Specifically, they taken the natural frequencies as $\omega_i = k_i$, where k_i is the node degree (see Chapter 2), in a scale free network. Later, Leyva et.al. [43] demonstrated that the choice $\omega_i = k_i$ is not sufficient for explosive synchronization. Indeed abrupt transition to synchronization cannot be found in networks with homogeneous degree distribution, despite that choice of natural frequencies. Authors in [43] showed, instead, that every pair of nodes should satisfy

$$|\omega_i - \omega_j| > \epsilon$$

imposing a gap in the frequency mismatch. In [43] it has been showed that for sufficiently large ϵ the transition becomes discontinuous, a phenomenon not observed for the same network topology under the constraint $\omega_i = k_i$.
Recently, Zhang et.al. [97] proposed the adaptive model

$$\dot{\theta}_i = \omega_i + \lambda\alpha_i\sum_{j=1}^{N} A_{ij}\sin\left(\theta_j - \theta_i\right) \tag{3-12}$$

where ω_i is taken from a distribution $g(\omega)$. To define α_i authors refer to the local order parameter for the i-th oscillator $r_i e^{i\phi} = 1/k_i\sum_{j\in\mathcal{N}_i} e^{i\theta_j}$. Then they choose $\alpha_i = r_i$ for a

fraction f of nodes and $\alpha_i = 1$ for the remaining ones. Increasing the fraction f from 0 to 1, and considering the same network structure, it is possible to see emergence of explosive synchronization, as $f > f_c$. Analytical work confirmed the numerical evidence, showing that the proposed strategy avoids the merging of small synchronized groups, that would result in a large synchronized cluster, yielding explosive synchronization.

3.4 Summary

Kuramoto model, even though very essential, embodies lots of features that researchers have been studying for years. It clearly describes the form of the interaction in a group of coupled oscillators and tell us significant facts about the onset of synchronization. In this Chapter we just mentioned some of them (for an exhaustive review see [83, 65]). This Chapter completes the overview on the background that is needed for the rest of the thesis. Next Chapter addresses an extension, presented in [21], of edge snapping mechanism for directed networks and general types of consensus. Moreover, we will come back to Kuramoto oscillators in Chapter 5, where the method we will propose is based on coupled phase oscillators.

CHAPTER 4

Modified edge-snapping techniques

As discussed in Chapter 2, the design of the communication protocol among the agents is crucial in consensus problems. Many results are available in the literature for the case of (possibly switching and directed) diffusive linear protocols, see [53, 15, 62, 48] and references therein. Nonetheless, an interesting open problem is to find new adaptive strategies to evolve the structure of the interactions among agents so as to ensure the emergence of consensus. In this Chapter, focusing on networks of integrators, we aim at extending the classical edge snapping mechanism (see Chapter 2) so as to steer the nodes' dynamics towards a desired consensus value, which is in general different from average consensus. To achieve our goal, we explore the use of two novel strategies that allow the emergence of steady directed network configurations. Specifically, we propose an hybrid method to achieve min- or max- consensus proving its stability. We then conjecture that an alternative smooth strategy for network evolution can be used to steer the network dynamics towards consensus while guaranteeing the emergence of a directed interconnection structure among the agents. The effectiveness of the proposed approaches is investigated both theoretically and via representative numerical examples.

4.1 General consensus and three-well potential

Consider a network of N integrators, whose topology is described by the graph $\mathcal{G} = \{\mathcal{V}, \mathcal{E}\}$, where $\mathcal{V}$ is the set of nodes and $\mathcal{E}$ is the set of edges. The node dynamics can be described as

$$\dot{x}_i = u_i, \qquad i = 1, \dots, N, \tag{4-1}$$

where u_i is a linear distributed protocol, described by

$$u_i = \sum_{\substack{j=1 \\ j \neq i}}^{N} \sigma_{ij}(t)(x_j - x_i), \quad i = 1, \ldots, N, \tag{4-2}$$

with $\sigma_{ij}(t) \in \mathbb{R}$ being the time-varying coupling gain between nodes i and j: $\sigma_{ij}(t)$ is greater than zero if there is an edge between i and j, while it is zero otherwise. In matrix form, network (4-1)-(4-2) can be equivalently rewritten as

$$\dot{x} = -Lx, \tag{4-3}$$

where $x = [x_1, \ldots, x_N]^T$, and L is the Laplacian matrix of the networks, defined in Chapter 2, whose ij-th element is defined as

$$l(t) = \begin{cases} -\sigma_{ij} & i \neq j, \\ -\sum_{\substack{r=1 \\ r \neq i}}^{N} l_{ir} & i = j. \end{cases} \tag{4-4}$$

We say that network (4-1)-(4-2) achieves χ-consensus iff

$$\lim_{t \to \infty} e_i(t) = 0,$$

for all $i = 1, \ldots, N$, where

$$e_i = \chi(x(0)) - x_i. \tag{4-5}$$

with $\chi : \mathbb{R}^n \times \mathbb{R}$ being a real function of the initial conditions. Specifically, we say that *average consensus* is achieved if

$$\chi(x(0)) = \chi_{\text{ave}}(x(0)) := \frac{1}{n} \sum_{i=1}^{n} x_i(0),$$

while *max-consensus* and *min-consensus* are achieved when

$$\chi(x(0)) = \chi_{\max}(x(0)) := \max_{i=1,\ldots,N} x_i(0)$$

and

$$\chi(x(0)) = \chi_{\min}(x(0)) := \min_{i=1,\ldots,N} x_i(0),$$

respectively.

In what follows, we propose different modifications of the strategy first introduced in [20] to adapt the coupling gains σ_{ij} for all (i,j), so that average, min-, or max-consensus can be achieved. The edge snapping mechanism proposed in [20] (see also Chapter 2), is based on assigning to the coupling gains $\sigma_{ij}(t)$ a second order dynamics subject to the effects of a bistable potential $V : \mathbb{R} \to \mathbb{R}$, driven by a function of the error $e_{ij} = x_j - x_i$. Recall that the gains dynamics is given by

$$\ddot{s}_{ij} + d\dot{s}_{ij} + \frac{\partial}{\partial s_{ij}} V(s_{ij}) = g(e_{ij}), \tag{4-6a}$$

$$\sigma_{ij} = h(s_{ij}), \tag{4-6b}$$

where $s_{ij} \in \mathbb{R}$, d is the damping, and h is the scalar output function. Notice that, adopting the edge snapping approach for coupling adaptation, the network can be still described by equations (4-3)-(4-4), where the Laplacian matrix is now time-varying, that is, $L = L(t)$. Indeed, at the onset of the evolution, all nodes are disconnected, that is, all edges in the network are at the equilibrium state corresponding to edges being switched off. Edge snapping is induced as the external forcing (error between neighboring nodes) is strong enough to drive the corresponding gain to the other equilibrium associated to the edge being switched on. As can be noted from (4-6), network evolution can be controlled by choosing the potential V, the input function g, and the output function h. Specifically, we will define an certain rule to update the Laplacian L in (4-4) and choose a three-well potential V, see Figure **4-1**, defined by

$$V(\sigma_{ij}) = b\sigma_{ij}^2(\sigma_{ij} - 1)^2(\sigma_{ij} + 1)^2, \tag{4-7}$$

Next we discuss how an appropriate choice of functions g and h can be made to steer the network towards a desired consensus value $\chi(x(0))$.

4.2 Hybrid Edge Snapping

In this section, we illustrate how the snapping mechanism can be tailored to achieve χ-consensus, where χ is in general different from χ_{ave}. To achieve this goal, we need to allow the emergence of a directed network from the snapping evolution. To this aim, we define an hybrid rule to update the Laplacian L in (4-4) and choose the three-well potential V in Equation (4-7), see Fig. **4-1**, and a different input function g. Specifically, we select

$$g(x_j - x_i) = x_j - x_i, \tag{4-8}$$

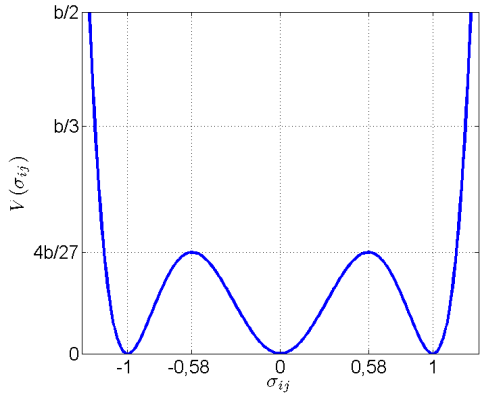

Figure **4-1**: Three-well potential (4-7) driving the evolution of each σ_{ij}.

and we set $h(s_{ij}) = s_{ij}$ so that (4-6) can be rewritten as

$$\ddot{\sigma}_{ij} = -d\dot{\sigma}_{ij} - \frac{\partial}{\partial \sigma_{ij}} V(\sigma_{ij}) + g(x_j - x_i). \tag{4-9}$$

For the sake of clarity, in what follows we refer to the case of max-consensus, but the proposed approach can be adjusted to achieve min-consensus.

Following an approach inspired from [15], we propose the following hybrid rule to achieve max-consensus:

$$l_{ij}(t) = \begin{cases} -|\sigma_{ij}| & x_j \geq x_i, i \neq j, \\ 0 & x_j < x_i, i \neq j, \\ -\sum\limits_{\substack{r=1 \\ r \neq i}}^{N} l_{ir} & i = j. \end{cases} \tag{4-10}$$

Rule (4-10) simply implies that an edge from node j to node i is fostered if $x_j > x_i$, i.e. the activation is promoted of edges directed from nodes with greater to lower state values. The analogy with energy flows is clear since energy spontaneously flows from higher to lower levels. We show the effectiveness of this rule in three steps: i) We show the boundedness of the error system, ii) we prove that the only possible consensus value is max-consensus, iii) we prove that max-consensus is asymptotically achieved.

Boundedness of the error system is trivial from contraction analysis (see Chapter 7). Indeed, from construction we have $\mu_\infty(-L(t)) = 0$ for all $t \geq 0$, which implies that $\|x\|_\infty$ is bounded. Then, $\|e\|_\infty$ is bounded, and consequently so is $\|e\|_2$, from norm equivalence. Now, let's define

$$M := \underset{i=1,\ldots,N}{\operatorname{argmax}}\, x_i(0).$$

Note that the hybrid rule (4-10) implies that

$$\dot{x}_i(t) \geq 0, \qquad i = 1, \ldots, N, \quad t \geq 0,$$

and that

$$\dot{x}_M(t) = 0, \qquad t \geq 0.$$

We will show by contradiction that $x_i(t) \leq x_M(0)$. Indeed, suppose a time instant $\bar{t}$ exists such that for all $t > \bar{t}$, $x_i(t) > x_M(0)$. Then, being x_i continuous, $x_i(\bar{t}) = x_M(0)$. Hence, from rule (4-10), $\dot{x}_i(t)$ would be locked to zero for all $t \geq \bar{t}$ against the hypothesis. Therefore, we can conclude that $x_i(t) \leq x_M(0)$, from which we have

$$e_i \geq 0, \dot{e}_i \leq 0, \qquad i = 1, \ldots, N, t \geq 0,$$

which implies that $\|e\|_2$ is decreasing. As $\|e\|_2$ is also bounded, then we can conclude that

$$\lim_{t \to \infty} \|e(t)\|_2 = c \leq \|e(0)\|_2 .$$

At steady-state, we have $\frac{d}{dt}\|e\|_2 = 0$, which implies that $\sigma_{ij} = 0$ for all (i, j) and/or $e_i = 0$ for all (i, j). Notice, nonetheless, that if for some i, $e_i \neq 0$, then equation (4-6) would imply that the corresponding σ_{ij} is different from 0 and thus $\frac{d}{dt}\|e\| < 0$. Hence, we would get a contradiction. Therefore, $c = 0$ and the network of integrators asymptotically reaches max-consensus.

To complement the analysis, we numerically test this approach on a network of 50 integrators. The nodes' initial conditions are selected from a normal distribution with zero mean and standard deviation equal to 15, while $s_{ij}(0)$ is set to 0 for all $i, j = 1, \ldots, N$. As reported in Figure **4-2**a, max-consensus is achieved and the agents asymptotically converge to the value 31.68 corresponding to $\max_i x_i(0)$, while the coupling gains settle to steady state bounded values, see Figure **4-2**b.

Remark 4.2.1. *Following a similar argument to that presented above, we can show that the hybrid rule can be adjusted to*

$$l_{ij}(t) = \begin{cases} -|\sigma_{ij}(t)| & x_j < x_i, i \neq j, \\ 0 & x_j \geq x_i, i \neq j, \\ -\sum\limits_{\substack{r=1 \\ r \neq i}}^{N} l_{ir}(t) & i = j, \end{cases} \tag{4-11}$$

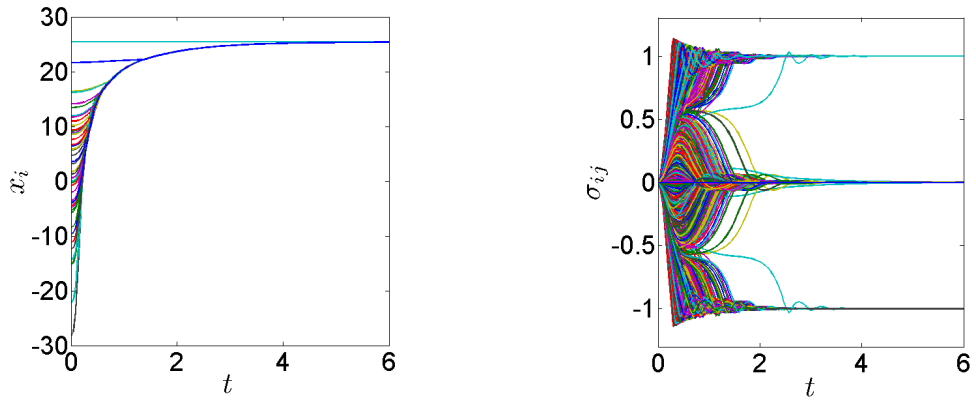

(a) (b)

Figure **4-2**: Network of $N = 50$ integrators: (a) Evolution of the agent states towards max-consensus; (b) evolution of the coupling gains.

if the goal is to achieve min-consensus, that is,

$$\lim_{t\to\infty} (x_i(t) - \chi_{\min}) = 0.$$

*In Figure **4-3**, we illustrate that min-consensus is achieved in a network of* $N = 50$ *integrators by means of rule* (4-11).

4.3 Directed edge snapping

As an illustration of the viability of the edge-snapping strategy to steer the dynamics of a network of interest, we present and investigate numerically the performance of a different gain evolving strategy guaranteeing the evolution of a digraph connecting nodes in the network so that consensus emerges.

Specifically, the potential V, the output function g, and the function $h(s_{ij})$ are those in equations (4-7), (4-8), and (4-9), respectively but the time varying Laplacian matrix is now described by

$$l_{ij} = \begin{cases} -\sigma_{ij} & \sigma_{ij} \geq 0, i \neq j, \\ 0 & \sigma_{ij} < 0, i \neq j, \\ -\sum\limits_{\substack{r=1 \\ r\neq i}}^{N} l_{ir} & i = j. \end{cases} \tag{4-12}$$

Under this choice, given any pair of nodes (i, j), we have three coexisting stable equilibria for the edge dynamics: $\sigma_{ij} = 0$ (no active edges), $\sigma_{ij} = 1$ (an edge from j to i is activated),

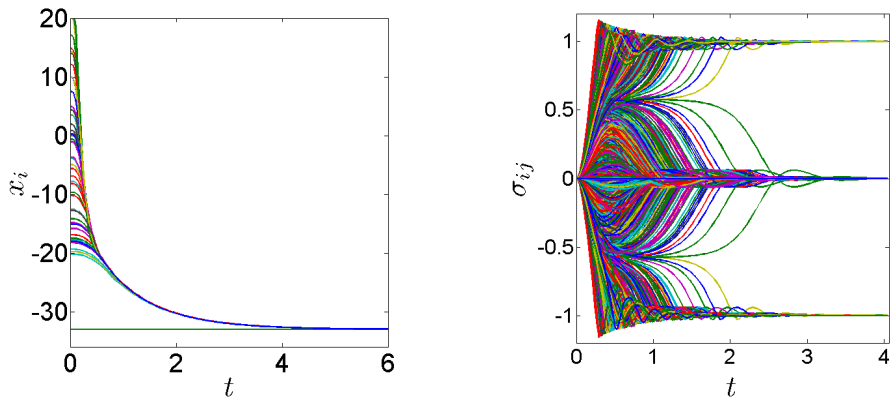

(a) (b)

Figure **4-3**: Network of $N = 50$ integrators: (a) Evolution of the agent states towards min-consensus; (b) evolution of the coupling gains.

and $\sigma_{ij} = -1$ (an edge from i to j is activated). Notice that, when $x_j > x_i$, the input g will be positive, and the activation of an edge from j to i will be facilitated. Otherwise, if $x_j < x_i$, then the bidirectional input g will be negative, thus fostering the activation of an edge from i to j.

To illustrate the effectiveness of the approach, we simulate the evolution of a network of $N = 50$ integrators, with nodes' initial conditions taken from a normal distribution with zero mean and standard deviation equal to 15. As usual, we set $s_{ij}(0) = 0$, for all $i, j = 1, \ldots, N$. As depicted in Figure **4-4**, consensus is achieved and the emerging topology achieves a steady-state configuration.

Note that in this case consensus is achieved onto the maximum value of the nodes' initial conditions (max consensus). This can be explained heuristically by noting that during the network evolution a directed spanning tree rooted in the node with the maximal initial condition has emerged and conditions for max consensus are fulfilled (a schematic of such spanning tree is omitted here for the sake of brevity). More generally, a spanning tree can be formed at a later stage of the evolution, and, in that case, consensus is still reached but on a different value. For example, in Figure **4-5**, we show the simulation where we selected node 1 to have a much smaller initial condition than the other nodes. In particular, we have set $x_1(0) = -300$, while the other initial conditions are the same as those used in the previous simulation. As we can observe from Figure **4-5**, agents agree on a value $\chi(x(0)) = 19.29 < \max_i x_i(0) = 25.02$. Notice that this approach can be easily adjusted to

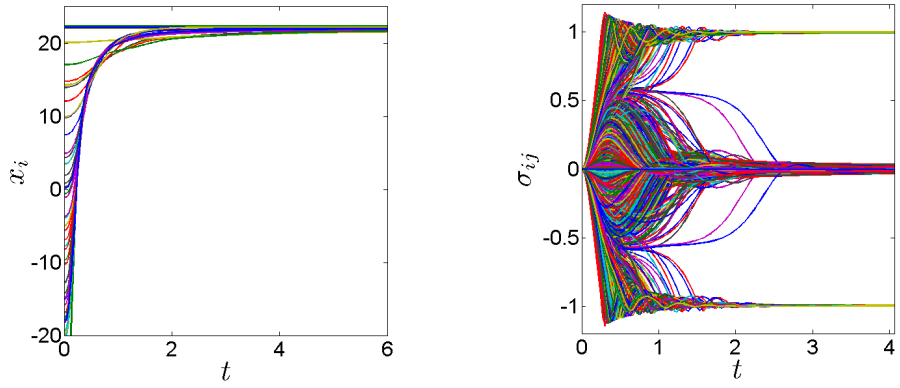

(a) (b)

Figure **4-4**: Network of $N = 50$ integrators: (a) Max-consensus is achieved through directed edge snapping; (b) all the coupling gains converge to the equilibrium values.

change the consensus value. For example, it suffices to choose

$$g(x_i - x_j) = x_j - x_i$$

in order to steer the dynamics of all nodes towards a minimal rather than maximal value. In Figure **4-6**, we report the outputs of the simulations with the same initial conditions as in Figure **4-4**.

4.4 Summary

In this Chapter, we presented some extensions of the edge snapping strategy for consensus of multiagent networks. We proposed two strategies, in which, differently from what derived in [20], a directed steady-state network is evolved to achieve different types of consensus. We showed that by appropriately selecting the structure of the edge adaptation rule, we can achieve both average (undirected edge snapping) and max/min consensus (hybrid edge snapping). Next we will address a slightly different problem. Indeed, we will show how to use edge snapping in an evolutionary manner so as to make undirected networks emerge. Structure and properties of those networks will be studied and their functionality will be analysed.

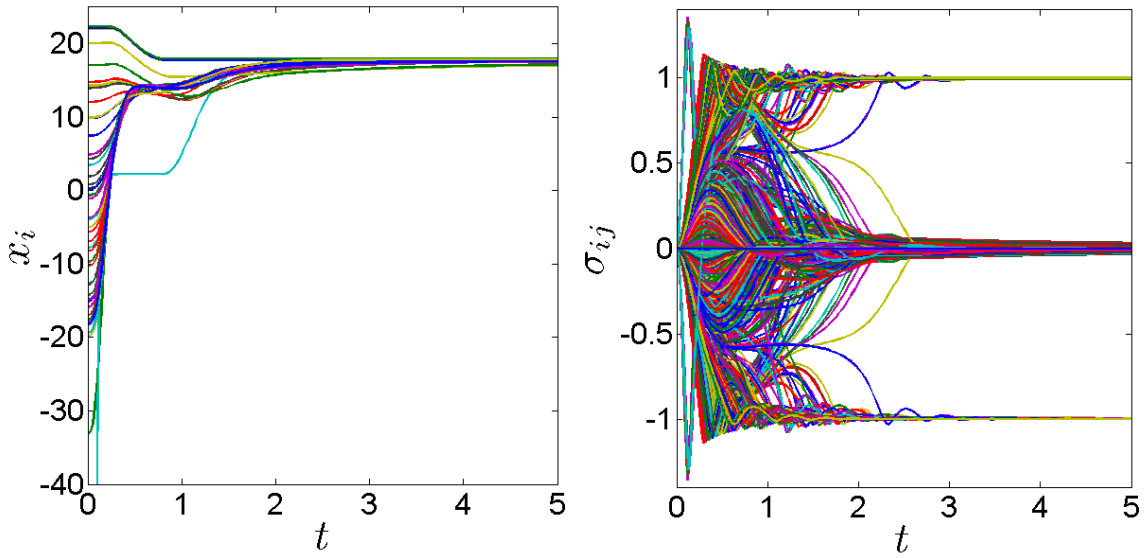

(a) (b)

Figure **4-5**: Network of $N = 50$ integrators with $x_1(0) = -300$: (a) χ-consensus is achieved through directed edge snapping, with $\chi < \chi_{\max}$; (b) all the coupling gains converge to the equilibrium values.

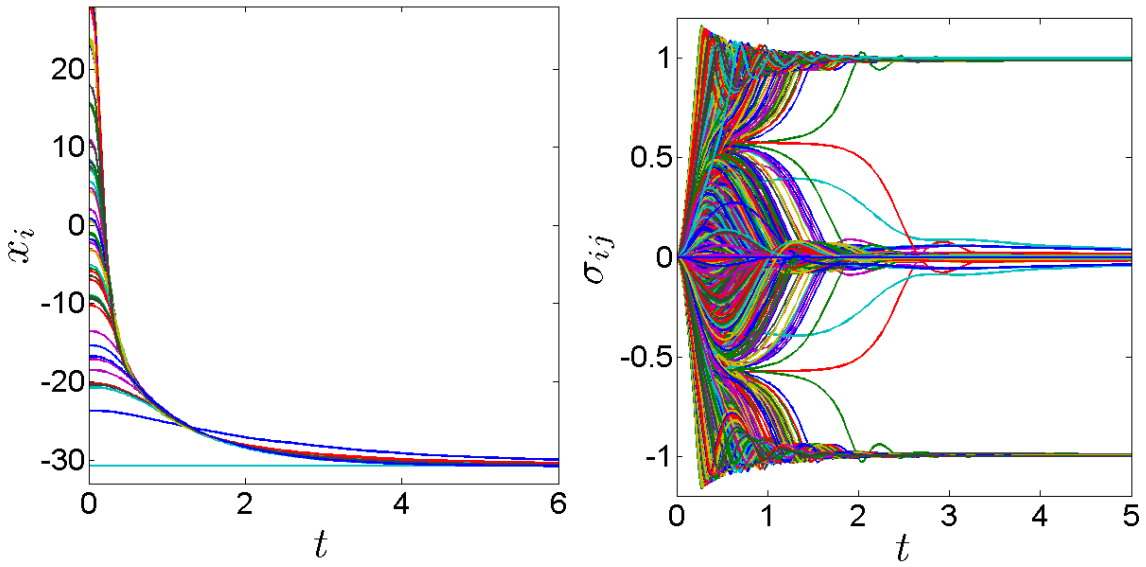

(a) (b)

Figure **4-6**: Network of $N = 50$ integrators: (a) Min-consensus is achieved through directed edge snapping; (b) all the coupling gains converge to the equilibrium values.

CHAPTER 5

An evolutionary strategy for network synchronization

Evolution is a central feature of many natural systems [16]. It consists of two key ingredients: mutation and selection. The first is based on the recombination within a class of organisms that yields the formation of new species. Then selection is the mechanism determining the survival of the fittest to perform a certain function. Evolutionary algorithms are known in the literature as genetic algorithms [17]. They are useful to optimize the behaviour of a given system with respect to a payoff function, through iterative mutation and selection. Recently, this mechanism has been successfully used in the field of complex networks [85] to explore and uncover mechanisms for the emergence of collective behaviours in a multi-agent network. Indeed, one of the most challenging open problems in Network Science [8] is aimed to uncover the intrinsic relation between structure and function of a complex dynamical network.

In this Chapter we will present a novel evolutionary method for network synchronization. The emergence of functional networks will be discussed together with their structural and dynamical properties that yield enhanced synchronizability. We will focus, for the sake of clarity, on a network of Kuramoto oscillators, though our method is very general and can be applied to a wide class of nonlinear oscillators.

The results of this Chapter were recently presented in [75, 76].

5.1 Problem statement

We start by considering a network of general nonlinear coupled oscillators

$$\dot{\mathbf{x}}_n = \mathbf{f}_n(x_n) + c\sum_{m=1}^{N} k_{nm}\mathbf{g}(\mathbf{x}_m, \mathbf{x}_n), \tag{5-1}$$

where $\mathbf{x}_n \in \mathbb{R}^p$ is the p-dimensional state of the n-th oscillator, $\mathbf{f}_n$ denotes its dynamics (note that oscillators can be slightly different from each other due to both parameters and model mismatches), $\mathbf{g}$ is a generic coupling function and k_{nm} are time-varying coupling gains determining the strength of the coupling between neighboring oscillators. We model the evolutionary pressures to reach synchronization by considering state-dependent second-order nonlinear dynamics for the gains dependent upon a double well potential $V(x) = bx^2(x-1)^2$. The gain dynamics are given by

$$\ddot{k}_{nm} + d\ \dot{k}_{nm} + \frac{\partial V(k_{nm})}{\partial k_{nm}} = h(\|\mathbf{x}_m - \mathbf{x}_n\|), \tag{5-2}$$

in which $h(\|\mathbf{x}_m - \mathbf{x}_n\|)$ is a generic increasing function such that $h(0) = 0$. Note that this is a very general adaptive network equation relying on a decentralized, local, state-dependent interconnection rule. This system can be systematically reduced, under a standard technique [42], to the network of adaptively coupled phase oscillators:

$$\dot{\theta}_n = \omega_n + \frac{1}{N}\sum_{m=1}^{N} k_{nm}\Gamma(\theta_m - \theta_n), \tag{5-3}$$

$$\ddot{k}_{nm} + d\ \dot{k}_{nm} + \frac{\partial V(k_{nm})}{\partial k_{nm}} = h(\|\theta_m - \theta_n\|), \tag{5-4}$$

in which θ_n is the phase of the n-th generic oscillator, $\Gamma(\theta_m - \theta_n)$ is a generic 2π-periodic function. We set the overall coupling strength K to a unitary value, since it can be absorbed into a parameter defining the heterogeneity of the natural frequencies by rescaling time, i.e. by setting $\tau = Kt$. In this paper we analyze, for the sake of clarity, the simplest case

$$\Gamma(\theta_m - \theta_n) = \sin(\theta_m - \theta_n), \tag{5-5}$$

$$h(\|\theta_m - \theta_n\|) = \alpha\left[1 - \frac{1}{2}|e^{i\theta_n} + e^{i\theta_m}|\right]. \tag{5-6}$$

The differences in the natural frequencies of the oscillators originate from the heterogeneity of the node dynamics $\mathbf{f}_n$ in weakly coupled nonlinear oscillators [42]. In what follows, these

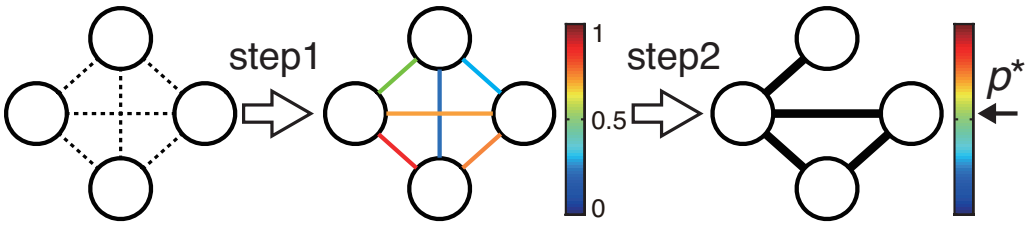

Figure **5-1**: Schematic description of the evolutionary edge-snapping strategy. Step 1 (variation): computation of link activation probabilities by running the edge-snapping strategy from many different random initial conditions. Step 2 (selection): selection of those links whose activation probability is above some threshold value p^*.

natural frequencies are selected deterministically from a Gaussian distribution with zero mean and standard deviation equal to σ. Therefore, the parameter σ can be used to "tune" the level of heterogeneity among nodes.

We note here that when the number of nodes is not so large, such as $N = 6$ or 7, the natural frequencies sampled from a distribution can be biased. To avoid the effect of the biased sampling, we deterministically select the natural frequencies of the oscillators, similarly to [93], as the N-tuple satisfying the constraints:

$$\int_{-\infty}^{\omega_1} g(\omega)d\omega = \frac{1}{N+1}, \quad (i = 1)$$
$$\int_{-\omega_{i-1}}^{\omega_i} g(\omega)d\omega = \frac{1}{N+1}, \quad (i = 2, \ldots, N)$$

where $g(\omega)$ is the probability density function of a given distribution. It should be noted that for a large network, we performed our simulation taking the natural frequencies randomly from a distribution and the obtained results are qualitatively the same.

Next, we investigate how the evolution of the network is affected by tuning the heterogeneity in the nodes. To this aim we use the edge snapping strategy described above in a novel evolutionary manner (see Figure **5-1**) as explained in the next section.

5.2 Methodology

The evolutionary Edge-Snapping technique is based on two fundamental steps: one implementing the *variation ingredient* of evolution, the other its *selection mechanism*.

To implement the *variation ingredient* of evolution, a set of unweighted networks is generated using equations (5-3) and (5-4) starting the process from different sets of initial conditions. We consider a set of n_S initial conditions randomly selected using a Latin Hypercube strategy [47] in the range $\theta_n(0) \in [0, 2\pi[$, $n = 1, 2, \ldots, N$. To obtain the "fitness" of each link, we next compute the probability p_{ij} of each link being activated as the fraction between the number of generated networks where that link is present, say n_{ij}, and the total number of trials, e.g. $p_{ij} = n_{ij}/n_S$. This yields a stochastic $N \times N$ matrix P whose elements are the probabilities of activation of every possible link among nodes.

The *selection rule* is obtained by selecting only those links whose activation probability is above a certain critical threshold value p^*, i.e. such that $p_{ij} > p^*$. We choose p^* so as to guarantee that the resulting network is connected and has the smallest number of links. We shall term such a network as the *minimal edge-snapping (ES) network*.

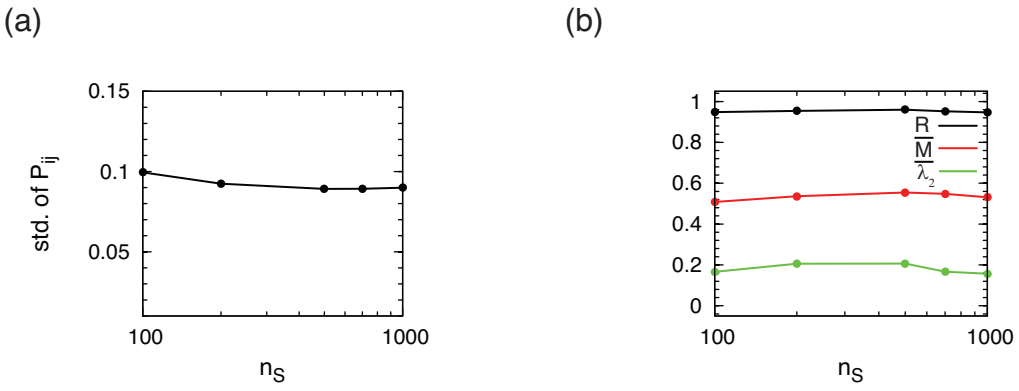

Figure **5-2**: (a) Standard deviation of the link activation probability p_{ij} as a function of the number of trials n_S. (b) Order parameter and relative number of links of the minimal ES structure as a function of the number of trials n_S.

The variation step of our evolutionary strategy relies on the generation of a set of n_S unweighted network using equations (5-3) and (5-4) and starting the process from a different set of initial condition. With the aim of choosing a reasonable value for the number of trials n_S, we plot in Figure **5-2**(a) the standard deviation of the link activation probability p_{ij} as a function of n_S. As can be noted, the differentiation in the p_{ij} is quite constant as n_S varies from 100 to 1000. Thus we select $n_S = 100$ in all of our simulations. Indeed this guarantees a good degree of variation with the least computational cost. Finally, Figure **5-2**(b) confirms that the dynamical and structural properties of the emerging ES minimal structure do not show significant fluctuations when the value of n_S is increased.

Note that the state space of the initial phases of many oscillators is a high-dimensional space (i.e. the aggregate N-dimensional state space obtained collecting the phase of each oscillator in the stack vector $\Theta = [\theta_1, \theta_2, \ldots, \theta_N]$). To obtain effective samplings from that space, we adopted a Latin Hypercube Sampling (LHS) strategy first proposed in [47]. LHS is a statistical method for generating a sample of plausible collections of parameter values from a multidimensional distribution. Specifically, let X denote a N variate random variable with probability density function $f(x)$ for $x \in S$. Then the range space of each of the N components of X is partitioned in n_S disjoint intervals S_i of size $p_i = P(X \in S_i) = 1/n_S$. Taking the Cartesian product of these intervals yields n_S^N cells each of probability size n_S^{-N}. Each cell can be labeled by a set of N coordinates $m_i = (m_{i1}, m_{i,2}, \ldots, m_{iN})$ where m_{ij} is the interval number of component X_j represented in cell i. A LHS is obtained from a random selection of the cells $m_1, \ldots, m_{n_S}$, with the condition that for each j the set $\{m_{ij}\}_{i=1}^{n_S}$ is a permutation of integers $1, 2, \ldots, n_S$. As a result, one random observation is made in each cell. The main advantage of the LHS strategy is that it does not require more samples for more dimension of the range space S. This is the main reason why we use LHS in our method.

To measure the synchronization performance of a ES network, we consider an ensemble of phase oscillators connected by that network and evaluate Kuramoto order parameter as $Re^{i\psi} = \frac{1}{N}\sum_{n=1}^{N} e^{i\theta_n}$.

5.3 Analysis of emergent network structures

We first test our strategy by applying it to a small size network with $N = 6$ and $\sigma = 0.3$ (Figure **5-3**). We obtain the P matrix visualized in Figure 2(a). In Figure 2(b), as the threshold value p is increased, the number of edges, M, rapidly decreases while the value of the order parameter R remains near unity.

In the figure, the normalized number of edges, which is divided by maximum links between N nodes, i.e. $\bar{M} = M/M^{a2a}$, is plotted. Also above a certain threshold the network becomes disconnected. Therefore we choose $p^* = 0.57$ obtaining the minimal ES network depicted in Figure 2(c) which is characterized by $M = 7$ edges and $R = 0.96$. We compare the minimal ES structure with the optimal network structure shown in Figure 2(d) obtained from an exhaustive search and a Monte Carlo based method [33] maximizing the value of R with the constraint that the total number of edges M is equal to 7. We notice that the two networks share the same links.

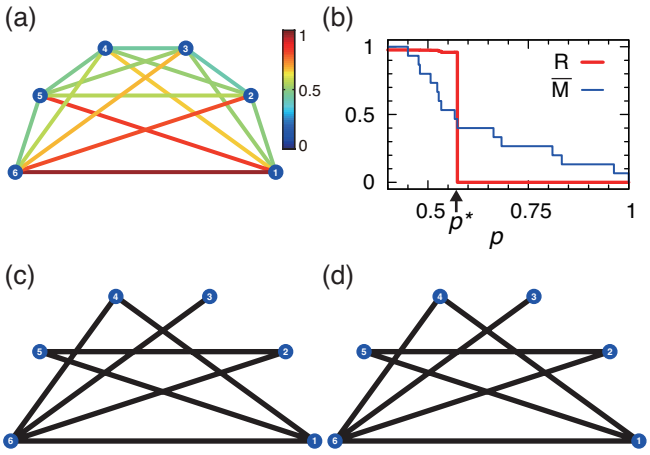

Figure **5-3**: (a) Link activation probabilities p_{ij} in the case of $N = 6$ generated by the variation stage of the evolutionary ES strategy; (b) Selection of the threshold probability value p: order parameter R, relative number of links $\bar{M}$. The arrow on the x-axis indicates the critical threshold p^* which gives the minimal ES network; (c) Minimal Edge-Snapping Network; (d) Optimal network maximizing R obtained by Exhaustive search and a Monte Carlo based method.

Next, we study how heterogeneity induces functional structural properties of the network. Figure **5-4** shows the P matrix as a function of the heterogeneity parameter σ when $N = 20$. We see that as σ is increased a differentiation becomes more and more apparent in the distribution of the link activation probabilities p_{ij} with edges between oscillators with relatively different frequencies becoming more likely to occur in the minimal ES structure. Figure **5-5**(a) shows the standard deviation of the link activation probabilities p_{ij} as a linear function of σ in a larger network of $N = 100$ oscillators. The structural properties of the emerging network are therefore induced by the node heterogeneity. This is confirmed in Figure **5-5**(b) where the maximum and minimum values of the node degree k_i, corresponding

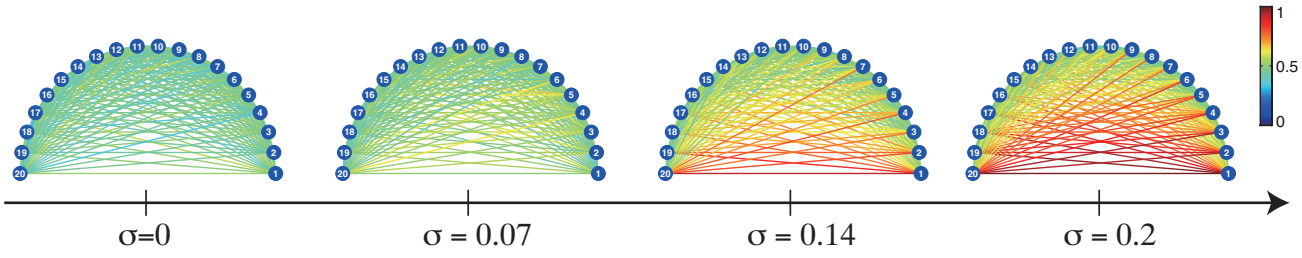

Figure **5-4**: Heterogeneity induces functional structural properties of the network. P matrix as a function of the heterogeneity parameter σ when $N = 20$.

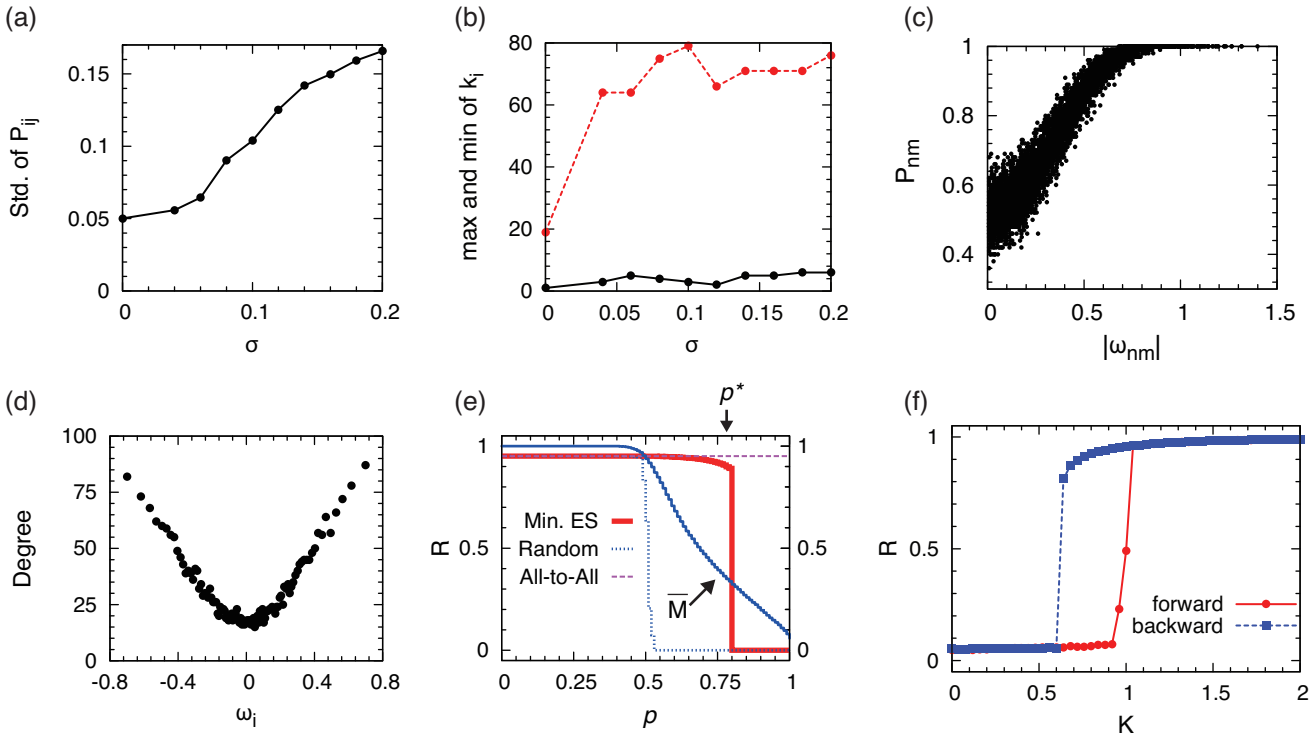

Figure **5-5**: Structural properties of the emergent minimal ES network with $N = 100$ and $\sigma = 0.2$. (a) Standard deviation of the link activation probabilities p_{ij} as a function of σ. (b) Maximum (red dashed line) and minimum (black solid line) value of Node Degree k_i as a function of σ. (c) Activation probability of each link against the value of the difference between the natural frequencies of the oscillators at the endpoints. (d) Node degree k_i vs. ω_i. (e) Order parameter R (red solid line) and relative number of links $\bar{M}$ (blue solid line) of the ES network as a function of the threshold probability value p. For comparison, the value R is depicted for an all-to-all network (purple dashed line) and for randomly generated networks (blue dot-dashed line) with the same number of links. The arrow on x-axis represents the threshold p^* to give the minimal ES network. (f) Order parameter R of the phase oscillators interconnected by the minimal ES network when the overall coupling strength K is increased (red solid) and decreased (blue dashed). We set $N = 300$ and $\sigma = 0.2$.

to each minimal ES network, is plotted as a function of σ. The behaviors of the maximum value of k_i (red dashed line) and the minimum of k_i (black solid line) show an abrupt transition when passing from $\sigma = 0$ to $\sigma > 0$. This suggests that the differentiation in the degree distribution of the minimal ES network becomes remarkable when heterogeneity in the nodes is increased from zero (identical oscillators) to a value greater than zero (non-identical oscillators).

The structural properties of the emergent minimal ES network are highlighted in Fig. **5-5**(c)-(f) for a network of highly heterogeneous $N = 100$ oscillators ($\sigma = 0.2$). The activation probability of each link is plotted in Figure **5-5**(c) against the value of the difference between the natural frequencies of the oscillators at the endpoints. Links connecting more distant nodes tend to be activated with a higher likelihood confirming that differentiation among links is induced by heterogeneity in the nodes. Also, as shown in Figure **5-5**(d), hubs tend to be associated with oscillators whose frequencies are farther away from the average. The functional advantage of the emerging network is shown in Figure **5-5**(e). Indeed, we observe that the order parameter of the minimal ES structure is close to its maximal value for an all-to-all network, even if the number of links in the minimal ES network is remarkably lower than that in an all-to-all configuration. For the sake of comparison, the values of R for a randomly generated network of the same number of edges is also depicted in Figure **5-5**(e). The sudden dip of R is due to the graph becoming disconnected beyond that critical value of the threshold p^*.

Notice that, as shown in Figure **5-5**(f), as the coupling strength K is varied, the order parameter R of the phase oscillators interconnected by the minimal ES network exhibits a sudden hysteretic change, associated to a discontinuous phase transition, whereas the system with a unimodal frequency distribution undergoes a continuous phase transition [42]. This discontinuous phase transition, also known as "explosive synchronisation", has been studied in the literature [55, 31, 43, 98], also in the case of adaptive networks [38, 97], revealing that the correlation between natural frequencies and the node degree, as shown in Figure 4(d), can induce this phenomenon. Here, we wish to emphasise that the proposed evolutionary strategy, which functionally organizes the network structure for synchronization, changes the type of phase transition that would be generically observed otherwise, inducing explosive synchronisation.

Our results clearly show the role of node heterogeneity in inducing functional structures using an evolutionary strategy for network synchronization. In particular, differences in the node dynamics do influence the evolution of the network determining a differentiation in the

link activation probabilities that is instrumental to obtain minimal structures with relatively high values of the order parameter. Also, hubs tend to emerge there where the distance from the average natural frequency is highest.
It is notable that the presence of hubs seems to characterize the emergent networks for synchronization when the nodes are heterogeneous as opposed to more homogenous structures, such as entangled networks, which have been suggested to be optimal structures in the homogeneous case [23]. This is also confirmed in the case of Monte Carlo based optimal networks in [93] where the presence of links between nodes with more distant frequencies is shown to be more likely and in the recent paper [80] based on the use of gradient-based methods. Here we obtain a further confirmation of these observations but via a generic local evolutionary strategy that is state-dependent and can be applied to a wider range of network synchronization and control problems.

5.4 Larger networks

Results obtained in previous sections could be biased by finite size effect [42]. Thus we provide the same analysis considering higher network sizes (we set $N = 1000$). We take into account four different values of standard deviation. Namely, $\sigma = 0.07$, $\sigma = 0.1$, $\sigma = 0.14$ and $\sigma = 0.2$. For each of them we repeat the evolutionary strategy presented above, obtaining results shown in Figure **5-6** where is clear that increasing heterogeneity, the emerging network becomes more and more heterogeneous. What we show in Figure **5-6** is nodes' degree as a function of natural frequency of each node, i.e. a degree-frequency plot. Notice the sparseness of such a plot when the heterogeneity in the nodes is small. Conversely, when $\sigma = 0.2$, nodes with highest and lowest natural frequencies tend to be connected to all other nodes in the network. This, in turn, results in a "saturating effect" affecting the degree-frequency plot.
Next we explore the structural features of the emergent network when $\sigma = 0.14$. Before that, we recall some assortativity[1] measures, introduced in the literature and well suited to the case of Kuramoto oscillators.

Definition 5.4.1 (Degree-frequency mixing coefficient [25])**.** *Given a network of oscillators with node degrees k_i and natural frequencies ω_i, we introduce degree-frequency mixing*

[1] In Chapter 2 we introduced the general concept of assortativity mixing in networks

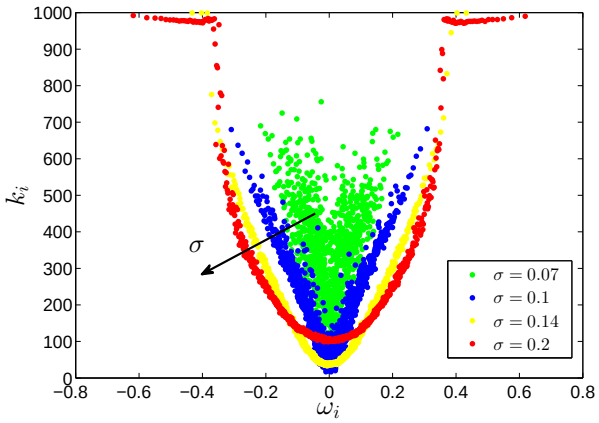

Figure **5-6**: Frequency-degree plots for different values of network heterogeneity σ. We set $N = 1000$.

coefficient

$$r_{k\omega} = \frac{N^{-1}\sum_{i=1}^{N} k_i\omega_i - \langle k\rangle\langle\omega\rangle}{\sqrt{N^{-1}\sum_{i=1}^{N} k_i^2 - \langle k\rangle^2}\sqrt{N^{-1}\sum_{i=1}^{N} \omega_i^2 - \langle\omega\rangle^2}}$$

where $\langle k\rangle = 1/N\sum_{i=1}^{N} k_i$ *and* $\langle\omega\rangle = 1/N\sum_{i=1}^{N}\omega_i$.

Definition 5.4.2 (frequency-frequency mixing coefficient [9]). *Given a network of oscillators with node degrees* k_i *and natural frequencies* ω_i*, a frequency-frequency mixing coefficient can be defined*

$$c_\omega = \frac{\sum_{i,j} a_{ij}(\omega_i - \langle\omega\rangle)(\omega_j - \langle\omega\rangle)}{\sum_{i,j} a_{ij}(\omega_i - \langle\omega\rangle)^2}$$

where $\langle\omega\rangle = 1/N\sum_{i=1}^{N}\omega_i$ *and* a_{ij} *are the entries of the adjacency matrix.*

Note that the coefficient $r_{k\omega}$ lies in the range $[-1, 1]$ and gives a measure of the correlation between the degrees and natural frequency of oscillators. Instead, c_ω quantifies how often nodes with large negative omega are adjacent to nodes with strongly positive omega.
Now, we provide a comparison of minimal network with the optimal structure obtained in [80]. Further, we compare our minimal network with what we call "NetworkCM". Namely we construct, through Configuration Model [50], a set of different networks sharing, with minimal network, the same degree distribution. Then we average the resulting characteristics of such networks, over 10 realizations, yielding results shown in third column of Table **5-1**, where the features of minimal and optimal networks are summarized too. Notice that NetworkCM has a different number of edges compared to minimal and optimal networks.

	Minimal	Optimal	NetworkCM
M(edges)	83746	83746	81110
Clustering	0.2143	0.2002	0.4679
Diameter	2	2	4
λ_2	32.9667	44.5288	32.4256
$r_{k\omega}$	0.9704	0.9706	0.9887
c_ω	-0.5664	-0.5280	-0.0016
R	0.8215	0.9171	0.1136

Table **5-1**: Comparison results ($N = 1000$). Minimal network is obtained for $\sigma = 0.14$. The optimal structure is computed as in [80]. NetworkCM was obtained with the Configuration Model algorithm [50], given the degree distribution of minimal network. All quantities referring to NetworkCM are averaged over 10 realizations.

Indeed, we used a Configuration Model algorithm in which self loops and multiple edges are not allowed. Thus, after a network is generated according to Configuration Model, such edges are cancelled resulting in a structure with a lower M. We note here minimal and optimal networks do not show the presence of multiple edges nor self loops. Clustering coefficient and diameter of NetworkCM are quite twice, compared to those of minimal and optimal networks. Degree frequency assortativity (see Chapter 2) does not show significant differences, while frequency-frequency assortativity is almost zero for NetworkCM and negative for the other two networks. Finally, NetworkCM ensures a value of the order parameter R that is very small compared to that of minimal structure, though they share the same degree distribution. Results shown in Table **5-1** suggest assortativity can enhance synchronizability. Nonetheless, degree-frequency assortativity is not sufficient to guarantee good performances, contrary to what is pointed out in [25]. Indeed frequency-frequency disassortativity is also a crucial feature. Notice that, in [9] only frequency-frequency assortativity c_ω is considered to enhance synchronization. We conjecture here that $r_{k\omega}$ and c_ω do both influence synchronizability. The resulting network shows the presence of hubs associated to nodes that are far from the average natural frequency (degree-frequency assortativity), with most of connections being established between nodes with opposite natural frequencies (frequency-frequency disassortativity).

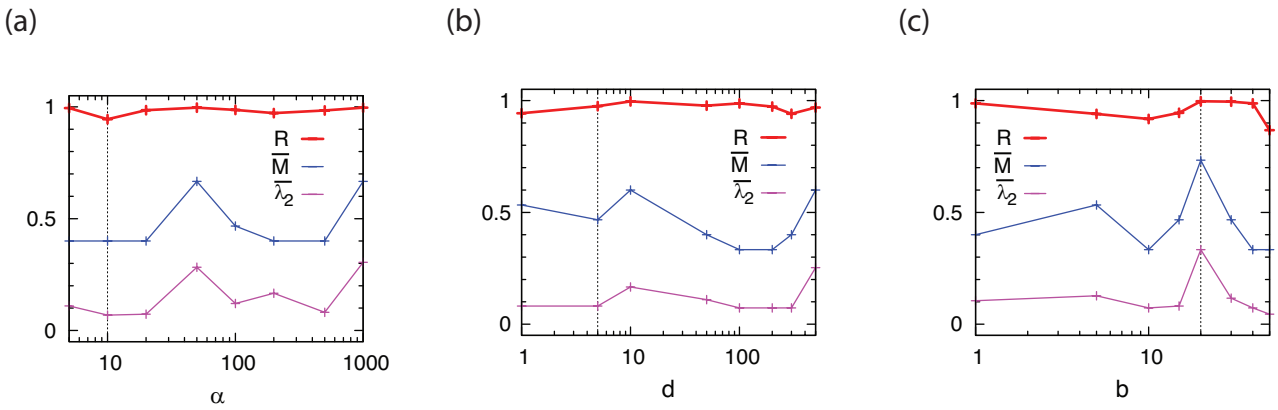

Figure **5-7**: Robustness analysis of the emergent minimal ES network. (a) Variations of the control input gain α (b) Variations of the damping factor d (c) Variations of the height of the barrier b

5.5 Robustness properties varying the parameters

Our strategy depends upon three parameters: b that is proportional to the height of the double-well potential barrier, d that is the damping coefficient in the edge snapping dynamics and α, a control input gain. To test the robustness of the proposed methodology to variations of such parameters, we selected a range of variation for each of them. Then we show the performance of the variation and selection methos, in terms of the order parameter R, the relative number of edges $\bar{M}$ and the relative smallest non-zero eigenvalue $\bar{\lambda}_2$ (these relative quantities are defined with respect to the values of the all-to-all configuration, namely $\bar{M} = M/M_{a2a}$, where M_{a2a} is the number of links of the all-to-all network with N nodes and M is the number of edges of the minimal ES network. Similarly, $\bar{\lambda}_2 = \lambda_2/\lambda_2^{a2a}$, where λ_2^{a2a} is the smallest non-zero eigenvalue of the all-to-all network with N nodes and λ_2 the smallest non-zero eigenvalue of the minimal ES network). We test the robustness of our approach on a network of Kuramoto oscillators.

From Figure **5-7** we can observe that varying α, b and d the order parameter is always close to 1, even if the number of edges and the smallest non-zero eigenvalue show fluctuations denoting the possible presence of local extrema whose investigation is left for future work.

5.6 Applications to networks of oscillators

In this section, we show the generality of our approach, by applying it to a network of diffusively coupled nonidentical Rossler oscillators. The network model is

$$\begin{aligned} \dot{x}_n &= -\omega_n\, y_n - z_n + c\sum_{m=1}^{N} k_{nm}(x_m - x_n) \\ \dot{y}_n &= \omega_n\, x_n + a y_n + c\sum_{m=1}^{N} k_{nm}(y_m - y_n) \\ \dot{z}_n &= b_r + z_i(x_i - c_r) + c\sum_{m=1}^{N} k_{nm}(z_m - z_n) \end{aligned} \tag{5-7}$$

$$\ddot{k}_{nm} + d\,\dot{k}_{nm} + \frac{\partial V(k_{nm})}{\partial k_{nm}} = |\theta_n - \theta_m| \tag{5-8}$$

where $\mathbf{x} = (x_n,\ y_n,\ z_n)^T \in \mathbb{R}^3$ is the state of the n-th chaotic Rossler oscillator. We use a complete coupling on each state variable. Moreover, the natural frequencies are taken from a normal distribution with mean and standard deviation equal to 1. We deterministically select the natural frequencies of the oscillators, similarly to what we have done for the Kuramoto oscillators. (We also performed our simulation taking the natural frequencies randomly from a normal distribution and the results are qualitatively the same).

We are interested in the so-called phase synchronization of chaotic oscillators. In [66] is showed that the classical notion of synchronization can be extended to chaotic oscillators. In this context, there is a need for the definition of the time-dependent amplitude $A(t)$ and phase $\theta(t)$ of a chaotic signal. There are several approaches in the literature. Here we choose to define $A(t)$ and $\theta(t)$ as [28]

$$A(t)e^{i\theta(t)} = s(t) + i\tilde{s}(t) \tag{5-9}$$

where $s(t)$ is the chaotic signal, while $\tilde{s}(t)$ is the Hilbert transorm of $s(t)$. When the phase of a chaotic signal is introduced in some way, one can define the phase synchronization as the occurence of a certain relation between the phases of interacting systems, while the amplitudes can remain chaotic and are, in general, not correlated [54], i.e. only phase locking is important. We recall (see Chapter 3) phase locking occurs when the difference between the phases of the oscillators does not grow with time, but remains bounded.

As the phase of the Rossler oscillator is well defined, the adaptation rule can be chosen as in Equation (5-8). In Figure **5-8** we show the p_{ij} distribution of a network of $N = 10$ Rossler oscillators. In the numerical simulation we set $n_S = 100$, the height of the barrier $b = 300$ and the Rossler parameters $a = b_r = 0.1$, $c = 18$ in order to obtain a chaotic behaviour [59].

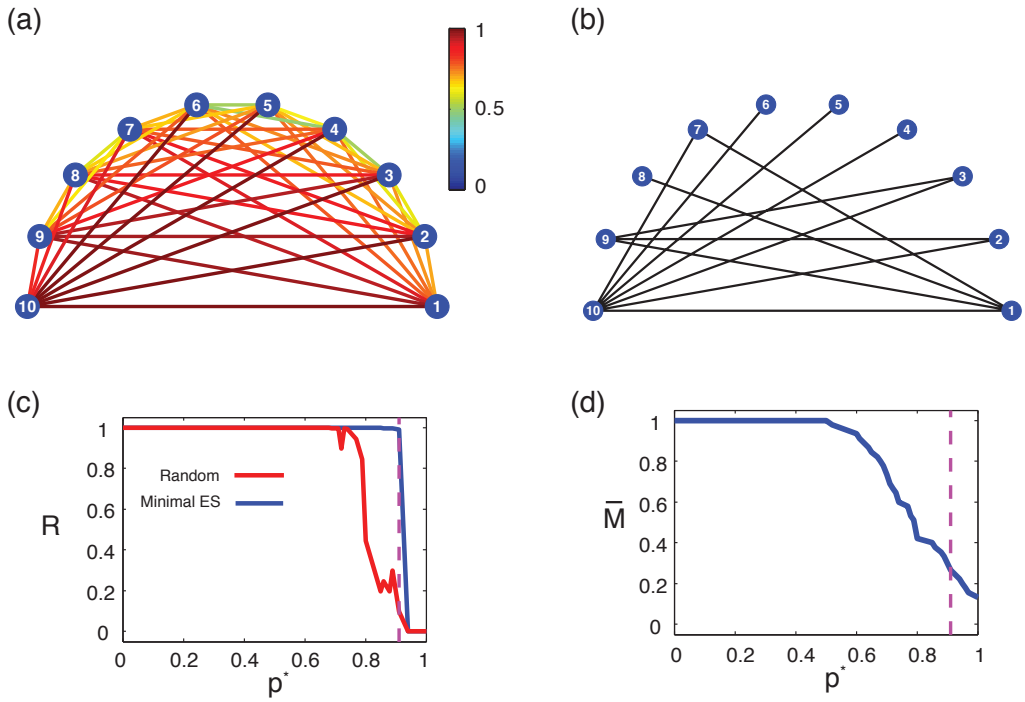

Figure **5-8**: Emergent minimal ES network with $N = 10$ and $\sigma = 1$. (a) Link activation probabilities p_{ij} generated by the variation stage of the evolutionary ES strategy; (b) Minimal ES network obtained selecting $p^* = 0.91$. (c) Order parameter of the minimal ES network as a function of the threshold probability value p^* (blue solid line). For comparison, the value is depicted of the order parameter for randomly generated networks (red solid line) with the same number of links. The vertical (purple dotted line) represents the threshold we choose at the selection stage to find the minimal ES network. As can be seen, the order parameter of the minimal ES network rapidly decrease in the proximity of the threshold we choose. Indeed the network does not guarantee any phase locked solution above that threshold. (d) Relative number of links $\bar{M}$ of the minimal ES structure (when compared to the number of links of the all-to-all structure).

Moreover, we select the natural frequencies from a normal distribution with mean equal to 1 and standard deviation equal to 1.
The evolutionary and decentralized strategy presented in Section 5.2, allows us to find the minimal ES network (see Figure **5-8**) from the p_{ij} distribution, as the threshold $p^* = 0.91$ is selected. Similarly to the results in Section 5.3 , nodes with higher connectivity are those whose natural frequency is far from the average value. Figure **5-8** also shows the synchronization performance of the minimal ES network. As can be seen from Figure **5-8**(c), the order parameter of the minimal ES structure is close to its maximal value, i.e. $R = 1$. For the sake of comparison, the values of R^2 for a randomly generated network of the same size is also depicted in Figure **5-8**(c). It is remarkable that the value of the order parameter R remains near unity, even if, as the threshold value p^* is increased, the relative number of edges, $\bar{M}$ (when compared to the number of links of the all-to-all structure), rapidly decreases (see Figure **5-8**(d)). As a result, the minimal ES network is characterised by $M = 12$ edges, i.e. $\bar{M} = 0.27$, and $R = 0.99$.

5.7 Summary

We presented a novel strategy, based on evolution, for network synchronization. The adaptive edge snapping mechanism is used to generate a minimal network in an evolutionary manner. Indeed, our method consist of two key steps: *Variation* and *Selection*.
The minimal network emerging from that evolutionary strategy was investigated. Our results suggest that heterogeneity is the driving force determining the evolution of state-dependent functional networks. This can explain the structural properties detected in natural networks such as neural interconnections in the brain, gene regulatory networks or ecological networks where the states of the nodes typically affects the evolution of their interconnections [5, 7, 32]. Also assortativity is a central feature of emerging minimal ES networks, determining its synchronizability properties (see Table **5-1**).
Next, we will discuss the dynamics of two Kuramoto oscillators coupled via edge snapping mechanism. This model, yet very simple, will be used to study robustness properties of a network of N coupled Kuramoto oscillators, when a node is perturbed from the synchronized state.

[2]The values of R are the average over the simulation interval, i.e. $R = \frac{1}{T}\int_{t_0}^{t_0+T_s} R(t)dt$, where t_0 is the initial instant and T_s is the simulation time.

CHAPTER 6

Dynamics, stability and robustness of evolving strategies

The evolutionary strategy presented in Chapter 5, is based on adaptation of coupling gains through edge snapping. The output of variation stage is a collection of network structures emerging from several adaptation trials. Therefore, understanding the main dynamical features of such adaptation is of utmost importance. In [20] convergence properties of edge snapping, in the case of nonlinear oscillators at each node, are shown in terms of appropriate MSF functions (see Chapter 2). Nonetheless, the model we proposed for the variation step of the evolutionary strategy contains several parameters that do influence the emerging network structure. In this Chapter we provide an ad-hoc analysis of the dynamics, stability and robustness of the evolving strategies we proposed starting from the simplest case of two coupled oscillators. Moreover, in the last part we will see how that model can be useful in the general case of N coupled oscillators.

6.1 Dynamics of adaptively coupled Kuramoto oscillators: a brief overview

The dynamics of coupled Kuramoto oscillators has been studied extensively in the literature. As discussed in Chapter 3, results range from the case of all-to-all interconnection structure to sparse connected[1] networks. However, the case in which the coupling gains are subject

[1] Usually, when considering a generic network describing the interaction among oscillators, there is a nonzero hypothesis about the second smallest eigenvalue of the Laplacian matrix. That condition yields connect-

to evolving (adaptive) laws is poorly explored. In this Section a brief literature overview is provided, recalling works that are most related to that presented in this Thesis.

A novel adaptive strategy in a network of Kuramoto oscillators is introduced in [5]. Here, the idea is to design an adaptation mechanism for the coupling that promotes the connection strengths between those elements that are dynamically correlated. An instantaneous phase correlation p_{nm} between m-th and n-th oscillators is defined as $p_{nm} := \frac{1}{2}\left|e^{i\theta_m(t)} + e^{i\theta_n(t)}\right|$, where $\theta_m(t)$ and $\theta_n(t)$ are the phases of oscillators m and n, respectively. Then, the adaptation law is chosen as $\dot{k} = (p_{nm} - p_c)k_{nm}(1 - k_{nm})$, where p_c is a threshold and k_{nm} is the coupling gain between oscillators. The main result is that modularity and assortativity features (see Chapter 2) emerge spontaneously and simultaneously. Moreover, is proven in [5] that such an emergent structure is associated with an asymptotic arrangement of the collective dynamical state of the network into cluster synchronization.

A different approach is presented in [77], where a first order sinusoidal adaptive law is proposed for the coupling gains. Thus, the model considered is

$$\dot{\theta}_i = \omega_i + \tfrac{1}{N}\textstyle\sum_{j=1}^{N} k_{ij}\sin(\theta_j - \theta_i) \tag{6-1a}$$

$$\dot{k}_{ij} = \epsilon\left[\alpha\cos(\theta_i - \theta_j) - k_{ij}\right] \tag{6-1b}$$

i.e. a Kuramoto oscillator at each node, with an evolving coupling k_{ij} whose adaptation is described by Equation (6-1b). For small ϵ, one can expect that, for a couple of nonsynchronized oscillators, the driving term $\alpha\cos(\theta_i - \theta_j)$ is oscillating around zero. Thus, the the coupling gain k_{ij} is also oscillating around zero. Instead, for two synchronized oscillators, the driving term produces a constant nonzero value. Therefore, for large enough α, the coupling gain between the two synchronized oscillators will be strengthened. For the sake of simplicity, the analysis in [77] starts from two coupled oscillators. In this case the model can be recast as

$$\dot{\Phi} = \Delta\omega - k\sin\Phi \tag{6-2a}$$

$$\dot{k} = \epsilon(\alpha\cos\Phi - k) \tag{6-2b}$$

where $\Phi = \theta_2 - \theta_1$ is the phase difference between the oscillators, $\Delta\omega = \omega_2 - \omega_1$ is the difference between their natural frequencies and k the coupling gain. We note here that

edness of the network structure.

stable fixed points of system (6-2) correspond to phase-locked solutions of system (6-1), with $N = 2$. Moreover, unbounded solutions of system (6-2) are related to divergent solutions of the original model (6-1) when $N = 2$. One of the main results in [77] is that, varying the parameters α and ϵ, three situations are possible: (a) there are no fixed points, (b) there are only stable fixed points and (c) there is coexistence of fixed points and unbounded solutions. A converse approach in the adaptation rule is taken in [61]. Therein an evolving law is selected fostering coupling between pairs of nodes that are desynchronized, i.e. pairs of nodes which have larger phase incoherence. Thus, the network model becomes

$$\dot{\theta}_i = \omega_i + \tfrac{1}{N}\textstyle\sum_{j=1}^{N} k_{ij}\sin\left(\theta_j - \theta_i\right) \tag{6-3a}$$

$$\dot{k}_{ij} = \epsilon\left[\alpha\sin\left(\beta(\theta_i - \theta_j)\right) - k_{ij}\right] \tag{6-3b}$$

Authors in [61] point out that the evolving mechanism (6-3b) does make the whole network prone to synchronization. To this aim, a comparison is provided in [61] between the evolving network in Equation (6-3), and a static network with the same overall coupling strength. In other words, both static and evolving networks are such that $\sum_{i,j} k_{ij}^{static} = \sum_{i,j} k_{ij}^{evolving}$, with clear interpretation of superscripts. Results show that the evolving networks achieve better synchronization performance, in terms of relative phase difference (and thus in terms of the overall order parameter, see Chapter 3), compared to static ones. As a result, the synchronization speed and the steady-state phase difference can be adjusted and enhanced by appropriately tuning the parameters ϵ, α and β of the adaptive law. We note here, a similar adaptation law, given by $\dot{k}_{ij} = -\epsilon[\sin\left(\theta_j - \theta_i + \beta\right)]$, was introduced in [4]. Authors found that, depending on β, three fundamental states of collective behaviour are possible. Namely, there is a two state cluster in which the oscillators are, basically, organized in two synchronized groups. Another type is called coherent state, where oscillators are arranged sequentially in time. Finally in the chaotic state the relative phases between oscillators and their coupling weights are chaotically shuffled.

6.2 Dynamics of two oscillators coupled via Edge Snapping

As we discussed in Chapter 2, edge snapping is a viable method for network synchronization. Moreover, in Chapter 5 we investigated the structural and functional properties of

networks, emerging from the co-evolution of Kuramoto dynamics and edge snapping mechanism, through an evolutionary strategy based on variation and selection. In this Section, we will recall our model, analysing its dynamical features and its dependence upon network parameters. We will focus on the simplest case of two coupled Kuramoto oscillators via an edge snapping evolving strategy. For the sake of clarity, we recall the network model presented in Chapter 5

$$\begin{aligned}
\dot{\theta}_1 &= \omega_1 + \frac{k}{N}\sin(\theta_2 - \theta_1) \\
\dot{\theta}_2 &= \omega_2 + \frac{k}{N}\sin(\theta_1 - \theta_2) \\
\ddot{k} + d\ \dot{k} + \frac{\partial V(k)}{\partial k} &= \alpha\left(1 - \left|\frac{e^{i\theta_1} + e^{i\theta_2}}{2}\right|^2\right)
\end{aligned} \tag{6-4}$$

where the first two equations represent the phase evolution of two Kuramoto oscillators, while the latter describes an edge snapping mechanism. In particular, $V(k)$ is the potential and has been chosen as $V(k) = bk^2(k-1)^2$. Thus, the third equation can be rewritten as

$$\ddot{k} + d\ \dot{k} + 2b(2k^3 - 3k^2 + k) = \alpha\left(1 - \left|\frac{e^{i\theta_1} + e^{i\theta_2}}{2}\right|^2\right) \tag{6-5}$$

Note that in Chapter 5, the second term in Equation (6-5) was taken equal to $\alpha\left(1 - \left|\frac{e^{i\theta_1}+e^{i\theta_2}}{2}\right|\right)$ instead of $\alpha\left(1 - \left|\frac{e^{i\theta_1}+e^{i\theta_2}}{2}\right|^2\right)$. We emphasize that, as expected, similar results still hold with this choice. Moreover, defining $\psi = \theta_2 - \theta_1$ and $\Delta\omega = \omega_2 - \omega_1$, system (6-4) can be rewritten as the third order system

$$\begin{aligned}
\dot{\psi} &= \Delta\omega - k\sin\psi \\
\dot{k} &= v \\
\dot{v} &= -d\ v - 2b(2k^3 - 3k^2 + k) + \alpha\left(1 - \frac{2 + 2\cos\psi}{2}\right)
\end{aligned} \tag{6-6}$$

where k is still the coupling gain and $v = \dot{k}$ its derivative. We are interested in the dynamical features of system (6-6). Thus, we are looking for equilibria of the system, and we want to classify their stability. Setting the derivatives equal to zero yields

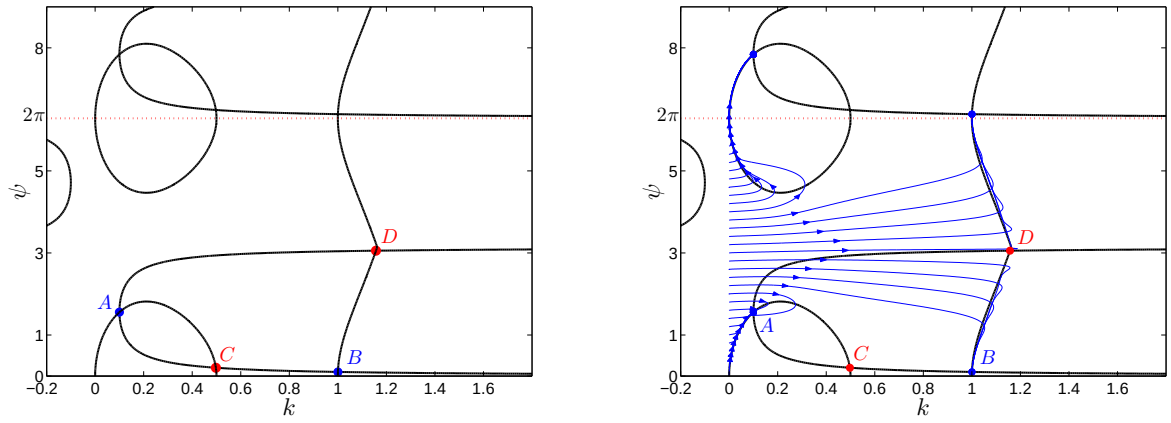

(a) (b)

Figure **6-1**: (a) Nullclines and equilibria of system (6-6). Blue dots are stable and red dots are unstable equilibria. (b) Some trajectories of system (6-6) rooted in several initial conditions, with $k = 0$ and ψ varying from 0 to 2π.

$$\begin{aligned} v &= 0 \\ \Delta\omega - k\sin\psi &= 0 \\ -2b(2k^3 - 3k^2 + k) + \alpha\left(1 - \frac{2 + 2\cos\psi}{2}\right) &= 0 \end{aligned} \tag{6-7}$$

Thus, we can study equilibria in the two-dimensional plane (k, ψ) defined by $v = 0$. In that plane, nullclines are those shown in Figure **6-1**(a), where blue dots represent stable equilibria (denoted as A and B) and the red ones are unstable equilibria (C and D). We recall that stable equilibria are related to phase-locked solutions. Moreover, nullclines in Figure **6-1**(b) are obtained for nominal values of model parameters $\Delta\omega = 0.1, b = 20, d = 10, \alpha = 10$.
As noticed above, there are several parameters characterizing our model. Nullclines and trajectories showed in Figure **6-1**, are obtained for nominal values of the parameters, given by $\Delta\omega = \ 0.1$, $b = 20, d = 10, \alpha = 10$. Next we study the structural robustness of system (6-6), against perturbations of parameters from their nominal values.
Robustness properties are analysed varying each parameter, one at a time, over a wide range. In detail, we considered 4 cases

1. $\Delta\omega = 0.1$, $b \in [0, 200], d = 10, \alpha = 10$;

2. $\Delta\omega = 0.1$, $b = 20, d \in [0, 500], \alpha = 10$;

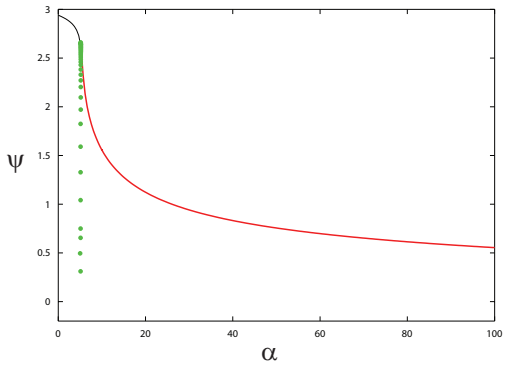

(a) Varying α.

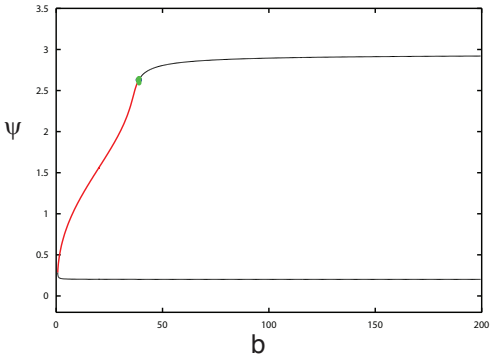

(b) Varying b

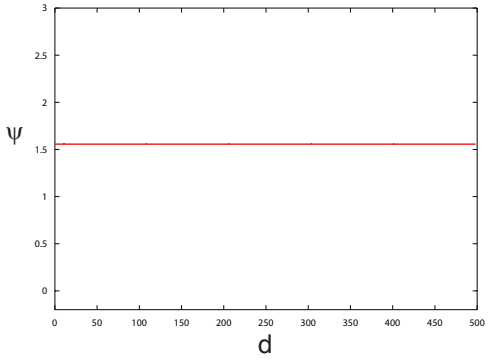

(c) Varying d

Figure **6-2**: Parameters variation (equilibrium A). Red(black) line are associated to stable(unstable) solutions. Green dots are related to the amplitude of stable limit cycles.

3. $\Delta\omega = 0.1$, $b = 20, d = 10, \alpha \in [0, 100]$;

4. $\Delta\omega \in [0, 2]$, $b = 20, d = 10, \alpha = 10$

Results of cases 1 to 3 are shown in Figure **6-2**. Bifurcation diagrams are obtained using XPP/Auto software. Figures **6-2**(a)-(b) show the onset of oscillations as limit cycles can appear varying b and α. Thus, if b and α are not appropriately selected, the coupling gain k and the phase difference ψ between oscillators, can start to persistently oscillate. On the contrary, varying d is not observed to produce any significant modification of the dynamics of system (6-9). When $\Delta\omega$ is varied, instead, equilibrium A moves as showed in Figure **6-3**. Here a Hopf bifurcation occurs. Then equilibria B and C collide and disappear.
Equilibrium B represents the situation in which phase locking occurs with link activation between nodes. Thus, the coupling gain k is close to 1, while the phase difference ψ is smaller,

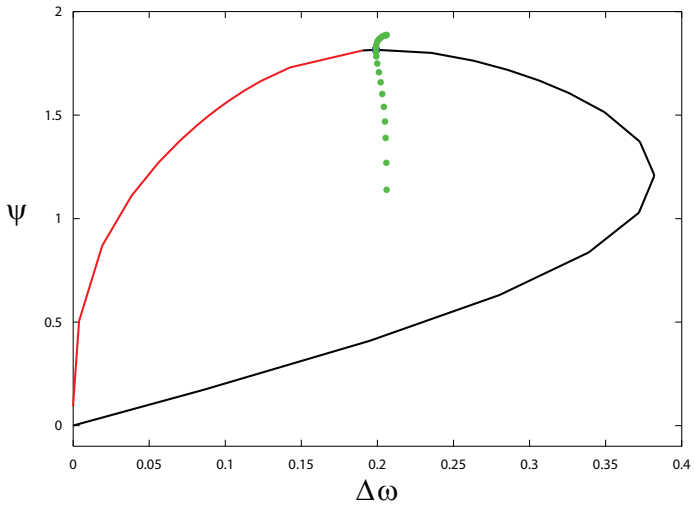

Figure **6-3**: Behaviour of equilibrium A varying $\Delta\omega$. Red(black) line are associated to stable(unstable) solutions. Green dots are related to the amplitude of stable limit cycles.

compared to Equilibrium A. Varying edge snapping parameters α, b and d, equilibrium A does not show significant variations, as illustrated in Figure **6-4**. Variations of $\Delta\omega$, instead, produces a saddle node bifurcation, as shown in Figure **6-5**.

6.3 Two oscillators model

In this Section we will explore robustness properties of the evolutionary method presented in Chapter 5. In order to asses such robustness features, we will assume that co-evolutionary dynamics converges to a synchronized state. In that state, each oscillator moves at same angular velocity Ω, forming what we call a "giant cluster". We note here, that the giant cluster rotates, at steady state, as a single unit. Nevertheless, within the cluster, oscillators display nonzero phase differences among each other, due to heterogeneity of their natural frequencies.

Now, let us perturb a node from the synchronized state, i.e. add a perturbing term to its dynamics kicking it out from the giant cluster. What happens to the whole system? Will the perturbed node be still entrained, after a transient?

To analyse what happens after a perturbation of a single node, it is convenient to have a snapshot of the dynamics before the perturbation. To this aim, let us denote N^+ as the

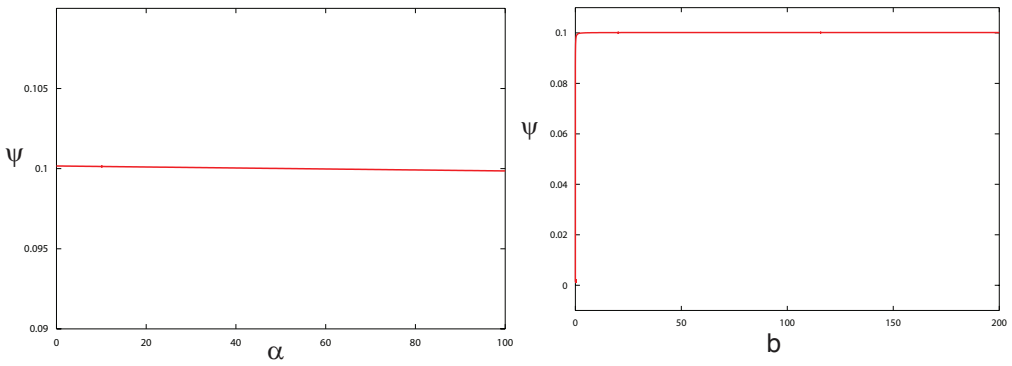

(a) Varying α. (b) Varying b.

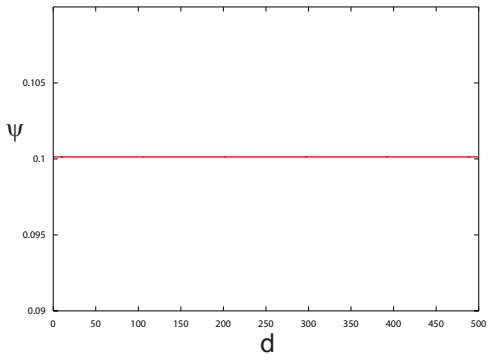

(c) Varying d.

Figure **6-4**: Parameters variation (equilibrium B). Red (black) lines are associated to stable (unstable) solutions.

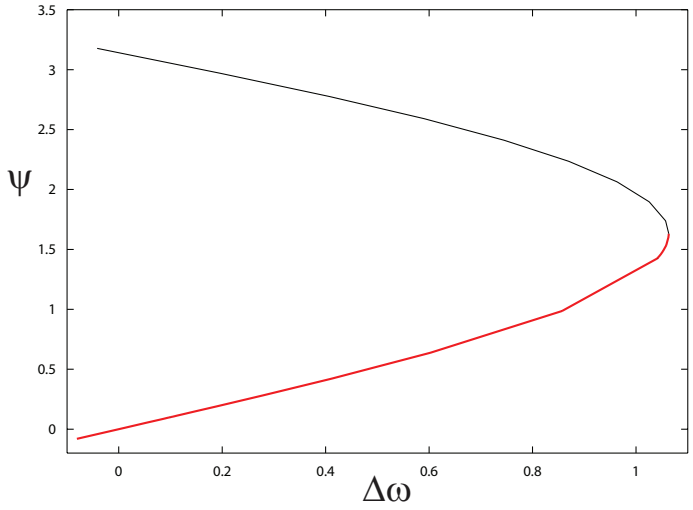

Figure **6-5**: Behaviour of equilibrium B varying $\Delta\omega$. Red (black) lines are associated to stable(unstable) solutions.

number of activated links between the perturbed node and the cluster, before the action of the disturbing term, and N^0 as the number of links that are switched off. Recall that $N^+ + N^0 = N - 1$. We can write

$$\dot{\Theta} = \Omega + \tfrac{1}{N}(N^+k^+ + N^0k^0)\sin(\phi - \Theta) \tag{6-8a}$$

$$\dot{\phi} = \omega + \tfrac{1}{N}(N^+k^+ + N^0k^0)\sin(\Theta - \phi) \tag{6-8b}$$

where Equation (6-8a) described the aggregate dynamics of the giant cluster and (6-8b) describes the dynamics of the oscillator which has been perturbed away from the cluster. Moreover, Θ is the average phase of oscillators within the cluster, ϕ and ω represent phase and natural frequency, respectively, of node subject to perturbation. We note here the that we have separated the activated links $k^+ \approx 1$ from those that have not been activated associated to $k^0 \approx 0$. Now, defining $\psi = \Theta - \phi$ and $\rho^+ = \frac{N^+}{N}$, model (6-8) can be rewritten as

$$\dot{\psi} = \Delta\omega - 2\rho^+ \sin\psi \tag{6-9}$$

If $\rho^+ < \Delta\omega/2$, system (6-9) has two equilibria, in the interval $\psi \in [0, 2\pi]$. One

$$\psi_1^* = \sin^{-1}\left(\frac{\Delta\omega}{2\rho^+}\right)$$

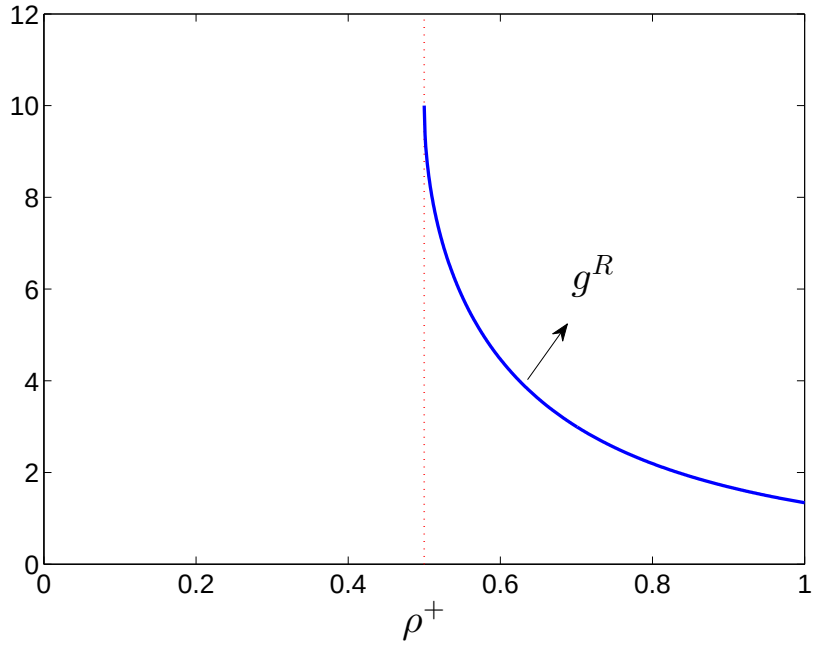

Figure **6-6**: Schematic illustration of condition (6-12). Red dotted line divides the plane in two regions $\rho^+ > \Delta\omega/2$ and $\rho^+ < \Delta\omega/2$. Function g^R is obtained for $\Delta\omega = 1$.

is stable and the other one

$$\psi_2^* \;=\; \sin^{-1}\left(\frac{\Delta\omega}{2\rho^+}\right) + \pi$$

is unstable. The existence of a stable equilibrium guarantees phase-locking of system (6-8). Thus, after a perturbation, cohesiveness of the giant cluster and the perturbed node can be achieved. Moreover, the phase difference between the two will correspond to ψ_1^*. Nevertheless, we still have to analyse edge dynamics, in order to find conditions under which network structure reacts to the perturbation, i.e. conditions ensuring new links will be activated after the perturbation. Note that, in the limit $d \to \infty$, we recover, for edge snapping, the static situation $\dot{k} = 0$. Thus, edge dynamics collapse into the equation

$$\frac{\partial V(k)}{\partial k} = \alpha\left[1 - \left(\frac{2 + 2\cos\psi}{4}\right)\right] \tag{6-10}$$

where the right-hand side is the driving force depending upon ψ and the left-hand side term represent a forcing term due to potential energy in the double-well potential. Therefore, the driving force has to be greater than the potential term, in order for the link to be activated.

Namely, a sufficient condition for link activation is given by

$$\left.\frac{\partial V(k)}{\partial k}\right|_{k=1/2} < \alpha \left[1 - \left(\frac{2+2\cos\psi}{4}\right)\right]\Bigg|_{\psi=\psi_1^*} \tag{6-11}$$

where we selected $k = 1/2$ to get the potential energy associated with the highest point of the barrier between two potential wells. Note that the analysis gives a sufficient condition, as we are neglecting the dynamical terms. The usual choice of the potential, $V(k) = bk^2(k-1)^2$, yields

$$b < g^R \tag{6-12}$$

where $g^R = \alpha\left(1 - \sqrt{1 - \frac{\Delta\omega^2}{4\rho^2}}\right)$ is depicted in Figure **6-6**. Thus, if b is selected below g^R, no links are activated. Otherwise new links will be activated through edge snapping. In both cases, phase-locking is achieved and the perturbed node will be entrained.

When $\rho^+ < \Delta\omega/2$ system (6-9) has no equilibria. This means the number of active links before perturbation, is not sufficiently high to entrain node subject to perturbation. Inspired by [94, 42], we can statisically characterize the generic solution ψ. Indeed, instead of the drifting solution ψ, we use an invariant measure, i.e. the probability density $p(\psi, \rho^+)$ such that $E[\psi] = \int_0^{2\pi} \psi \; p(\psi, \rho^+) d\psi$, which is inversely proportional to the drift velocity of ψ. Thus, $p(\psi, \rho^+) = C(\Delta\omega - 2\rho^+ \sin\psi)^{-1}$, where C is a normalization constant given by $C = \frac{\sqrt{\Delta\omega^2 - \rho^{+2}}}{2\pi}$. This invariant measure is used for replacing the driving force $u(\psi)$ with its statistical average $E[u(\psi)] = \int_0^{2\pi} u(\psi) \; p(\psi, \rho^+) d\psi$.

Now, characterizing the driving force $u(\psi) = \alpha\left[1 - \left(\frac{2+2\cos\psi}{4}\right)\right]$ yields

$$E[u(\psi)] = \int_0^{2\pi} u(\psi) p(\psi, \rho^+) d\psi = \frac{\alpha}{2} \tag{6-13}$$

Thus, following the same reasoning for the case $\rho > \Delta\omega/2$, we have

$$b < g_L \tag{6-14}$$

with $g_L = \alpha$. The inequality (6-14) provides a sufficient condition to activate new links. As shown in Figure **6-7**, if the heigh of the barrier b is selected below function g_L, new links are activated. Note that $b < g_L$ also guarantees entrainment of node subject to perturbation, i.e. phase-locking between node and the giant cluster. Contrariwise, if $b > g_L$ then incoherence will persist.

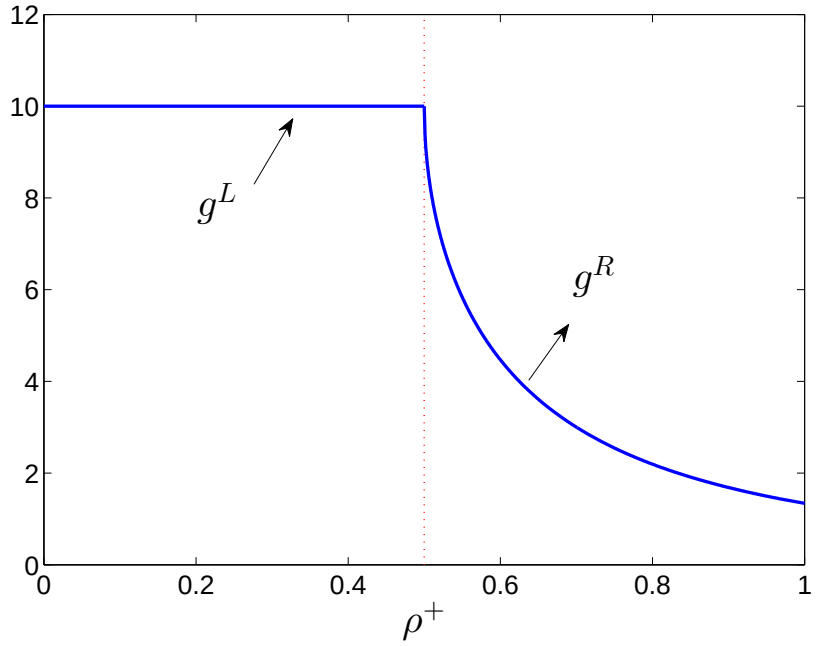

Figure **6-7**: Schematic illustration of functions g^R and g_L. Red dotted line divides the plane in two regions $\rho^+ > \Delta\omega/2$ and $\rho^+ < \Delta\omega/2$. Functions g^R and g^L are obtained for $\Delta\omega = 1$.

6.4 Summary

Co-evolution of Kuramoto dynamics with edge snapping mechanism results in a robust method to achieve synchronization via evolution of the network structure. Parameters can be adjusted to enhance synchronization performance in terms of phase difference between pairs of oscillators. The height of the barrier b of double-well potential, together with the control parameter α, strongly influence robustness properties of evolving mechanism. Of course, the increase of α has to be bounded. Indeed, the more α is increased the more the control effort is. Also, the barrier could be engineered to weaken link activation. Indeed, as we have seen in Section 6.3, if $\rho^+ > \Delta\omega/2$ there is no need to activate new links to recover synchronization, after a perturbation. Thus, in that case, the barrier b could be increased. On the other hand, when $\rho^+ < \Delta\omega/2$ the height of the barrier could be decreased to foster link activation.

Next Chapter deals with a further line of research related to convergence of multi-agent systems via Contraction theory, a tool recently proposed in the literature to study convergence of dynamical systems and networks.

CHAPTER 7

Synchronization via contraction theory

In Chapter 2 we presented the fundamental problem of steering the collective behaviour of a network of dynamical agents towards a desired common target solution. As an example, we analysed synchronization and consensus in a network of linear and nonlinear systems. Here, the key problem is to prove convergence of all agents towards the desired common behaviour. This convergence problem is usually solved locally, by means of MSF approach (see Section 2.2.1), or globally via Lyapunov theory [44]. Global results are very useful, particularly when dealing with noise or perturbations. Contraction theory has been recently proposed as an effective approach to study convergence between trajectories of a dynamical systems (see for example [46] and the more recent papers [70, 71, 27, 79, 1, 2]). The idea is to characterize within some metric the distance between trajectories and prove that the matrix measure of the system Jacobian is negative in that metric, over some connected forward-invariant set of the state space. Indeed, it can be showed that this condition implies global exponential incremental stability over the set of interest. Thus, two trajectories starting from different initial conditions in that set, will asymptotic converge towards each other. Moreover, this approach does not require finding explicitly Lyapunov functions for the system of interest. It has been shown that contraction is an extremely useful property to analyze convergence in networks and study problems such as the emergence of synchronization or consensus ([46, 87, 57, 70, 67, 69]). In this Chapter, we provide an overview on a further part of the work, dealing with contraction theory as a tool to study synchronization problems.

Table **7-1**: Vector Norms, Induced Matrix Norms and Matrix Measure

Vector Norm	Induced Matrix Norm	Matrix Measure
$\|x\|_1 = \sum_{i=1}^n \|x_i\|$	$\|A\|_{i1} = \max_j \sum_{i=1}^n \|a_{ij}\|$	$\mu_1(A) = \max_j[a_{jj} + \sum_{i\neq j} \|a_{ij}\|]$
$\|x\|_2 = (\sum_{i=1}^n \|x_i\|^2)^{1/2}$	$\|A\|_{i2} = \left[\lambda_{max}\left(A^T A\right)\right]^{1/2}$	$\mu_2(A) = \lambda_{max}\frac{A^T+A}{2}$
$\|x\|_\infty = \max_i \|x_i\|$	$\|A\|_{i\infty} = \max_i \sum_{j=1}^n \|a_{ij}\|$	$\mu_\infty(A) = \max_i[a_{ii} + \sum_{j\neq i} \|a_{ij}\|]$

7.1 Mathematical Preliminaries

Throughout this chapter, $\mathbb{R}^{n\times n}$ denotes the set of all $n \times n$ real matrices. We now introduce the matrix measure associated to a matrix $A \in \mathbb{R}^{n\times n}$, that is the function $\mu_i(\cdot) : \mathbb{R}^{n\times n} \to \mathbb{R}$ defined in the following way.

Definition 7.1.1 (Matrix measure [86])**.** *Given a real matrix $A \in \mathbb{R}^{n\times n}$ the corresponding matrix measure $\mu(A)$ is defined as*

$$\mu_i(A) = \lim_{h\to 0^+} \frac{\|I + hA\|_i - 1}{h}$$

The measure of a matrix A can be thought of as the directional derivative of the induced matrix norm function $\|\cdot\|_i$, evaluated at the identity matrix I, in the direction of A. In table **7-1**, three different types of vector norm are considered together with the respective induced matrix norm and matrix measure. In general, given a constant invertible matrix P, the matrix measure $\mu_{P,i}$ induced by the weighted vector norm $|x|_P = |Px|$ can also be defined as $\mu_{P,i} = \mu_i(PAP^{-1})$.

Definition 7.1.2 ($\mathcal{K}$ function [40])**.** *A scalar continuous function $\alpha(r)$ defined for $r \in [0, a)$ is said to belong to class $\mathcal{K}$ if it is strictly increasing and $\alpha(0) = 0$. It is said to belong to class $\mathcal{K}_\infty$ if it is defined for all $r \geq 0$ and*

$$\lim_{r\to\infty} \alpha(r) = \infty$$

Definition 7.1.3 ($\mathcal{KL}$ function [40])**.** *A scalar continuous function $\beta(r, t)$ defined for $r \in [0, a)$ and $t \in [0, \infty)$ is said to belong to class $\mathcal{KL}$ if, for each fixed $\bar{t}$, $\beta(r, \bar{t})$ belongs to class $\mathcal{K}$ with respect to r and for each fixed $\bar{r}$, the mapping $\beta(\bar{r}, t)$ is decreasing with respect to t and*

$$\lim_{t\to\infty} \beta(\bar{r}, t) = 0$$

7.2 Contraction Theory and Incremental Stability

Next, we provide some definitions concerning the stability of a nonlinear dynamical system of the form:

$$\dot{x} = f(x,t) \tag{7-1}$$

where $x \in \mathbb{R}^n$, $t \in R$ and $f : \mathbb{R}^n \times \mathbb{R} \mapsto \mathbb{R}^n$. We denote with $\phi(t - t_0, t_0, x_0)$ the value of the solution $x(t$ at time t of the differential equation (7-1) with initial value $x(t_0) = x_0$. We say that a set $C \subseteq \mathbb{R}^n$ is a *forward invariant* set for system (7-1), if for every $t_0 \geq 0$, $x(t_0) = x_0 \in C$ implies $\phi(t - t_0, t_0, x_0) \in C$ for all $t \geq t_0$.
Specifically, we are interested in characterizing the stability of any two arbitrary solutions of the system with respect to one another. We refer to this property as *incremental stability*, using the definition first presented in [3].

Definition 7.2.1 (Incremental stability [3])**.** *System (7-1) is said to be* Incrementally Asymptotically Stable *(δAS) in a forward invariant set $C \subseteq \mathbb{R}^n$, if there exists a class $\mathcal{KL}$ function β, such that, for any $x_0, z_0 \in C$ and $t \geq t_0$, any two of its trajectories, say $x(t) = \phi(t - t_0, t_0, x_0)$ and $z(t) = \phi(t - t_0, t_0, z_0)$, verify*

$$|x(t) - z(t)| \leq \beta(|x_0 - z_0|, t - t_0)$$

Moreover, if there exist real numbers $c > 0, K \geq 1$ such that for all $t \geq 0$

$$|x(t) - z(t)| \leq K |x_0 - z_0| e^{-c(t-t_0)}$$

we say that system (7-1) is *Incrementally Exponential Stable (δES)*. Finally, if $C = \mathbb{R}^n$, then system (7-1) is said to be *Globally Incrementally Asymptotically Stable* (δGAS) or *Globally Incrementally Exponentially Stable* (δGES), respectively.
An effective approach to prove incremental stability is to use the concept of contracting system as expounded in [46].

Definition 7.2.2 (Infinitesimal Contraction)**.** *System* (7-1) *is said to be infinitesimally contracting on a set $\mathcal{C} \subseteq \mathbb{R}^n$ if there exits a norm in $\mathcal{C}$, with associated matrix measure $\mu_i(\cdot)$, such that, for some constant $c > 0$ (termed as contraction rate), it holds that:*

$$\mu(J(x,t)) \leq -c, \qquad \forall x \in \mathcal{C}, \quad \forall t \geq 0.$$

In [46, 71] it is shown that the following sufficient condition for δES holds

Theorem 7.2.1. *[71] Suppose $\mathcal{C}$ is a convex subset of $\mathbb{R}^n$ and that system (7-1) is infinitesimally contracting with contraction rate c. Then for every two solutions $x(t) = \varphi(t, 0, x_0)$, $z(t) = \varphi(t, 0, z_0)$ it holds that:*

$$|x(t) - z(t)| \leq e^{-ct} |x_0 - z_0| \tag{7-2}$$

Proof. See [71].

□

Remark 7.2.1. *From Theorem 7.2.1, it is clear that if $\mathcal{C} = \mathbb{R}^n$, then system (7-1) is δGES.*

7.2.1 Example

As a representative example, we consider the model

$$\begin{cases} \dot{x}_1 = x_1(x_1^2 + x_2^2 - 1) + x_2 \\ \dot{x}_2 = -x_1 + x_2(x_1^2 + x_2^2 - 1) \end{cases}$$

The Jacobian matrix of the system is

$$J = \begin{bmatrix} -1 + 3x_1^2 + x_2^2 & 1 + 2x_1x_2 \\ -1 + 2x_1x_2 & -1 + x_1^2 + 3x_2^2 \end{bmatrix}$$

and its symmetric part is given by

$$J_s := \frac{J + J^T}{2} = \begin{bmatrix} -1 + 3x_1^2 + x_2^2 & 2x_1x_2 \\ 2x_1x_2 & -1 + x_1^2 + 3x_2^2 \end{bmatrix}$$

Now, computing the eigenvalues $\lambda_i(J_s)$ yields

$$\begin{aligned} \lambda_1 &= x_1^2 + x_2^2 - 1 \\ \lambda_2 &= 3x_1^2 + 3x_2^2 - 1 \end{aligned}$$

It is simple to verify that

$$\lambda_2 > \lambda_1 \qquad \forall\, x \in \mathbb{R}^2$$

Thus $\mu_2(J_s) < 0$ implies

$$3x_1^2 + 3x_2^2 - 1 < 0$$

i.e. $\mu_2(J_s) < 0$ for all x in the circle of radius $\sqrt{3}/3$ centred at the origin. Thus, we select the set $\mathcal{C}$ as

$$\mathcal{C} := \{x \in \mathbb{R}^2 : |x| < \sqrt{3}/3\}$$

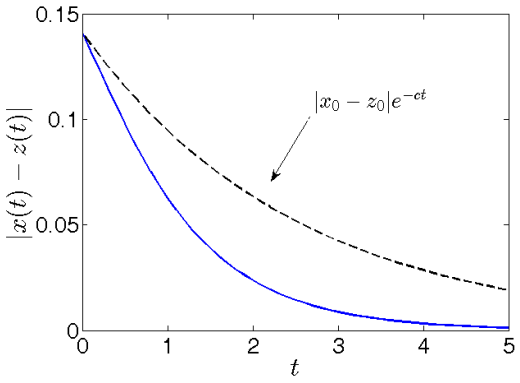

Figure **7-1**: Norm of the error (blue solid line) between two trajectories $x(t)$ and $z(t)$ rooted in different initial conditions $x_0 = [0.4 \quad 0.2]^T$, $z_0 = [0.3 \quad 0.1]^T$. For the sake of comparison, the behaviour of $|x_0 - z_0|e^{-ct}$ is depicted (dashed black line). (Reproduced from [22]).

Since the origin is an equilibrium point and it belongs to $\mathcal{C}$, we can conclude that the set $\mathcal{C}$ is a forward invariant set for the system.
In Figure **7-1** the norm of the error is showed, between two trajectories $x(t)$ and $z(t)$ rooted in different initial conditions $x_0 = [0.4 \quad 0.2]^T$, $z_0 = [0.3 \quad 0.1]^T$.
The contraction rate c can be estimated as

$$c = \min\{|3x_{0,1}^2 + 3x_{0,2}^2 - 1|, \quad |3z_{0,1}^2 + 3z_{0,2}^2 - 1|\}$$

where $x_{0,i}$ and $z_{0,i}$ are the i-th component of the vectors x_0 and z_0, respectively. Thus, we have $c = 0.4$.

7.2.2 Properties of contracting systems

Contracting systems have been shown to possess several useful properties. Consider a system of the following form:

$$\dot{x} = f(x, t)$$
$$\dot{y} = g(x, y, t)$$

where $x(t) \in \mathcal{C}_1 \subseteq \mathbb{R}^{n_1}$ and $y(t) \in \mathcal{C}_2 \subseteq \mathbb{R}^{n_2}$ for all t.
The Jacobian of this system is

$$J = \begin{bmatrix} A & 0 \\ B & C \end{bmatrix} \tag{7-3}$$

where we have written the Jacobian of f with respect to x as $A(x,t) = \frac{\partial f}{\partial x}(x,t)$, the Jacobian of g with respect to x as $B(x,y,t) = \frac{\partial g}{\partial x}(x,y,t)$, and the Jacobian of g with respect to y as $C(x,y,t) = \frac{\partial g}{\partial y}(x,y,t)$.

Theorem 7.2.2. *[71] Suppose that*

- *the system $\dot{x} = f(x,t)$ is infinitesimally contracting with contraction rate c_1*
- *the system $\dot{y} = g(x,y,t)$ is infinitesimally contracting with contraction rate c_2 when x is viewed as a parameter*
- *the mixed Jacobian $B(x,y,t)$ is bounded, that is $\|B(x,y,t)\| \leq k$, $k > 0$*

then the cascade system is infinitesimally contracting. More precisely, pick any two positive numbers p_1 and p_2 such that $c_1 - \frac{p_2}{p_1}k > 0$ and let $c := \min\left\{c_1 - \frac{p_2}{p_1}k,\ c_2\right\}$ then $\mu(J) \leq -c$.

Proof. See [71]. □

Another useful property, often exploited in applications of contraction theory to synchronization and entrainment problems, refers to the case where a contracting system is forced by an external periodic signal. In particular, given a number $T > 0$, we will say that system (7-1) is *T-periodic* if it holds that

$$f(x, t+T) = f(x,t) \qquad \forall t \geq 0$$

Notice that a system $\dot{x} = f(x, u(t))$ with input $u(t)$ is T-periodic if $u(t)$ is itself a periodic function of period T. We can then state the following basic result about existence and stability of periodic orbits.

Theorem 7.2.3. *[71] Suppose that*

- *$\mathcal{C}$ is a closed convex subset of $\mathbb{R}^n$;*
- *f is infinitisimally contracting with contraction rate c;*
- *f is T-periodic.*

Then there is a unique periodic orbit $\widehat{\omega}$ in $\mathcal{C}$ of (7-1) of period T and, for every solution $x(t)$ starting in $\mathcal{C}$, it holds that $\mathrm{dist}(x(t), \widehat{\omega}) \to 0$ as $t \to \infty$.

This property was used in [71] to prove global entrainment of transcriptional biological networks and can be effectively used whenever the goal is to prove entrainability of a system or network of interest.

7.3 Synchronization and Contraction Theory

Next we discuss how contraction analysis can be used to prove convergence in networks of nonlinear systems and prove their synchronization. We consider a generic homogeneous network whose nodes' dynamics can be described by the following set of differential equations

$$\dot{x}_i = f(x_i, t) + \tilde{h}_i(x_1, \dots, x_N, t), \qquad i = 1, \dots, N \tag{7-4}$$

where $x_i \in \mathbb{R}^n$ is the state vector of node i, the vector field $f : \mathbb{R}^n \times \mathbb{R}^+ \to \mathbb{R}^n$ describes the intrinsic dynamics of the i-th node, and the function $\tilde{h}_i : \mathbb{R}^n \times \cdots \times \mathbb{R}^n \times \mathbb{R}^+ \to \mathbb{R}^n$ represents the coupling function describing how the i-th node interacts with the other nodes in the network. We assume the network structure is connected.
In the case of diffusive coupling, we can write

$$\dot{x}_i = f(x_i, t) + \sum_{j \in \mathcal{N}_i} [h(x_j) - h(x_i)] \qquad i = 1, \dots, N$$

where $h : \mathbb{R}^n \to \mathbb{R}^n$ is some nonlinear coupling function, and $\mathcal{N}_i$ is the set of the neighbours of node i, that is the set of nodes connected to node i. If the coupling is linear and diffusive, the network equations then become

$$\begin{aligned} \dot{x}_i &= f(x_i, t) + \sigma \sum_{j \in \mathcal{N}_i} (x_j - x_i) \\ &= f(x_i, t) - \sigma \sum_{j=1}^{N} l_{ij} x_j \end{aligned} \tag{7-5}$$

for $i = 1, \dots, N$, where l_{ij} is the ij-th element of the Laplacian matrix L associated with the graph describing the network topology, and σ is the overall coupling strength.
In some cases it is useful to rewrite the network equations in block form

$$\dot{X} = F(X) - \sigma(L \otimes I_n)X \tag{7-6}$$

where $X = \left[x_1^T, \ \dots \ , x_n^T\right]^T \in \mathbb{R}^{nN}$, $F(X) = \left[f^T(x_1), \ \dots \ , f^T(x_N)\right]^T$ is the stack vector of all node vector fields, and $\otimes$ denotes the Kronecker product.
To prove synchronization of a complex network such as (7-6) using contraction theory several alternative approaches are available, each with its own advantages and limitations. In what follows we will expound some of the most common methodologies presented in the literature highlighting their advantages and limitations. Specifically we will discuss the following strategies: (i) virtual system method; (ii) contraction to flow-invariant subspaces; (iii) hierarchical approach.

7.4 Virtual system method

The virtual system method, firstly presented in [46, 87], is based on proving synchronization by constructing a virtual (or *auxiliary*) system whose particular solutions are the solutions of each of the nodes in the network. Specifically, the virtual system has as solutions all the solutions $x_i(t)$ of the original network and a particular solution, say $y_\infty(t)$, that verifies a smooth specific property. Then, if the virtual system is proved to be contracting then all its trajectories converge exponentially towards each other and towards y_∞. Therefore, all trajectories of the nodes in the network verify the same property exponentially. If a virtual system exist, then the original system (or network) is said to be *partially contracting*.
To illustrate the previous idea let us consider as a simple example, a network of two diffusively coupled identical nodes

$$\begin{cases} \dot{x}_1 = f(x_1) + h(x_2) - h(x_1) \\ \dot{x}_2 = f(x_2) + h(x_1) - h(x_2) \end{cases}$$

To prove convergence of x_1 and x_2 towards each other, we can construct the following virtual system

$$\dot{y} = f(y) - 2h(y) + h(x_1) + h(x_2)$$

Indeed, it is immediate to verify that this system has $x_1(t)$ and $x_2(t)$ as particular solutions, and if it is contracting, that is if for all x_1 and x_2,

$$\mu\left(\frac{\partial f(y)}{\partial y} - 2\frac{\partial h(y)}{\partial y}\right) \leq -c \quad \forall y \in \mathcal{C}, \ \ \forall t \geq 0$$

then the two node trajectories exponentially converge towards each other in $\mathcal{C}$ and the network synchronizes.

7.4.1 Synchronization of networks with an all-to-all topology

As discussed in [87], constructing virtual systems is not, in general, an easy task given a generic network structure. It becomes immediate in the case of fully connected networks. Specifically, consider the all-to-all network

$$\begin{aligned} \dot{x}_i =& f(x_i) + \sum_{j=1}^{N} [h(x_j) - h(x_i)] \\ =& f(x_i) - Nh(x_i) + \sum_{j=1}^{N} h(x_j) \end{aligned}$$

for $i = 1, \ldots, N$. The virtual system can then be selected as

$$\dot{y} = f(y) - Nh(y) + \sum_{j=1}^{N} h(x_j)$$

and it is contracting if some matrix measure μ exists such that

$$\mu\left(\frac{\partial f(y)}{\partial y} - N\frac{\partial h(y)}{\partial y}\right) \leq -c \quad \forall y \in \mathcal{C}, \ \ \forall t \geq 0$$

Unfortunately the simplicity of the method is lost when more generic topologies are considered.

7.4.2 Example

As a representative example of application of the virtual system approach let us consider the all-to-all network of biological oscillators presented in [73].
The Repressilator is a synthetic biological circuit of three genes inhibiting each other in a cyclic way [**?**]. As shown in Fig. **7-2**a, gene *lacI* (associated to the state variable c_i in our model) expresses protein *LacI* (C_i), which inhibits transcription of gene *tetR* (a_i). This translates into protein *TetR* (A_i), which inhibits transcription of gene *cI* (b_i). Finally, the protein *CI* (B_i) translated from *cI* inhibits expression of *lacI*, completing the cycle. The resulting mathematical model for the network is

$$\begin{aligned}
\dot{a}_i &= -a_i + \frac{\alpha}{1 + C_i^2} \\
\dot{b}_i &= -b_i + \frac{\alpha}{1 + A_i^2} \\
\dot{c}_i &= -c_i + \frac{\alpha}{1 + B_i^2} + \frac{kS_i}{1 + S_i} \\
\dot{A}_i &= \beta_A a_i - d_A A_i \\
\dot{B}_i &= \beta_B b_i - d_B B_i \\
\dot{C}_i &= \beta_C c_i - d_C C_i \\
\dot{S}_i &= -k_{s0} S_i + k_{s1} A_i - \eta(S_i - S_e) \\
\dot{S}_e &= -k_{se} S_e + \eta_{ext} \sum_{j=1}^{N} (S_j - S_e) + u(t)
\end{aligned} \tag{7-7}$$

For further details on the mathematical model see [73].
The network is an all-to-all network of identical nodes, hence the virtual system can be

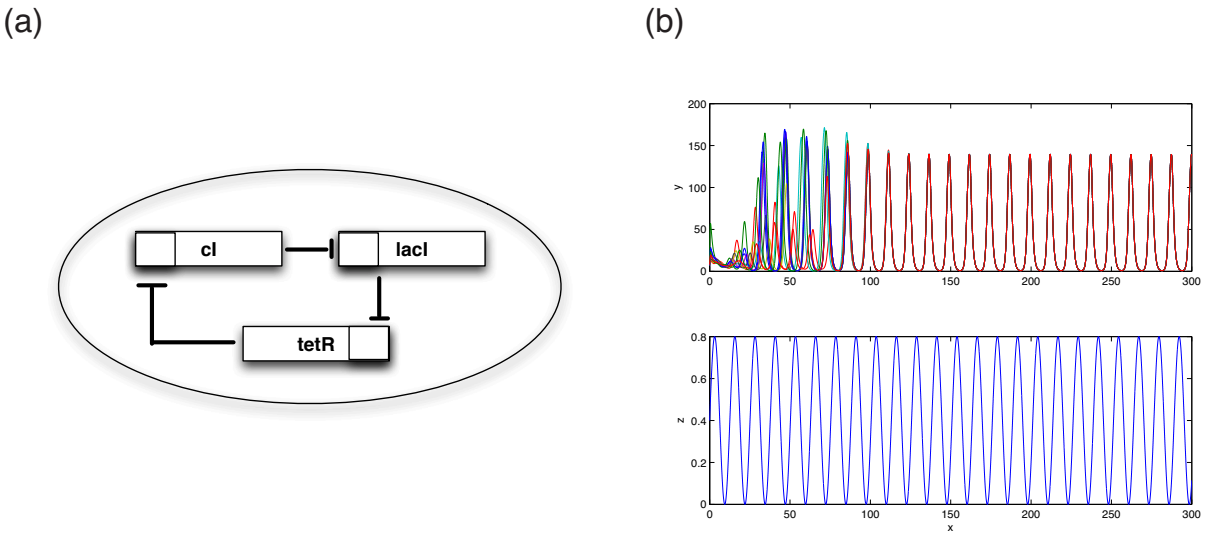

Figure **7-2**: A schematic representation of the three-genes Repressilator circuit (a). Simulation results (b). (Reproduced from [22])

chosen as having the same dynamics as the individual Repressilator circuit, forced by the external coupling signal S_e, i.e.

$$\begin{aligned}
\dot{a} &= -a + \frac{\alpha}{1+C^2} \\
\dot{b} &= -b + \frac{\alpha}{1+A^2} \\
\dot{c} &= -c + \frac{\alpha}{1+B^2} + \frac{kS}{1+S} \\
\dot{A} &= \beta_A a - d_A A \\
\dot{B} &= \beta_B b - d_B B \\
\dot{C} &= \beta_C c - d_C C \\
\dot{S} &= -k_{s0} S + k_{s1} A - \eta(S - S_e) \\
\dot{S}_e &= -k_{se} S_e + \eta_{ext}(S_1 + \cdots + S_N) - \eta_{ext} N S_e + u(t)
\end{aligned} \tag{7-8}$$

Indeed, by direct inspection it is easy to check that, by substituting the state variables of the nodes dynamics for the virtual variables (i.e., $[a_i,\ b_i,\ c_i,\ A_i,\ B_i,\ C_i,\ S_i,\ S_e]$ for $[a,\ b,\ c,\ A,\ B,\ C,\ S,\ S_e]$), the equations of each Repressilator circuit in the network can be obtained. In this sense, the virtual system embeds the trajectories of all network oscillators as particular solutions. Thus, contraction of the virtual system (7-8) implies synchronization of (7-7). Differentiation

of (7-8) yields the Jacobian matrix

$$J = \begin{bmatrix} -1 & 0 & 0 & 0 & 0 & f_1(C) & 0 & 0 \\ 0 & -1 & 0 & f_1(A) & 0 & 0 & 0 & 0 \\ 0 & 0 & -1 & 0 & f_1(B) & 0 & f_2(S) & 0 \\ \beta_A & 0 & 0 & -d_A & 0 & 0 & 0 & 0 \\ 0 & \beta_B & 0 & 0 & -d_B & 0 & 0 & 0 \\ 0 & 0 & \beta_C & 0 & 0 & -d_C & 0 & 0 \\ 0 & 0 & 0 & k_{s1} & 0 & 0 & -k_{s0} - \eta & \eta \\ 0 & 0 & 0 & 0 & 0 & 0 & 0 & -k_q \end{bmatrix}$$

where f_1 and f_2 denote the partial derivatives of decreasing and increasing Hill functions with respect to the state variable of interest and $k_q = k_{se} + \eta_{ext} N$.
Note that the Jacobian matrix J has the (transposed) structure of a cascade in (7-3), i.e.

$$J = \begin{bmatrix} A & B \\ 0 & C \end{bmatrix}$$

with

$$A = \begin{bmatrix} -1 & 0 & 0 & 0 & 0 & f_1(C) & 0 \\ 0 & -1 & 0 & f_1(A) & 0 & 0 & 0 \\ 0 & 0 & -1 & 0 & f_1(B) & 0 & f_2(S) \\ \beta_A & 0 & 0 & -d_A & 0 & 0 & 0 \\ 0 & \beta_B & 0 & 0 & -d_B & 0 & 0 \\ 0 & 0 & \beta_C & 0 & 0 & -d_C & 0 \\ 0 & 0 & 0 & k_{s1} & 0 & 0 & -k_{s0} - \eta \end{bmatrix},$$

$B = [0\ 0\ 0\ 0\ 0\ 0\ \eta]^T$, $C = -k_q$. Thus, to prove contraction of the virtual system Theorem 7.2.2 can be used. Specifically, it suffices to prove that there exist two matrix measures, μ_* and μ_{**} such that

1. $\mu_*(A) \leq -c_1$, with $c_1 > 0$
2. $\mu_{**}(C) \leq -c_2$, with $c_2 > 0$
3. $\|B\| \leq k$, with $k > 0$

Clearly, since k_q and η are positive real parameters, the second and third conditions above are satisfied. On the other hand, the matrix measure of A can be made negative by choosing the values of the parameters adequately (see [73] for further details). Thus, we can conclude that (7-8) is contracting, and in turn this implies that all the nodes of (7-7) synchronize on

the same solution, as can be noted in Fig.**7-2**b. Furthermore, if $u(t)$ is a T-periodic function, the N interconnected dynamical systems *entrain* onto a T-periodic trajectory (see Theorem 7.2.3).

7.4.3 Synchronization of networks with a generic topology

Constructing the virtual system for more generic network structures is cumbersome. A possible approach is presented in [87] where it is noted that in some cases the virtual system for a generic network structure can be written as

$$\dot{Y} = F(Y) - \sigma(L \otimes I_n)Y - (1_{N\times N} \otimes K_0)(Y - X) \tag{7-9}$$

where $Y = \left[y_1^T, \ \dots \ , y_n^T\right]^T \in \mathbb{R}^{nN}$ is the set of virtual state variables, K_0 is some constant symmetric positive definite matrix and $1_{N\times N}$ is the $N \times N$ matrix whose elements are all equal to 1.
It can again be noticed that this virtual system is such that it embeds all the solutions of the original network as particular solutions, in fact for $Y = X$ (7-9) gives (7-6). Furthermore this system admits the particular solution $y_1 = \cdots = y_N = y_\infty$ with

$$\dot{y}_\infty = f(y_\infty) - nK_0 y_\infty + K_0 \sum_{j=1}^{N} x_j(t)$$

Therefore if the virtual system is proved to be contracting then all its trajectories converge exponentially towards each other and towards y_∞, this in turns implies synchronization of the network (7-6), which is said to be *partially contracting*.
Notice that K_0 is a virtual quantity used to prove contraction of the virtual system, and thus it cannot affect the synchronization of the original network.
For a full proof of the virtual system method see [87], while the link between this approach and the Master Stability Function, see Chapter 2 is discussed in [72]. The most notable difference is that, while the MSF approach guarantees *local* transversal stability of the synchronization manifold, contraction analysis gives a *global* result in the region of interest.

7.5 Convergence to a flow-invariant linear subspace

Contraction theory can also be used to guarantee convergence of system trajectories towards some flow-invariant linear manifold [57]. Hence, synchronization can be proved by using

contraction analysis to prove global convergence of the network nodes towards the synchronization manifold defined in (2-5). A more general description of this approach is presented in [57], where the problem of concurrent sychronization is discussed.
Assume that for the dynamical system $\dot{x} = f(x,t)$ there exists a linear flow-invariant subspace $\mathcal{M}$ of dimension p. Let $[e_1, \dots, e_n]$ be an orthonormal basis of $\mathbb{R}^n$ where the first p vectors form a basis of $\mathcal{M}$ and the last $n-p$ a basis of $\mathcal{M}^\perp$. Define now the following matrices

$$U := \begin{bmatrix} e_1^T \\ \vdots \\ e_p^T \end{bmatrix}, \qquad V := \begin{bmatrix} e_{p+1}^T \\ \vdots \\ e_n^T \end{bmatrix}$$

The following result holds

Theorem 7.5.1. *All trajectories of $\dot{x} = f(x,t)$ globally exponentially converge towards $\mathcal{M}$ if there exist some matrix measure and some $c > 0$ such that*

$$\mu\Big(VJ(x,t)V^T\Big) \leq -c \qquad \forall x \in \mathbb{R}^n,\ \forall t \geq 0$$

where $J(x,t)$ is the system Jacobian.

The previous theorem can be used to prove synchronization of a complex network by considering as linear subspace $\mathcal{M}$ the synchronization manifold $\mathcal{S}$ in (2-5) and V as the orthonormal matrix spanning $\mathcal{S}^\perp$. The matrix V can be obtained as the orthonormalization of the following $n(N-1) \times nN$ matrix

$$\begin{bmatrix} I_n & -I_n & O & O & \dots & O \\ O & I_n & -I_n & O & \dots & O \\ \vdots & & \ddots & \ddots & & \vdots \\ O & O & \dots & I_n & -I_n & O \\ O & O & \dots & O & I_n & -I_n \end{bmatrix}$$

Let $F(X,t)$ be the stack of all the node vector fields and $H(X,t)$ the stack vector of all the coupling functions $\tilde{h}_i$ in (7-4).
Using contraction towards the synchronization subspace, we can prove the following result [**?**].

Theorem 7.5.2. *Assume that for network (7-4) the subspace $\mathcal{S}$ exists, then network synchronization is attained if there exists some matrix measure such that*

$$\mu\Big(V\frac{\partial F}{\partial X}V^T\Big) < -\mu\Big(V\frac{\partial H}{\partial X}V^T\Big) \quad \forall x \in \mathbb{R}^n,\ \ \forall t \geq 0$$

Proof. Indeed, from Theorem 7.5.1 we have that all network trajectories converge towards the synchronization subspace $\mathcal{S}$ if

$$\mu\left(V\left(\frac{\partial F}{\partial X}+\frac{\partial H}{\partial X}\right)V^T\right)$$

is uniformly negative definite. Now, by the subadditivity property of matrix measure [86] we have that the above condition is satisfied if

$$\mu\left(V\frac{\partial F}{\partial X}V^T\right)+\mu\left(V\frac{\partial H}{\partial X}V^T\right)$$

is uniformly negative definite. This proves the result.

□

If we consider a network of diffusively coupled nonlinear nodes as in (7-5)-(7-6), the following result holds from applying contraction using Euclidean matrix measures. (An historical overview of similar results and further proofs can be found in [1, 2]. Here we report alternative proofs based on contraction to make the chapter self contained.)

Theorem 7.5.3. *All network trajectories converge towards $\mathcal{S}$ if*

$$\max_{x,t}\lambda_{\max}\left(\frac{\partial f}{\partial x}\right)\leq\sigma\lambda_2\quad\forall x\in\mathbb{R}^n,\ \ \forall t\geq 0$$

where λ_2 is the algebraic connectivity of the network.

Proof. Let V be the orthonormal matrix spanning $\mathcal{S}^\perp$, this can be chosen as

$$V=(Q\otimes I_n)^T, \tag{7-10}$$

where Q is the orthonormal $N-1\times N-1$ matrix such that

$$Q^TLQ=\Lambda$$

and Λ is the $N-1\times N-1$ diagonal matrix containing on its main diagonal the eigenvalues $\lambda_2,\dots,\lambda_N$ of L.
Now, let J be the Jacobian of (7-6) then from Theorem 7.5.1 we have that all network trajectories converge towards $\mathcal{S}$ if $\mu_2\left(VJV^T\right)$ is uniformly negative definite. That is if

$$\mu_2\left(V\frac{\partial F}{\partial X}V^T-V(\sigma(L\otimes I_n))V^T\right)\leq -c,\quad c>0$$

Then

$$\mu_2\left(V\frac{\partial F}{\partial X}V^T - V(\sigma(L\otimes I_n))V^T\right) \leq \mu_2\left(V\frac{\partial F}{\partial X}V^T\right) + \mu_2\left(-V(\sigma(L\otimes I_n))V^T\right) \qquad (7\text{-}11)$$

Remembering that for the Kronecker product the following property holds

$$(A\otimes B)(C\otimes D) = (AC)\otimes(BD),$$

we have

$$\begin{aligned} V(L\otimes I_n)V^T &= (Q\otimes I_n)^T(L\otimes I_n)(Q\otimes I_n) = \\ &= (Q^T\otimes I_n)(L\otimes I_n)(Q\otimes I_n) = \\ &= (Q^TL\otimes I_n)(Q\otimes I_n) = \\ &= Q^TLQ\otimes I_n = \\ &= \Lambda\otimes I_n \end{aligned}$$

Therefore

$$\mu_2\left(-V(\sigma(L\otimes I_n))V^T\right) = \sigma\mu_2\left(-\Lambda\right) = -\sigma\lambda_2$$

Furthermore

$$\mu_2\left(V\frac{\partial F}{\partial X}V^T\right) = \lambda_{\max}\left(V\left[\frac{\partial F}{\partial X}\right]_s V^T\right)$$

where $\left[\frac{\partial F}{\partial X}\right]_s$ denotes the symmetric part of $\frac{\partial F}{\partial X}$. To evaluate the above matrix measure, consider the quadratic form

$$v^TV\left[\frac{\partial F}{\partial X}\right]_s V^Tv = a^T\left[\frac{\partial F}{\partial X}\right]_s a.$$

Notice that, since the matrix $\frac{\partial F}{\partial X}$ is a block diagonal matrix, we have for any $a\neq 0$

$$\min_{x,t}\lambda_{\min}\left(\frac{\partial f}{\partial x}\right)a^Ta \leq a^T\frac{\partial F}{\partial X}a \leq \max_{x,t}\lambda_{\max}\left(\frac{\partial f}{\partial x}\right)a^Ta,$$

where $\frac{\partial f}{\partial x}$ is the Jacobian of the intrinsic dynamics of the node. On the other hand $a^Ta = v^TVV^Tv = v^Tv$. Thus (7-11) become

$$\mu_2\left(V\frac{\partial F}{\partial X}V^T - V(\sigma(L\otimes I_n))V^T\right) \leq \max_{x,t}\lambda_{\max}\left(\frac{\partial f}{\partial x}\right) - \sigma\lambda_2.$$

Since the above quantity is uniformly negative definite by hypotheses, we have that all network trajectories globally exponentially converge towards $\mathcal{S}$. This proves the result. □

In the specific case where all the network nodes are linear systems and the coupling is linear and diffusive, that is when

$$\dot{x}_i = A(t)x_i + \Gamma \sum_{j \in \mathcal{N}_i} (x_j - x_i) \qquad i = 1, \dots, N \tag{7-12}$$

where $A(t)$ is the dynamical matrix of each node and Γ is some inner coupling matrix, it is possible to prove the following theorem. (We include here a proof for the sake of completeness although other proofs of the same result are also available, see for example [1] for an overview.)

Theorem 7.5.4. *Network (7-12) synchronizes if there exist some matrix measure μ and constant $c > 0$ such that*

$$\mu\Big(A(t) - \lambda_2 \Gamma\Big) \leq -c \qquad \forall t \geq 0$$

Proof. Let J be the Jacobian of (7-12) given as

$$J(t) = I_N \otimes A(t) - L \otimes \Gamma,$$

and V be the orthonormal matrix spanning $\mathcal{S}^{\perp}$ as in (7-10). Following Theorem 7.5.1 network (7-12) synchronizes if

$$\mu\left(V(I_N \otimes A(t) - L \otimes \Gamma)V^T\right) \leq -c,$$

that is

$$\mu\left(V(I_N \otimes A(t))V^T - V(L \otimes \Gamma)V^T\right) \leq -c \tag{7-13}$$

Now using (7-10) the first term in (7-13) can be recast as

$$\begin{aligned} V(I_N \otimes A(t))V^T &= (Q \otimes I_N)^T (I_N \otimes A(t))(Q \otimes I_N) = \\ &= (Q^T \otimes I_N)(I_N \otimes A(t))(Q \otimes I_N) = \\ &= (Q^T \otimes A(t))(Q \otimes I_N) = \\ &= I_N \otimes A(t) \end{aligned}$$

On the other hand, the second term of (7-13) can be written as

$$\begin{aligned} V(L \otimes \Gamma)V^T &= (Q \otimes I_n)^T (L \otimes \Gamma)(Q \otimes I_n) = \\ &= (Q^T \otimes I_n)(L \otimes \Gamma)(Q \otimes I_n) = \\ &= (Q^T L \otimes \Gamma)(Q \otimes I_n) = \\ &= Q^T L Q \otimes \Gamma = \\ &= \Lambda \otimes \Gamma \end{aligned}$$

This means that (7-13) become

$$\mu\left(I_N \otimes A(t) - \Lambda \otimes \Gamma\right) \leq -c.$$

Since $I_N \otimes A(t)$ and $\Lambda \otimes \Gamma$ are block diagonal matrices, we have

$$\mu\left(I_N \otimes A(t) - \Lambda \otimes \Gamma\right) = \mu\left(A(t) - \lambda_2 \Gamma\right) \leq -c,$$

thus proving the result.

□

As for the MSF approach, these results nicely link the contraction properties of the node vector fields with the structural properties of the network and the strength of the coupling.

7.5.1 Example

To illustrate how contraction to a flow-invariant subspace can be successfully applied to networked dynamical systems, we consider the directed network of four FitzHugh-Nagumo neurons whose structure is depicted in Fig. **7-3**a.
A single FN neuron can be described as [26]

$$\begin{cases} \dot{v} = f(v,w) = c\left(v + w - \frac{1}{3}v^3 + u(t)\right) \\ \dot{w} = g(v,w) = -\frac{1}{c}(v - a + bw) \end{cases} \tag{7-14}$$

where v is the membrane potential, w is a recovery variable, $u(t)$ is the magnitude of the stimulus current assumed to be periodic. The parameters a, b and c are non negative and they are set to $a = 0$, $b = 2$, $c = 6$.
In particular we want to prove that a subgroup of system nodes converges towards a specific manifold. The mathematical model of the network is

$$\begin{aligned} \dot{v}_1 &= f(v_1, w_1) + k_1 v_2 + \sigma_1(v_3 - v_1) \\ \dot{w}_1 &= g(v_1, w_1) \\ \dot{v}_2 &= f(v_2, w_2) + k_2 v_3 + \sigma_2(v_4 - v_2) \\ \dot{w}_2 &= g(v_2, w_2) \\ \dot{v}_3 &= f(v_3, w_3) + k_1 v_4 + \sigma_1(v_1 - v_3) \\ \dot{w}_3 &= g(v_3, w_3) \\ \dot{v}_4 &= f(v_4, w_4) + k_2 v_1 + \sigma_2(v_2 - v_4) \\ \dot{w}_4 &= g(v_4, w_4) \end{aligned} \tag{7-15}$$

As a representative example assume we want to prove convergence between nodes 1 and 3, that is we want to prove convergence of the network towards the manifold

$$\mathcal{M} := \left\{ [(v_1, w_1)^T, \dots, (v_4, w_4)^T] \in \mathbb{R}^8 \ : \ (v_1, w_1)^T = (v_3, w_3)^T \right\}$$

and therefore contraction on $\mathcal{M}^\perp$, whose basis is

$$V = \begin{bmatrix} I_2 & O_2 & -I_2 & O_2 \end{bmatrix}$$

where I_2 and O_2 are respectively 2×2 identity and zero matrices.
The system Jacobian is

$$J = \begin{bmatrix} J_1 - \Sigma_1 & K_1 & \Sigma_1 & O \\ O & J_2 - \Sigma_2 & K_2 & \Sigma_2 \\ \Sigma_1 & O & J_3 - \Sigma_1 & K_1 \\ K_2 & \Sigma_2 & O & J_4 - \Sigma_2 \end{bmatrix}$$

where

$$J_i = \begin{bmatrix} \frac{\partial f}{\partial v_i} & \frac{\partial f}{\partial w_i} \\ \frac{\partial g}{\partial v_i} & \frac{\partial g}{\partial w_i} \end{bmatrix} = \begin{bmatrix} c(1 - v_i^2) & c \\ -\frac{1}{c} & -\frac{b}{c} \end{bmatrix}$$

and

$$\Sigma_i = \begin{bmatrix} \sigma_i & 0 \\ 0 & 0 \end{bmatrix}, \quad K_i = \begin{bmatrix} k_i & 0 \\ 0 & 0 \end{bmatrix}.$$

To prove contraction towards $\mathcal{M}^\perp$ Theorem 7.5.1 can be applied, therefore we need to study the matrix measure μ of

$$VJV^T = J_1 + J_3 - 4\Sigma_1 = \begin{bmatrix} \frac{\partial f}{\partial v_1} + \frac{\partial f}{\partial v_3} - 4\sigma_1 & 2c \\ -\frac{2}{c} & -\frac{2b}{c} \end{bmatrix}$$

Using the ∞-vector norm we get the condition

$$\mu_\infty \left(VJV^T \right) = \max \left\{ \frac{\partial f}{\partial v_1} + \frac{\partial f}{\partial v_3} - 4\sigma_1 + |2c| \, ; \ -\frac{2b}{c} + \left| -\frac{2}{c} \right| \right\} < 0 \tag{7-16}$$

Since $\frac{\partial f}{\partial v_i} = c(1 - v_i^2) < c \quad \forall v_i$, the first term in (7-16) is negative definite if

$$c + c - 4\sigma_1 < -2c \quad \Longrightarrow \quad \sigma_1 > c$$

while the second term is negative if $b > 1$.

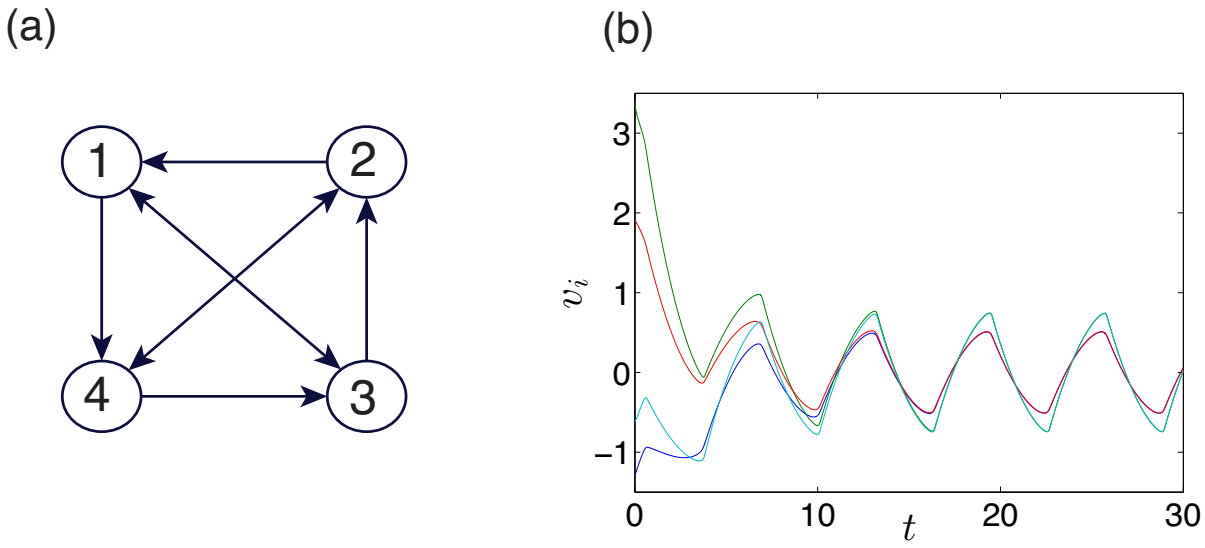

Figure **7-3**: The network structure of the example 7.5.1 (left panel). Simulation of the network (7-15) with parameters $a = 0$, $b = 2$, $c = 6$, coupling gains $\sigma_1 = 7$, $\sigma_2 = 10$, $k_1 = 1$, $k_2 = 10$, and $u(t) = 3\sin(t)$. The initial conditions are uniformly distributed in the interval $[-4,\ 4]$ (right panel). (Reproduced from [22])

Therefore condition (7-16) is fulfilled if

$$\begin{cases} \sigma_1 > c \\ b > 1 \end{cases}$$

A numerical simulation is reported in Fig. **7-3**b showing that nodes 1 and 3 synchronize. Furthermore, node 2 and 4 synchronize as well on a different solution in $\mathcal{M}$, reaching the so-called *cluster synchronization* [57].

7.6 Hierarchical approach

A final alternative which is particularly useful in the case of large networks of interconnected systems is to use a hierarchical approach to obtain a conservative estimate of the matrix measure of the Jacobian of the system or network of interest using multiple norms [74]. Specifically, contraction of the overall system can be guaranteed if some matrix measure of the Jacobian of each individual node is upper bounded and the measure of a reduced-order matrix associated to the interconnection is negative.

Let us consider two norms, a *local* norm $|\cdot|_L$ on $\mathbb{R}^n$ and a *structure* norm $|\cdot|_S$ on $\mathbb{R}^N$ assumed to be monotone. Given any vector $X = [x_1^T, \dots, x_n^T]^T \in \mathbb{R}^{nN}$, with $x_i \in \mathbb{R}^n$, $i = 1, \dots, N$,

we define a *global* norm on $\mathbb{R}^{nN}$ as

$$|X|_G := \left| \left[|x_1|_L, \dots, |x_N|_L \right]^T \right|_S . \tag{7-17}$$

Furthermore we use the notations $\mu_L(\cdot)$, $\mu_S(\cdot)$ and $\mu_G(\cdot)$ to denote the matrix measures associated to $\|\cdot\|_L$, $\|\cdot\|_S$ and $\|\cdot\|_G$ respectively.
Let $J(x,t)$ denote the $nN \times nN$ Jacobian matrix of (7-4) and consider the following partition

$$J(x,t) = \begin{bmatrix} J_{11} & J_{12} & \dots & J_{1k} \\ J_{21} & J_{22} & \dots & J_{2k} \\ \vdots & \vdots & \ddots & \vdots \\ J_{k1} & J_{k2} & \dots & J_{kk} \end{bmatrix}$$

and define the $k \times k$ *structure Jacobian* matrix as

$$J_S(x,t) = \begin{bmatrix} \tilde{J}_{11} & \tilde{J}_{12} & \dots & \tilde{J}_{1k} \\ \tilde{J}_{21} & \tilde{J}_{22} & \dots & \tilde{J}_{2k} \\ \vdots & \vdots & \ddots & \vdots \\ \tilde{J}_{k1} & \tilde{J}_{k2} & \dots & \tilde{J}_{kk} \end{bmatrix} \tag{7-18}$$

with

$$\begin{cases} \tilde{J}_{ii} = \mu_L \left(J_{ii}(x,t) \right) & \text{for } i \in \{1, \dots, k\} \\ \tilde{J}_{ij} = \|J_{ij}(x,t)\|_L & \text{for } i,j \in \{1, \dots, k\},\ i \neq j \end{cases}$$

The following result holds

Theorem 7.6.1 ([22]). *For every local norm on $\mathbb{R}^n$, every monotone structure norm on $\mathbb{R}^N$ and every matrix $J \in \mathbb{R}^{nN \times nN}$*

$$\mu_G(J) \leq \mu_S(J_S) \tag{7-19}$$

Therefore, let $\mathcal{C}$ be a convex set in $\mathbb{R}^{nN}$, if

$$\mu_S \left(J_S(x,t) \right) \leq -c \qquad \forall x \in \mathcal{C},\ \forall t \geq 0$$

then system (7-4) is contracting in $\mathcal{C}$.

Since (7-19) is conservative, the analysis is robust in the sense that a large degree of uncertainty can be tolerated in the components as long as the estimations are met for the network subsystems and their couplings.
The hierarchical approach described above can be effectively used to prove that a system or network is contracting. In the latter case, if the synchronization manifold is embedded into

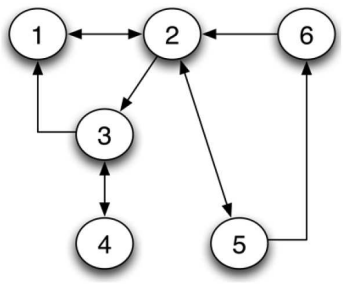

Figure **7-4**: The network used for the simulation of FN neurons. (Reproduced from [22])

the region where the network is contracting, as it is invariant all trajectories will converge towards it and synchronization will remain proved. More generally, the hierarchical approach can reduce the problem of evaluating the matrix measure of the Jacobian of the virtual system or that of the matrix used when proving contraction to a manifold. Hence, it is a useful tool when proving synchronization of large networks with a well identified hierarchical structure.

7.6.1 Example

We illustrate how the hierarchical approach can be used to give sufficient conditions for the convergence of networks of nonlinear agents and hence as an effective design tool to select appropriate coupling functions. We focus again on a representative network of FitzHugh-Nagumo neurons (7-14) which was first presented in [74].
The key steps of this methodology can be summarised as follows:

1. we first compute the reduced-order structured matrix J_S in (7-18);
2. we then use such reduced-order matrix to design appropriate coupling protocols between the network nodes in order to guarantee network convergence.

The network topology considered in this example is shown in Fig. **7-4**.
We assume the coupling protocol among nodes to be similar to the so-called *excitatory-only coupling*, specifically the FN oscillators are coupled via the coupling function

$$\tilde{h}_i(v_i, w_i) := -\gamma_1 \sum_{j \in \mathcal{N}_i} v_j - (\gamma_2 + c)v_i, \qquad \gamma_1, \gamma_2 > 0 \tag{7-20}$$

which is added to the first state equation in (7-14). Thus, the network dynamics become

$$\begin{cases} \dot{v}_i = c\left(v_i + w_i - \frac{1}{3}v_i^3 + u(t)\right) + \tilde{h}_i(v_i, w_i) \\ \dot{w}_i = -\frac{1}{c}(v_i - a + bw_i) \end{cases} \qquad i = 1, \dots, N \tag{7-21}$$

To guarantee that all nodes converge towards a unique trajectory in state space, it now suffices to choose the parameters of the coupling protocol (7-20) so as to make the closed-loop network (7-21) contracting. Indeed, the synchronization manifold (2-5), with $x_i = [v_i, w_i]^T$, is flow invariant for the network dynamics (that is, trajectories with initial conditions in $\mathcal{S}$ remain in it for all $t \geq t_0$). Hence, if the network is contracting, trajectories starting from any two initial conditions will converge exponentially towards each other. As trajectories in $\mathcal{S}$ remain therein for all time, it immediately follows that all trajectories must converge towards $\mathcal{S}$ and asymptotically towards each other; that is, nodes will synchronize. Moreover, from Theorem 7.2.3, network contraction also yields that the synchronous evolution will be periodic with the same period of $u(t)$.

Now, to study contraction of the network dynamics we would need to study the Jacobian of (7-21), which is a $2N \times 2N$ matrix. Using the hierarchical approach, we can look instead at the structure Jacobian, which is, in this case, an $N \times N$ matrix, defined in (7-18). To compute J_S we use as *local* norm on $\mathbb{R}^2$ the one induced by the ∞-norm, and choosing $\gamma_2 > c + b - 1/c$ we have

$$J_S = \begin{bmatrix} -\frac{b-1}{c} & \gamma_1 & \gamma_1 & 0 & 0 & 0 \\ \gamma_1 & -\frac{b-1}{c} & 0 & 0 & \gamma_1 & \gamma_1 \\ 0 & \gamma_1 & -\frac{b-1}{c} & \gamma_1 & 0 & 0 \\ 0 & 0 & \gamma_1 & -\frac{b-1}{c} & 0 & 0 \\ 0 & \gamma_1 & 0 & 0 & -\frac{b-1}{c} & 0 \\ 0 & 0 & 0 & 0 & \gamma_1 & -\frac{b-1}{c} \end{bmatrix}$$

Now to ensure network contraction (and hence synchronization) we have to tune the parameters b and γ_1 so that a uniformly negative structure matrix measure in $\mathbb{R}^6$ for J_S exists. Choosing as *structure* norm the 1-vector norm, we have that the matrix measure $\mu_1(J_S)$ is uniformly negative if

$$\{J_s\}_{ii} < 0$$
$$|\{J_S\}_{ii}| > \textstyle\sum_{i \neq j} |\{J_S\}_{ij}|$$

Notice that the first condition above is fulfilled if $b > 1$. The second condition is instead guaranteed if

$$3\gamma_1 < \frac{b-1}{c}$$

Thus if this last condition is fulfilled, all network trajectories will converge towards a unique synchronous solution. A simulation for such a network is reported in Fig. **7-5**, confirming the theoretical predictions.

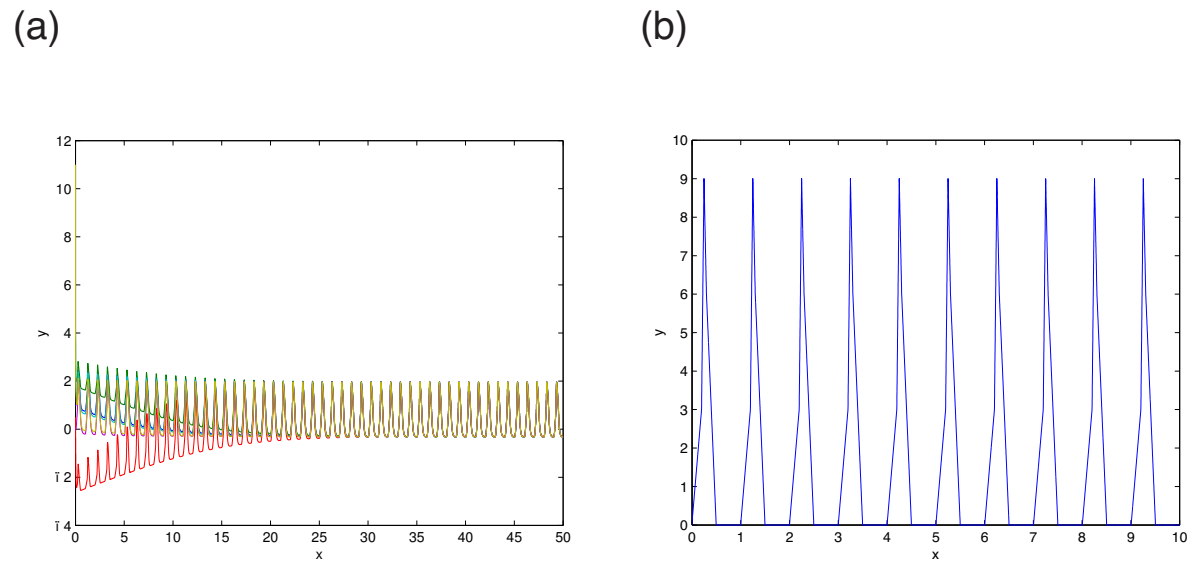

Figure **7-5**: Simulation of (7-21) with $\gamma_1 = 0.05$ and $\gamma_2 = 7$ (left panel). The behaviour of $u(t)$ is shown $(0 \geq t \geq 10)$ in the right panel. (Reproduced from [22].)

7.7 Summary

We reviewed some approaches to study synchronization from a contraction theory viewpoint. Specifically we analysed three strategies: virtual systems method, convergence to a flow-invariant subspace and hierarchical approach. Note that the latter is well suited, differently from the former, when the dimensionality of the problem does grow. Numerical examples confirms all theoretical results showed throughout the Chapter.

CHAPTER 8

Conclusions

We derived several strategies for the evolution of a network of dynamical agents, so as to achieve synchronization and consensus.

In Chapter 4 we investigated two strategies for general types of consensus in directed networks. We built on edge snapping and derived proper modifications to achieve this objective. A three-well potential was introduced to describe unidirectional links in the network. Then we defined two rules to adapt network structure, based on nodes' state. Theoretical results have been confirmed by numerical simulations.

In Chapter 5 we investigated synchronization of coupled oscillators via an evolutionary strategy. Results show that heterogeneity in the nodes dynamics is fundamental for the emergence of minimal ES networks. A thorough analysis of the emergent networks also suggest that increasing the heterogeneity in the nodes, the structure of minimal networks tends to be characterized by the presence of hubs. Thus, the degree distribution becomes more heterogeneous. Also, our adaptive, local strategy induces the type of phenomena described in the literature on explosive synchronization.

An analysis of robustness properties regarding edge snapping mechanism is provided in Chapter 6. As a result, the height of the barrier of the potential V used in the edge snapping mechanism, can be adjusted to enhance robustness properties. Indeed, below a certain threshold, a node subject to a perturbation can recover the synchronized state via the activation of new links. Moreover, it is shown how to improve the performance of synchronization by acting on model parameters.

In Chapter 7 we analysed some approaches to study synchronization from a contraction theory viewpoint. Specifically we analysed three strategies: virtual systems method, conver-

gence to a flow-invariant subspace and hierarchical approach. We note that the latter is well suited, differently from the former, when the dimensionality of the problem does grow.

Bibliography

[1] Zahra Aminzare and Eduardo D. Sontag. Contraction methods for nonlinear systems: a brief introduction and some open problems. In *IEEE Conference on Decision and Control*, pages 3835–3847, December 2014.

[2] Zahra Aminzare and Eduardo D. Sontag. Remarks on diffusive-link synchronization using non-Hilbert logarithmic norms. In *IEEE Conference on Decision and Control*, pages 6086–6091, December 2014.

[3] David Angeli. A Lyapunov approach to incremental stability properties. *IEEE Transactions on Automatic Control*, 47(3):410–421, 2002.

[4] Takaaki Aoki and Toshio Aoyagi. Co-evolution of phases and connection strengths in a network of phase oscillators. *Phys. Rev. Lett.*, 102:034101, 2009.

[5] Vanesa Avalos-Gaytán, Juan A. Almendral, David Papo, Satu Elisa Schaeffer, and Stefano Boccaletti. Assortative and modular networks are shaped by adaptive synchronization processes. *Phys. Rev. E*, 86:015101, 2012.

[6] Albert-Lázslo Barabási and Réka Albert. Emergence of scaling in random networks. *Science*, 286:509–512, 1999.

[7] Igor Belykh, Mario di Bernardo, Jürgen Kurths, and Maurizio Porfiri. Evolving dynamical networks. *Physica D: Nonlinear Phenomena*, 267:1–6, 2014.

[8] S. Boccaletti, V. Latora, Y. Moreno, M. Chavez, and D.-U. Hwang. Complex networks: Structure and dynamics. *Physics Reports*, 424(4–5):175 – 308, 2006.

[9] Markus Brede. Synchrony-optimized networks of non-identical kuramoto oscillators. *Physics Letters A*, 372(15):2618 – 2622, 2008.

[10] D.A. Burbano Lombana and M. di Bernardo. Multiplex pi control for consensus in networks of heterogeneous linear agents. *Automatica*, 67:310–320, 2016.

[11] Guan-Rong Chen. Problems and challenges in control theory under complex dynamical network environments. *Acta Automatica Sinica*, 39(4):312 – 321, 2013.

[12] J.-M. Chen, J.-J Lu, and Q.-H. Wang. Research and improvement of adaptive topology algorithm leach for wireless sensor network. In *4th International Conference on Wireless Communications, Networking and Mobile Computing*, pages 1–4, 2008.

[13] T. Chen, X. Liu, and W. Lu. Pinning complex networks by a single controller. *IEEE Transactions on Circuits and Systems I: Regular Papers*, 54(6):1317–1326, 2007.

[14] N. Chopra and M. W. Spong. On exponential synchronization of kuramoto oscillators. *IEEE Transactions on Automatic Control*, 54(2):353–357, 2009.

[15] J. Cortés. Distributed algorithms for reaching consensus on general functions. *Automatica*, 44(3):726–737, 2008.

[16] C. Darwin. *The Origin of Species by Means of Natural Selection, or the Preservation of Favoured Races in the Struggle for Life*. London: Murray, 1859.

[17] L. Davis. *Handbook of genetic algorithms*. Van Nostrand Reinhold, 1991.

[18] P. De Lellis, M. di Bernardo, T. E. Gorochowski, and G. Russo. Synchronization and control of complex networks via contraction, adaptation and evolution. *IEEE Circuits and Systems Magazine*, 10(3):64–82, 2010.

[19] P. De Lellis, M. di Bernardo, and M. Porfiri. Pinning control of complex networks via edge snapping. *Chaos: An Interdisciplinary Journal of Nonlinear Science*, 21, 2011.

[20] Pietro De Lellis, Mario di Bernardo, Franco Garofalo, and Maurizio Porfiri. Evolution of complex networks via edge snapping. *IEEE Transactions on Circuits and Systems I*, 57(8):2132–2143, 2010.

[21] P. DeLellis, M. di Bernardo, and F. Scafuti. Consensus via adaptation of the network structure. In *IEEE 52nd Annual Conference on Decision and Control (CDC), 2013*, pages 660–665, Dec 2013.

[22] M. di Bernardo, D. Fiore, G. Russo, and F. Scafuti. *Complex Systems and Networks*, chapter Convergence, Consensus and Synchronization of Complex Networks via Contraction Theory, pages 313–339. Springer Berlin Heidelberg, 2016.

[23] Luca Donetti, Pablo I. Hurtado, and Miguel A. Muñoz. Entangled networks, synchronization, and optimal network topology. *Phys. Rev. Lett.*, 95:188701, Oct 2005.

[24] F. Dörfler and F. Bullo. On the critical coupling for kuramoto oscillators. *SIAM Journal on Applied Dynamical Systems*, 10(3), 2011.

[25] J. Fan and D. J. Hill. Enhancement of synchronizability of the kuramoto model with assortative degree-frequency mixing. In J. Zhou, editor, *Complex Sciences*, volume 5, pages 1967–1972. Springer-Verlag, Berlin, Heidelberg, 2009.

[26] Richard FitzHugh. Mathematical models of threshold phenomena in the nerve membrane. *The bulletin of mathematical biophysics*, 17(4):257–278, 1955.

[27] F. Forni and R. Sepulchre. A differential lyapunov framework for contraction analysis. *IEEE Transactions on Automatic Control*, 59:614–628, 2014.

[28] D. Gabor. Theory of communication. part 1: The analysis of information. *Journal of the Institution of Electrical Engineers*, 93(26), 1946.

[29] Fei Ge and Yuanni Wang. An adaptive energy efficient topology for wireless sensor networks. In *Proceedings of the Second International Conference on Future Generation Communication and Networking, FGCN '08*, volume 2, pages 187–192, 2008.

[30] J. Gómez-Gardeñes, S. Gómez, A. Arenas, and Y. Moreno. Explosive synchronization transitions in scale-free networks. *Phys. Rev. Lett.*, 106:128701, 2011.

[31] Jesús Gómez-Gardeñes, Sergio Gómez, Alex Arenas, and Yamir Moreno. Explosive synchronization transitions in scale-free networks. *Phys. Rev. Lett.*, 106:128701, Mar 2011.

[32] Thomas E. Gorochowski, Mario Di Bernardo, and Claire S. Grierson. Evolving dynamical networks: A formalism for describing complex systems. *Complexity*, 17(3):18–25, 2011.

[33] Thomas E. Gorochowski, Mario di Bernardo, and Claire S. Grierson. Evolving enhanced topologies for the synchronization of dynamical complex networks. *Phys. Rev. E*, 81:056212, May 2010.

[34] T. Gross and B. Blasius. Adaptive coevolutionary networks: a review. *Journal of the Royal Society Interface*, 5, 2008.

[35] Andrew M Hein, Sara Brin Rosenthal, George I Hagstrom, Andrew Berdahl, Colin J Torney, and Iain D Couzin. The evolution of distributed sensing and collective computation in animal populations. *eLife*, 4:e10955, 2015.

[36] J. L. Hemmen and W. F. Wreszinski. Lyapunov function for the kuramoto model of nonlinearly coupled oscillators. *Journal of Statistical Physics*, 72(1):145–166, 1993.

[37] P. Holmes. A nonlinear oscillator with a strange attractor. *Philosophical Transactions of the Royal Society of London, Series A*, 292(1394):419–448, 1979.

[38] Jiang Hui-Jun, Wu Hao, and Hou Zhong-Huai. Explosive synchronization and emergence of assortativity on adaptive networks. *Chinese Physics Letters*, 28(5), 2011.

[39] A. Jadbabaie, N. Motee, and M. Barahona. On the stability of the kuramoto model of coupled nonlinear oscillators. In *Proceedings of the 2004 American Control Conference*, volume 5, pages 4296–4301, 2004.

[40] Hassan K Khalil. *Nonlinear systems*. Prentice Hall, 3rd edition, 2002.

[41] Y. Kuramoto. Lecture notes in physics. In H. Araki, editor, *International Symposium on Mathematical Problems in Theoretical Physics*, volume 39, pages 420–422, 1975.

[42] Y. Kuramoto. *Chemical Oscillations, Waves, and Turbulence*. Springer, New York, 1984.

[43] I. Leyva, A. Navas, I. Sendina-Nadal, JA Almendral, JM Buldú, M. Zanin, D. Papo, and S. Boccaletti. Explosive transitions to synchronization in networks of phase oscillators. *Scientific Reports*, 3, 2013.

[44] Zhi Li and Guanrong Chen. Global synchronization and asymptotic stability of complex dynamical networks. *IEEE Transactions on Circuits and Systems II: Express Briefs*, 53(1):28–33, 2006.

[45] Yang-Yu Liu, Jean-Jacques Slotine, and Albert-László Barabási. Controllability of complex networks. *Nature*, 473:167–173, 2011.

[46] W. Lohmiller and J. J. E. Slotine. On contraction analysis for non-linear systems. *Automatica*, 34:683–696, 1998.

[47] M. D. McKay, R. J. Beckman, and W. J. Conover. Comparison of three methods for selecting values of input variables in the analysis of output from a computer code. *Technometrics*, 21(2):239–245, 1979.

[48] M. Mesbahi and M Egerstedt. *Graph Theoretic Methods in Multiagent Networks*. Princeton University Press, Princeton, NJ, 2010.

[49] Ciamac C. Moallemi and Benjamin Van Roy. Distributed optimization in adaptive networks. In *in Advances in Neural Information Processing Systems*, page 2004. MIT Press, 2003.

[50] M. Molloy and B. Reed. A critical point for random graphs with a given degree sequence. *Random Structures and Algorithms*, 6(2-3):161–179, 1995.

[51] M. E. J. Newman. The structure and function of complex networks. *SIAM Review*, 45(2):167–256, 2003.

[52] R. Olfati-Saber, J.A. Fax, and R.M. Murray. Consensus and cooperation in networked multi-agent systems. *Proceedings of the IEEE*, 95(1):215–233, 2007.

[53] R. Olfati-Saber and R.M. Murray. Consensus problems in networks of agents with switching topology and time-delays. *IEEE Transactions on Automatic Control*, 49(9):1520–1533, 2004.

[54] Grigory V. Osipov, Arkady S. Pikovsky, Michael G. Rosenblum, and Jürgen Kurths. Phase synchronization effects in a lattice of nonidentical rössler oscillators. *Phys. Rev. E*, 55:2353–2361, Mar 1997.

[55] Diego Pazó. Thermodynamic limit of the first-order phase transition in the kuramoto model. *Phys. Rev. E*, 72:046211, Oct 2005.

[56] Louis M. Pecora and Thomas L. Carroll. Master stability functions for synchronized coupled systems. *Phys. Rev. Lett.*, 80:2109–2112, 1998.

[57] Quang-Cuong Pham and Jean-Jacques Slotine. Stable concurrent synchronization in dynamic system networks. *Neural Networks*, 20(1):62–77, 2007.

[58] M. Porfiri and D.J. Stilwell. Consensus seeking over random weighted directed graphs. *IEEE Transactions on Automatic Control*, 52(9):1767–1773, 2007.

[59] Maurizio Porfiri and Francesca Fiorilli. Node-to-node pinning control of complex networks. *Chaos: An Interdisciplinary Journal of Nonlinear Science*, 19(1):–, 2009.

[60] Amirreza Rahmani, Meng Ji, Mehran Mesbahi, and Magnus Egerstedt. Controllability of multi-agent systems from a graph-theoretic perspective. *SIAM Journal on Control and Optimization*, 48(1):162–186, 2009.

[61] Quansheng Ren and Jianye Zhao. Adaptive coupling and enhanced synchronization in coupled phase oscillators. *Phys. Rev. E*, 76, 2007.

[62] W. Ren and R. W. Beard. *Distributed Consensus in Multi-vehicle Cooperative Control*. Springer, London, UK, 2008.

[63] Wei Ren, R.W. Beard, and E.M. Atkins. A survey of consensus problems in multi-agent coordination. In *Proceedings of the American Control Conference, 2005*, pages 1859–1864 vol. 3, 2005.

[64] Wei Ren, R.W. Beard, and E.M. Atkins. Information consensus in multivehicle cooperative control. *IEEE Control Systems Magazine*, 27(2):71–82, 2007.

[65] F.A Rodrigues, K. DM. T. Peron, P. Ji, and J. Kurths. The kuramoto model in complex networks. *Physics Reports*, 610:1–98, 2016.

[66] Michael G. Rosenblum, Arkady S. Pikovsky, and Jürgen Kurths. Phase synchronization of chaotic oscillators. *Phys. Rev. Lett.*, 76:1804–1807, Mar 1996.

[67] G. Russo and M. di Bernardo. How to synchronize biological clocks. *Journal of Computationa Biology*, 16:379–393, 2009.

[68] G. Russo and M. di Bernardo. Solving the rendezvous problem for multi-agent systems using contraction theory. In *Proceedings of the 48th IEEE Conference on Decision and Control, 2009 held jointly with the 2009 28th Chinese Control Conference. CDC/CCC 2009.*, pages 5821–5826, 2009.

[69] G. Russo and M. di Bernardo. Solving the rendezvous problem for multi-agent systems using contraction theory. In *Proceedings of the International Conference on Decision and Control*, 2009.

[70] G. Russo, M. di Bernardo, and J.J. Slotine. A graphical algorithm to prove contraction of nonlinear circuits and systems. *IEEE Transactions on Circuits And Systems I*, 58:336–348, 2011.

[71] G. Russo, M. di Bernardo, and E. D. Sontag. Global entrainment of transcriptional systems to periodic inputs. *PLoS Computational Biology*, 6:e1000739, 2010.

[72] Giovanni Russo and Mario Di Bernardo. Contraction Theory and Master Stability Function: Linking Two Approaches to Study Synchronization of Complex Networks. *IEEE Transactions on Circuits and Systems*, 56(2):177–181, 2009.

[73] Giovanni Russo, Mario Di Bernardo, and Eduardo D Sontag. Global entrainment of transcriptional systems to periodic inputs. *PLoS computational biology*, 6(4):e1000739, 2010.

[74] Giovanni Russo, Mario Di Bernardo, and Eduardo D Sontag. A contraction approach to the hierarchical analysis and design of networked systems. *IEEE Transactions on Automatic Control*, 58(5):1328–1331, 2013.

[75] Francesco Scafuti, Takaaki Aoki, and Mario di Bernardo. An evolutionary strategy for adaptive network control and synchronization and its applications. *IFAC-PapersOnLine*, 48(18):193–198, 2015.

[76] Francesco Scafuti, Takaaki Aoki, and Mario di Bernardo. Heterogeneity induces emergent functional networks for synchronization. *Phys. Rev. E*, 91:062913, 2015.

[77] Philip Seliger, Stephen C. Young, and Lev S. Tsimring. Plasticity and learning in a network of coupled phase oscillators. *Phys. Rev. E*, 65:041906, 2002.

[78] D.D. Siljak. Dynamic graphs. *Nonlinear Analysis: Hybrid Systems*, 2(2):544–567, 2008.

[79] J.W. Simpson-Porco and F. Bullo. Contraction theory on riemannian manifolds. *Systems and Control Letters*, 65:74–80, 2014.

[80] Per Sebastian Skardal, Dane Taylor, and Jie Sun. Optimal synchronization of complex networks. *Phys. Rev. Lett.*, 113:144101, Sep 2014.

[81] Jean-Jacques E Slotine and Weiping Li. *Applied nonlinear control*. Prantice-Hall, Englewood Cliffs, 1991.

[82] S.H. Strogatz. *Nonlinear Dynamics and Chaos*. AddisonŰWesley, Reading, MA, 1994.

[83] S.H. Strogatz. From kuramoto to crawford: exploring the onset of synchronization in populations of coupled oscillators. *Physica D: Nonlinear Phenomena*, 143(1-4):1–20, 2000.

[84] S.H. Strogatz. Exploring complex networks. *Nature*, 410:268–276, 2001.

[85] S. Tan, J. Lu, G. Chen, and D. Hill. When structure meets function in evolutionary dynamics on complex networks. *Circuits and Systems Magazine, IEEE*, 14(4):36–50, Fourthquarter 2014.

[86] Mathukumalli Vidyasagar. *Nonlinear systems analysis*. Siam, 2002.

[87] Wei Wang and Jean-Jacques E Slotine. On partial contraction analysis for coupled nonlinear oscillators. *Biological cybernetics*, 92(1):38–53, 2005.

[88] Xiao Fan Wang. Complex networks: Topology, dynamics and synchronization. *International Journal of Bifurcation and Chaos*, 12(5):885–916, 2002.

[89] Duncan J. Watts and Steven H. Strogatz. Collective dynamics of 'small-world' networks. *Nature*, 393:440–442, 1998.

[90] N. Wiener. *Nonlinear Problems in Random Theory*. MIT Press, Cambridge, MA, 1958.

[91] Ryan K Williams and Gaurav S Sukhatme. Topology-constrained flocking in locally interacting mobile networks. *IEEE International Conference on Robotics and Automation (submitted)*, 2013.

[92] A.T. Winfree. Biological rhythms and the behavior of populations of coupled oscillators. *Journal of Theoretical Biology*, 61(1):15–42, 1967.

[93] Tatsuo Yanagita and Alexander S. Mikhailov. Design of easily synchronizable oscillator networks using the monte carlo optimization method. *Phys. Rev. E*, 81:056204, May 2010.

[94] Dorjsuren Battogtokh Yoshiki Kuramoto. Coexistence of coherence and incoherence in nonlocally coupled phase oscillators. *Nonlinear Phenomena in Complex Systems*, 5(4):380–385, 2002.

[95] Wenwu Yu, Guanrong Chen, Ming Cao, and J. Kurths. Second-order consensus for multiagent systems with directed topologies and nonlinear dynamics. *IEEE Transactions on Systems, Man, and Cybernetics, Part B: Cybernetics*, 40(3):881–891, 2010.

[96] M. M. Zavlanos and G. J. Pappas. Distributed connectivity control of mobile networks. *IEEE Transactions on Robotics*, 24(6):1416–1428, 2008.

[97] X. Zhang, S. Boccaletti, S. Guan, and Z. Liu. Explosive synchronization in adaptive and multilayer networks. *Phys. Rev. Lett.*, 114:038701, 2015.

[98] Xiyun Zhang, Xin Hu, J. Kurths, and Zonghua Liu. Explosive synchronization in a general complex network. *Phys. Rev. E*, 88:010802, Jul 2013.